AN ABSTRACT OF THE DISSERTATION OF

Gamika Arun Wickramasuriya for the degree of Doctor of Philosophy in Mechanical Engineering presented on December 10, 2009.

Title: Reduced Order Modeling of Legged Locomotion in the Horizontal Plane

Abstract approved: _____

John Schmitt

Sprawled-posture insects exhibit a remarkable ability to rapidly run in a stable manner over complex terrain, a feat that has yet to be equaled by man-made legged robots. Recent experimental results suggest that these insects may employ a hierarchical control structure, in which locomotion performance emerges from a combination of insect structure and leg function, which is only augmented by neural reflexes in the presence of large or persistent disturbances. In this study, we utilize a previously developed reduced order model for lateral plane locomotion and extend it by developing leg positioning and actuation strategies that are consistent with insect leg function evidenced in experiments. We examine improvements in locomotion performance obtained by utilizing these strategies in terms of gait stability and robustness to external perturbations, such as those that might be encountered when running over rough terrain. Leg positioning strategies examined include leg angle control based upon previous leg angles and leg recirculation strategies that prescribe, in

a feedforward manner, the motion of the leg as it swings from its lift-off to touch-down positions. Both these protocols provide control authority in re-orienting system momentum and are shown to improve gait stability and robustness to external perturbations. While the original reduced order template models leg dynamics by an energy-conserving spring, we incorporate energetic variations through leg actuation that varies the force-free leg length during the stance phase while preserving qualitatively correct force and velocity profiles. In contrast to the partially asymptotically stable gaits identified in previous analyses, incorporating leg actuation in conjunction with the leg positioning strategies produces completely asymptotically stable gaits in body coordinates. Locomotion performance of the resulting model is subsequently analyzed by computing the basin of stability of our model in response to energetic perturbations of the type experimentally implemented on running, sprawled-posture insects.

Reduced Order Modeling of Legged Locomotion in the Horizontal Plane

by

Gamika Arun Wickramasuriya

A DISSERTATION

submitted to

Oregon State University

in partial fulfillment of
the requirements for the
degree of

Doctor of Philosophy

Presented December 10, 2009
Commencement June 2010

Doctor of Philosophy dissertation of Gamika Arun Wickramasuriya presented on December 10, 2009.

APPROVED:

Major Professor, representing Mechanical Engineering

Head of the School of Mechanical, Industrial, and Manufacturing Engineering

---

Dean of the Graduate School

I understand that my dissertation will become part of the permanent collection of Oregon State University libraries. My signature below authorizes release of my dissertation to any reader upon request.

Gamika Arun Wickramasuriya, Author

ACKNOWLEDGEMENTS

I take this opportunity to convey my deep appreciation to all who have impacted me positively during my years at Oregon State University. I express my sincere gratitude to my doctoral thesis adviser Dr. John Schmitt for mentoring, teaching and guiding me over the years. I thank Dr. Charles E. Smith from whom I've learnt advanced engineering dynamics. I thank all the instructors who have thought me at Oregon State University. I have obtained valuable transferable skills and knowledge from them for which I'm deeply grateful. I thank my doctoral thesis committee for their valuable input and cooperation. I would like to thank Shai Revzen for providing individual leg position data and individual leg angular velocity data he collected from experiments with running cockroaches.

Next, I extend my sincere thanks to all my friends at OSU from whom I've learned a lot. Specifically, I would like to thank Ben Dickinson, Matt Knudson, Cody Ray, Arun Selvaraj, Scott Bonnono and Ehsan Shams.

I am most grateful to my wife Kishani, my mother Kumarini, other family members and our family friends for supporting me and standing beside me. Finally, let me express my deep gratitude to Raeda and Jim Poirot and Joan and Alan Knudtson for all the strength, support and encouragement they gave me over the years.

TABLE OF CONTENTS

TABLE OF CONTENTS (Continued)

LIST OF FIGURES

LIST OF TABLES

LIST OF APPENDIX FIGURES

DEDICATION

I dedicate this thesis to my wife Kishani, my mother Kumarini and my father Sena.

Chapter 1 – Introduction

Sprawled-posture insects are highly maneuverable, exhibiting a remarkable ability to rapidly run over complex terrain [52, 14] and quickly recover from large external perturbations [24]. In contrast to humans and many larger mammals whose movement is predominantly in the vertical plane with respect to the ground, insect motion occurs primarily in the horizontal plane. Insects are relatively stable in the vertical plane due to their sprawled posture and multiple leg supports. Thus, our model will be restricted to the horizontal plane dynamics of the insect. The sprawled posture employed by these insects naturally produces large lateral forces, yielding locomotion dynamics that occur largely in the horizontal plane.

Reduced order modeling of these lateral plane locomotion dynamics has been performed primarily through analyses of the lateral leg spring (LLS) model [43, 42]. The model has been shown to qualitatively reproduce the force, velocity and moment profiles exhibited by the cockroach *Blaberus discoidalis* during fast locomotion [41], have relevance to other sprawled-posture creatures via the analysis of non-dimensional model parameters [44], and exhibit partially asymptotically stable gaits without utilizing neural feedback [43, 42, 41, 44].

Reduced order models have been utilized to effectively represent the underlying dynamics of legged locomotion in both the sagittal [4, 5, 50, 18] and lateral planes [43, 42, 41] for a variety of animals and insects. Analyses of these reduced order mod-

els have often focused on the dynamics and stability of periodic gaits for a fixed leg angle touch-down protocol, where the leg touch-down angle is fixed to the same value at the beginning of each stance phase. While utilizing this protocol produces stable gaits for appropriate choices of the relevant system parameters for both the sagittal [50, 18] and lateral [43, 44] plane models, implementing a similar leg touch-down protocol in a three dimensional spatial reduced order model produces only unstable periodic gaits [47]. Prescribing fixed leg touch-down angles in the bipedal spatial model evidently precludes proper reorientation of the system momentum in response to perturbations, leading to gait instability. While the foot placement control law proposed for the spatial reduced order model is capable of stabilizing the periodic gaits [47], it utilizes sensory information that may not either be readily available or easily sensed.

While the existing LLS models are capable of recovering from external perturbations in the velocity heading angle and body angular velocity these models are unable to recover mass center velocity and leg touch down angle values of the original periodic gait. This is due to energy conservation and fixed leg touch down protocol respectively which are inherent in the existing LLS models. Also, none of the previous LLS model formulations have specified the motion of the leg during the swing phase required to attain a specific touch-down angle which would contribute to stability by re-orienting momentum.

In this research we endeavor to introduce biologically inspired control mechanisms for leg touch down angle control, swing leg recirculation and muscle actuation to ultimately obtain complete asymptotic stability for the point mass LLS model by combining the control strategies stated above. Thus, we show that the point mass model is capable

recovering the original gait when subjected to energetic perturbations as in [24, 6].

The purpose of our leg angle control work is to develop a method for systematically varying the leg touch-down angle to aid in recovering from external perturbations, utilizing easily sensed variables. To that end, we utilize the simple models of insect locomotion in the horizontal plane, examined in [42, 43, 44, 31], to obtain analytical and numerical results concerning the stability properties of gaits utilizing a prescribed leg touch-down angle control law. Consistent with the limited sensory feedback evidently utilized by sprawled-posture insects during locomotion [52], the leg touch-down angle control law developed in this work will depend upon a limited number of variables that are easily sensed by insect mechanoreceptors and will apply control at only a single point during a stance phase rather than continuously during stance. Experimental studies on the cockroach *Blaberus discoidalis* suggest that while the intrinsic force-length properties of muscles produce mechanical feedback that is largely responsible for perturbation recovery within a stance phase, stride to stride gait variations can occur as a result of neural reflexes [24, 34, 52]. Additionally, when recovering from significant external perturbations, experimental studies suggest that cockroaches change foot touch-down positions from those utilized during unperturbed strides [23]. While gaits of the original horizontal plane model benefit from a simplistic model of preflexes via the elastic leg spring, the model has no prescription for varying the leg touch-down angle in response to external perturbations. In our leg angle control work, we wish to combine the effect of preflexes with low level neural control to improve gait stability by modifying the leg touch-down angle based upon previous leg angle measurements. In future studies, we intend to utilize the insight gained from this study, as well as a similar

one for the sagittal plane model [37, 38], to design a leg touch-down angle control to stabilize gaits of the spatial model in a similar manner.

While previous LLS model formulations have employed a constant [43, 42, 31] leg touch-down angle, none have specified the motion of the leg during the swing phase required to attain a specific touch down angle. However, the development and incorporation of leg recirculation strategies into a reduced order model of vertical plane locomotion, the spring loaded inverted pendulum (SLIP), has yielded performance benefits. Seyfarth et al. [51] demonstrated that retracting the leg of the SLIP model at a constant angular velocity, beginning at the apex of the flight phase, improved both gait stability and the basin of stability. Altendorfer et. al [2] showed that an open-loop controller, similar to that developed for the hexapedal robot Rhex [36], utilizing piecewise-linear leg angle trajectories yielded stable gaits for appropriate parameter ranges of both the point mass and rigid body SLIP models. It appears that no such studies of leg recirculation have been performed for the LLS model.

Recent experimental investigations into cockroach locomotion over rough terrain suggest that leg activation during swing and stance is prescribed primarily in a feedforward manner, with neural reflexes serving to modulate activation levels on a longer timescale [52]. Variations in foot touch-down positions evidenced experimentally in response to external perturbations [23] may therefore arise largely from this feedforward action rather than neural control. Based upon these analyses and experimental results, we extend the original LLS model by developing a leg recirculation policy that specifies the angular velocity of the leg during its swing phase in a feedforward manner. From a theoretical perspective, this study was motivated by the stability improvements obtained

for small, controlled changes in leg touch-down angles for the LLS model in response to external perturbations in our leg angle control work introduced above and by the instability of all periodic gaits in the spatial spring loaded inverted pendulum model for a constant leg touch-down protocol [47]. In this work, we combine the simplistic model of preflexes of the LLS model with low level neural control required for feedforward leg recirculation, and determine the effects of this policy on gait stability and robustness. It is hoped that the results of this swing leg recirculation work will provide insight into the importance of leg recirculation in insect locomotion and the design of leg recirculation policies for multi-legged and spatial reduced order models.

The original LLS formulation is energetically conservative, with an elastic leg serving to store and return energy during the course of a stance phase, yet no physical mechanisms have been identified in animals or insects that function in this manner without also dissipating or producing energy[12]. Instead, the apparently conservative operation during steady state locomotion results from a variety of muscles working in concert to produce both negative and positive work during a stance phase, with the net result resembling dynamics that are well represented by the LLS model. While the original LLS model yields force and velocity profiles representative of steady state animal locomotion, transitions to different speeds and recovery from external energetic perturbations requires non-conservative leg function. Recent experimental investigations into leg function in insects [12] have begun to provide insight into how non-conservative leg function may impact gait stability and robustness to external perturbation. Further insight into leg function in the presence of external perturbations is obtained from experiments with cockroaches running over rough terrain [52]. While locomotion over uneven

terrain would seem to require significant neural feedback, muscle activation evidenced in cockroaches running over rough terrain appears to be prescribed in a feedforward manner; a leg that misses the ground continues to retract, exhibiting muscle activation levels similar to those employed by legs in contact with the ground [52]. We utilize these insights into leg function and develop an energetically non-conservative LLS model capable of recovery from energetic external perturbations via mechanisms similar to those of its animal counterparts. In our work, energy variations are introduced into the LLS model through clock-driven actuation of the force-free leg length during each stance phase. The actuation protocol investigated is employed in a feedforward manner, similar to the consistent muscle activation patterns evidenced for cockroaches running over rough terrain.

Stability and robustness to external perturbations is investigated for the point mass LLS model with leg actuation and a fixed leg touch down angle. Finally we investigate improving gait stability and robustness by combining leg actuation with leg angle control, thus obtaining complete asymptotic stability of periodic gaits for the point mass LLS model.

The thesis is structured as follows. Chapter 2 provides a review of the offset pivot lateral leg spring (LLS) model [31], which is an extension of the original horizontal plane model that produces qualitatively correct yawing motions without a moving leg attachment point. Chapter 3 details the construction of a simple control law that prescribes the leg touch-down angle based upon previous leg angle measurements. Analytical stability criteria are developed for periodic gaits and are used to confirm the results obtained from numerical simulation. Numerical simulations are subsequently utilized

to investigate the performance of the leg angle control law in response to significant external perturbations in the heading angle. We also numerically investigate the performance of the leg angle control law for the rigid body model with the leg attachment offset from the center of mass, and show that improved performance is also attained in this instance. Chapter 4 details the construction of a simple leg swing protocol that prescribes the leg touch down angle primarily in a feedforward manner during stance. Similar analytical and numerical analysis as described above for leg angle control is also carried out for leg swing in Chapter 4. We later modify the swing protocol in order to better match the more "insect like" swing protocol as calculated from experimental data and carry out numerical simulations to show improved performance with this refined swing protocol. Similarity between leg touch down angles employed by the refined leg recirculation protocol and the leg touch down angle control law developed earlier in Chapter 3 is examined via perturbation simulations. Chapter 5 details the incorporation of leg actuation. The leg actuation protocol is discussed in detail followed by stability and robustness results obtained numerically for the actuated point mass model with fixed leg touch down control. Lastly in Chapter 5 we combine leg actuation with leg angle control to further improve stability and obtain complete asymptotic stability for the point mass model. Results of gait stability and robustness to external perturbation for this combined strategy is presented in Chapter 5. We draw conclusions and present avenues for future work in Chapter 6.

Chapter 2 – Lateral leg spring (LLS) model

Nomenclature

k	spring stiffness
m	body mass
I	body moment of inertia
l	force-free leg length
d	distance between center of mass and leg attachment point
η	spring leg length ($\eta(0) = l$)
ζ	distance between foot placement and center of mass
ψ	angle ζ makes with local horizontal axis
v	center of mass velocity
δ	velocity heading angle
θ	body rotation angle
$\dot{\theta}$	body angular velocity
β	leg angle with respect to body axes
t_{des}	desired swing phase duration
β_{des}	desired leg angle at $t = t_{des}$
	Terms used in Chapter 4:
$\dot{\beta}$	leg angular velocity with respect to body axes
ω	leg recirculation amplitude
a	leg recirculation frequency
ϕ	leg recirculation phase shift
$\dot{\beta}_{des}$	desired leg angular velocity at $t = t_{des}$

Hexapedal insects, such as the the cockroach *Blaberus discoidalis* illustrated in Fig. 2.1, run and climb in an alternating tripod gait with at least three legs in contact with the ground at any instant. The left tripod consists of the left front, left rear, and the right middle leg, while the right tripod is comprised of the contralateral legs. While cockroaches run in an alternating tripod gait, experiments have shown that the forces produced by these legs during each stance phase may be represented by a single effective force [17, 15, 54]. This result, in conjunction with the fact that the mass of all the legs of the insect constitute less than 6% of the total mass, suggests modeling each tripod of legs by a single, massless effective leg represented by a linear, elastic spring with force-free length l. In the offset pivot LLS formulation [31], the leg attachment point is laterally offset from the center of mass by a distance d. For $d > 0$, as illustrated for the left stance phase in Fig. 2.1 (b), the leg is attached to the right of the center of mass. In the corresponding right stance phase for $d > 0$, the leg attachment point is reflected about the center of mass. Attaching the leg laterally offset from the center of mass results in the effective leg force moving fore to aft across the body centerline during stance, thereby yielding qualitatively correct moment and yawing profiles. As illustrated in panel (b) of Fig. 2.1, the resulting LLS model is comprised of a rigid body of mass m, moment of inertia I, and a pair of massless legs, each represented by an elastic spring. The rigid body represents the head, thorax and abdomen of the insect, and each effective leg represents the collective effect of the tripod of legs in contact with the ground during a stance phase. Each effective leg is modeled by a tangentially rigid, axially-elastic linear spring with force-free length l and spring stiffness k.

A full stride consists of a left and right stance phase. Each stance phase begins when

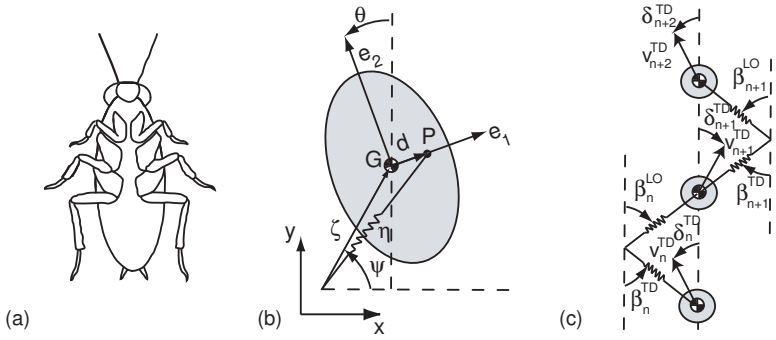

Figure 2.1: (a) Cockroach morphology (b) LLS rigid body model and (c) illustration of a single stride (left and right stance phases) for $d = 0$. Relevant quantities are as explained in the text: velocity magnitude (v), velocity direction defined from the vertical body axis (δ), leg angle (β), leg length (η), distance from the foot placement to the center of mass (ζ), and angle of that ζ makes with respect to the horizontal axis (ψ). Superscripts TD and LO denote lift-off and touch-down events, while subscripts indicate the particular stance phase. Leg touch-down and lift-off angles are measured from the body axes but are illustrated with respect to the inertial axes for clarity. Locomotion occurs in the positive y direction, from bottom to top in each panel.

one effective leg, extended at its force-free length l, touches the ground at an angle β_n^{TD} with respect to the body centerline. Superscripts of TD and LO denote values at touch-down and lift-off respectively, whereas subscripts identify the specific stance phase. The foot placement point remains fixed during the stance phase and is represented by a moment free pin joint. Under the influence of its own momentum, the body moves forward during the stance phase, compressing and extending the elastic leg. When the force in the leg returns to zero, the leg is lifted from an angle β_n^{LO} and the opposite stance leg is placed down at an angle β_{n+1}^{TD}. A duty factor of 0.5 is employed, such that the next effective leg touches down at the instant the previous leg is lifted. While simple feedback control is utilized for leg placement in this work, no energy is required to move the leg to the prescribed position since the leg has no mass. As a result, energy

is globally conserved, since no impacts or impulses occur.

The equations of motion for each stance phase are derived via Lagrange's equations in [31] and summarized here, implemented with a linear spring leg:

$$\ddot{\zeta} = \zeta\dot{\psi}^2 - \frac{k(\eta - l)\left[\zeta + d\cos(\theta - (-1)^n\psi)\right]}{m\eta} \tag{2.1}$$

$$\zeta\ddot{\psi} = -2\dot{\psi}\dot{\zeta} - \frac{(-1)^n k(\eta - l)d\sin(\theta - (-1)^n\psi)}{m\eta} \tag{2.2}$$

$$I\ddot{\theta} = \frac{k(\eta - l)d\zeta\sin(\theta - (-1)^n\psi)}{\eta} \tag{2.3}$$

As illustrated in second panel of Figure 2.1, η is the spring leg length, ζ is the distance between the foot placement point and the center of mass, d is the distance between the leg attachment point (P) and the center of mass (G), θ is the body rotation, and ψ denotes the angle ζ makes with the lateral inertial axis. Superscripts of n in the equations of motion denote the stance phase, with n even corresponding to left stance phases and n odd corresponding to right stance phases.

While the equations of motion (2.1-2.3) are essential for locomotion simulations of the model, insight into the stability properties of the resulting periodic gaits are more easily obtained with the state of the system defined at each leg touch-down and lift-off instant by $(v, \delta, \theta, \dot{\theta}, \beta)$. Here, v represents the center of mass velocity and δ represents the velocity heading angle with respect to the body centerline, as illustrated in the third panel of Fig. 2.1. A Poincaré map is defined, as in previous studies of stability of locomotion models [32, 28, 43, 18, 2, 9], to identify periodic orbits and characterize gait stability. In this work, the Poincaré section is defined as the instant of leg touch-down. Since no external torques or forces act on the system, both system energy and angu-

lar momentum about the foot placement point are conserved. Using these conserved quantities, in conjunction with the stance phase geometry illustrated in the third panel of Figure 2.1, yields the following Poincaré map for $d = 0$ and a fixed leg touch-down angle:

$$v_{n+1}^{TD} = v_n^{TD} \tag{2.4}$$

$$\delta_{n+1}^{TD} = \delta_n^{TD} + \beta_n^{LO} - \beta_n^{TD} + (-1)^n \omega\tau \tag{2.5}$$

$$\theta_{n+1}^{TD} = \theta_n^{TD} + \omega\tau \tag{2.6}$$

$$\beta_{n+1}^{TD} = \beta_{des}^{TD} \tag{2.7}$$

where $\omega = \dot{\theta}_n^{TD}$, $\beta_n^{LO} = \pi - \Delta\psi - \beta_n^{TD}$ and β_{des}^{TD} denotes a constant, desired leg touch-down angle for a periodic gait. For the point mass case ($d = 0$), a fixed point of the mapping, which represents a periodic orbit in the continuous system, requires $\omega = 0$ and $\beta_n^{TD} = \beta_n^{LO}$. Linearizing the mapping about a fixed point yields the Jacobian matrix, whose eigenvalues govern local stability of the orbit.

Chapter 3 – Improving horizontal plane locomotion via leg angle control

While utilizing a fixed leg touch-down angle protocol produces stable gaits for the planar LLS model [43, 42, 44, 31], improving the stability and disturbance rejection properties of the spatial spring loaded inverted pendulum (SLIP) model requires a protocol for systematically varying the leg touch-down angle in response to perturbations. Objectives guiding the development of a leg touch-down angle control for the LLS model include: enabling stabilization of previously unstable periodic gaits, producing improvements in periodic gait stability, improving gait robustness to external perturbations, and incorporating easily sensed variables and limited neural feedback. Pursuant to the last objective, the control formulation proposed in this work utilizes variables that are easily sensed by insect mechanoreceptors, such as the chordotonal organs that provide information regarding joint angles [55], rather than those that would prove more difficult, such as heading angle. Developing a control formulation based upon joint angles defined in the body frame also simplifies sensing and control in practical applications [2], increasing the relevance of this work for legged robotic applications. Given the limited neural feedback apparently utilized by the insect during stance, control is applied only at the start of each stance phase, through the leg touch-down angle, rather than continuously during stance. The construction and analysis of such a protocol for the LLS model can be viewed as a first step in the development of a similar protocol for the spatial LLS model.

The composition of the left and right stance phase locomotion dynamics result in a

hybrid system. As in previous analyses of the LLS model [43, 44, 31], it is anticipated that even controlled periodic gaits of the system will exhibit, at best, partial asymptotic stability. As long as the control formulation introduced does not destroy the symmetries (rotational invariance) and conserved quantities (energy) of the model, periodic gaits will retain one or more neutral eigendirections with a unity eigenvalue. Perturbations to partially asymptotically stable gaits in these neutral eigendirections will therefore result in convergence to a new gait rather than re-stabilization to the unperturbed gait. For example, for an energetically conservative system such as the LLS model, energetic perturbations that change the touch-down velocity of the center of mass will result in the attainment of a new periodic gait characteristic of a different energy level, since the LLS model contains no mechanism by which energy can be added or removed from the system. However, perturbations in the direction of the eigenvectors of stable eigenvalues will result in convergence to the unperturbed gait.

3.1 Leg touch-down angle control for $d = 0$

3.1.1 Control law formulation

The leg touch-down control law is developed by representing the Poincaré map (2.4-2.7), linearized about the fixed point, in a standard linear control formulation as

$$\bar{x}_{n+1}^{TD} = A\bar{x}_n^{TD} + Bu_n^{TD} \tag{3.1}$$

$$u_n^{TD} = \beta_n^{TD} - \beta_{des}^{TD} \tag{3.2}$$

where A is the Jacobian matrix, $\bar{x} = [(v - v_{des})\ (\delta - \delta_{des})]^T$, and B represents the effect of the control parameter (u_n) on the system dynamics. As in traditional state feedback control, the control is formulated based upon the deviation from a desired operating point

$$\beta_n^{TD} - \beta_{des}^{TD} = -\begin{bmatrix} j & k \end{bmatrix} \begin{bmatrix} v_n^{TD} - v_{des}^{TD} \\ \delta_n^{TD} - \delta_{des}^{TD} \end{bmatrix} \tag{3.3}$$

where $(v_{des}^{TD}, \delta_{des}^{TD}, \beta_{des}^{TD})$ represent the fixed point values of the linearization, or the initial conditions of a periodic orbit in the continuous system. Since no mechanism exists in this model formulation to add or remove energy during a stance phase, $v_n^{TD} = v_{des}^{TD}$, such that

$$\beta_n^{TD} - \beta_{des}^{TD} = -k\left(\delta_n^{TD} - \delta_{des}^{TD}\right)\ . \tag{3.4}$$

This intuitive control law is similar in nature to that utilized by Seipel and Holmes for stabilization of gaits in the spatial SLIP model [47]. As the heading angle deviates further from the desired value, the leg touches down at an increased angle from the body centerline to properly reorient the momentum. However, stabilization via this control law still requires sensing of the heading angle at the beginning of each stance phase, as well as explicit knowledge of the desired heading angle. To eliminate this explicit dependence on the heading angle, we first apply control to successive iterates of the mapping, yielding

$$\bar{x}_{n+1}^{TD} - \bar{x}_n^{TD} = A(\bar{x}_n^{TD} - \bar{x}_{n-1}^{TD}) + B(\beta_n^{TD} - \beta_{n-1}^{TD}) \tag{3.5}$$

$$\beta_n^{TD} - \beta_{n-1}^{TD} = -k(\delta_n^{TD} - \delta_{des}^{TD}) + k(\delta_{n-1}^{TD} - \delta_{des}^{TD}) = -k(\delta_n^{TD} - \delta_{n-1}^{TD})\ . \tag{3.6}$$

Subsequently, we employ the heading angle map (2.5) to remove the dependence of the control law on the heading angle such that

$$\beta_n^{TD} = \beta_{n-1}^{TD} - k(\beta_{n-1}^{LO} - \beta_{n-1}^{TD}) \, . \tag{3.7}$$

While this representation yields a control law in terms of leg touch-down and lift-off angles that are easily sensed by insect mechanoreceptors, it removes any dependence on the reference leg touch-down angle that identifies the desired periodic gait. Utilizing this control law for appropriate values of k results in gaits that are Lyapunov stable; perturbations in δ_n^{TD} or β_n^{TD} result in stabilization to a nearby periodic gait rather than re-stabilization to the original periodic gait. To ensure convergence to the original gait in response to external perturbations, we reintroduce the dependence on a desired leg touch-down angle and generalize the control law as

$$\beta_{n+1}^{TD} = c_1\beta_n^{TD} + c_2\beta_n^{LO} + c_3\beta_{des}^{TD} \tag{3.8}$$

where c_1, c_2 and c_3 are constants.

While periodic gaits exist such that $\beta_{n+2}^{TD} = \beta_n^{TD} = \beta_{des}^{TD}$ with $\beta_{n+1}^{TD} \neq \beta_n^{TD} \neq \beta_n^{LO}$, we seek to stabilize only reflection symmetric periodic gaits in this generalized control formulation. For reflection symmetric periodic gaits, the right stance phase is a mirror image of the left, which requires $\beta_{n+1}^{TD} = \beta_n^{TD} = \beta_n^{LO} = \beta_{des}^{TD}$. To ensure that the generalized control formulation proposed in (3.8) admits reflection symmetric periodic gaits,

we substitute this symmetry relationship into the control law to obtain the constraint

$$c_1 + c_2 + c_3 = 1 \ . \tag{3.9}$$

As a result, only two of the three constants are free parameters, with the third derived from the above relationship.

3.1.2 Periodic gait stability with control

Both analytical and numerical analyses are performed to determine the effectiveness of the proposed control law in terms of gait stability and robustness to external perturbations. The analytical periodic gait eigenvalue approximations developed in this section serve to validate our numerical computations. Numerical model simulations are performed using the Runge-Kutta integrator *ode45* in Matlab, with leg lift-off events determined numerically to a precision of 10^{-11} using the events functionality of *ode45*. Periodic orbits of the continuous system are identified by examining the difference between the initial states $(v_n^{TD}, \delta_n^{TD}, \beta_n^{TD})$ and those at the next leg touchdown $(v_{n+1}^{TD}, \delta_{n+1}^{TD}, \beta_{n+1}^{TD})$. Utilizing this difference in a Newton-Raphson iteration, implemented in *fsolve* in Matlab, results in the periodic gaits presented in this paper.

As in previous analyses [32, 28, 18, 43, 42], gait stability is governed by the eigenvalues of the Poincaré map linearized about the fixed point. Numerically, central difference approximations are utilized to generate the Jacobian matrix. Eigenvalues of the resulting matrix determine gait stability, with unstable gaits having at least one eigen-

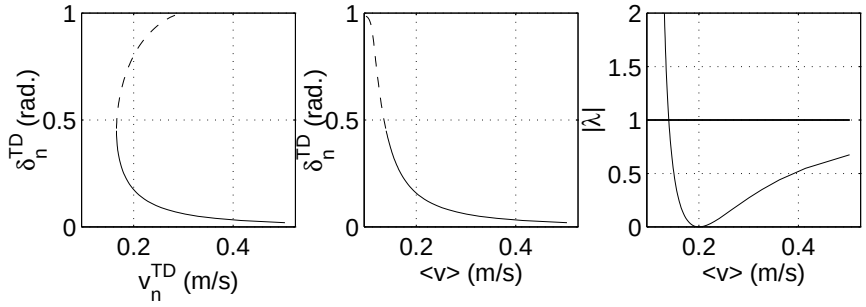

Figure 3.1: Family of periodic gaits (v, δ) for $d = 0$ and $\beta_{des}^{TD} = 1$ as a function of (a) the touch-down velocity, v_n^{TD} and (b) the mean forward speed throughout the stride $< v >$. Stable and unstable periodic gaits of the gait family are denoted by solid and dashed lines, respectively (c) Eigenvalue magnitudes of each periodic gait, with the gait identified by the mean forward speed. All other model parameters are held constant at values characteristic of *Blaberus discoidalis*, as described in the text.

value greater than unity in magnitude. Stable gaits have all eigenvalue magnitudes less than or equal to unity, with unity eigenvalues identifying directions of neutral stability. As explained previously, due to conserved quantities, stable gaits are therefore only partially asymptotically stable and cannot recover to the original fixed point if perturbed in the direction of a neutrally stable eigenvector.

Analytical and numerical investigations are performed with model parameters set to values similar to those utilized in previous locomotion studies of the cockroach *Blaberus discoidalis* [54, 25, 26, 42, 41]: spring stiffness (k) of 2.25 N/m, mass (m) of 0.0025 kg, force-free leg length (l) of 0.01 m, moment of inertia (I) of 2.06×10^{-7} kg m^2, and a desired leg touch-down angle (β_{des}^{TD}) of 1.0 radians. Model parameters are chosen to accurately reproduce insect force and velocity profiles, as well as stride length and frequency [54] at the desired running speed of the insect, 0.25 m/s.

For the standard parameter set, a one parameter family of periodic gaits exists, pa-

rameterized by the touch-down velocity v_n^{TD}. For each touch-down velocity, numerical computation of the fixed point of the Poincaré map and the associated eigenvalues of the Jacobian lead to the plots of Fig. 3.1. While periodic gaits exist over the whole speed range utilized by *Blaberus discoidalis*, not all gaits are stable for the nominal leg touch-down protocol used, $\beta_{n+1}^{TD} = \beta_n^{TD}$. As illustrated in panel (c) of Fig. 3.1 for $(c_1, c_2, c_3) = (1, 0, 0)$, the only non-unity eigenvalue for these gaits corresponds to the heading angle (δ). As a result, periodic gaits for the leg touch-down policy of $\beta_{n+1}^{TD} = \beta_n^{TD}$ cannot recover from perturbations in β_n^{TD} or v_n^{TD}, due to the unity eigenvalues corresponding to these states. As illustrated in panel (a), the family of periodic gaits is divided into upper and lower branches that differ in terms of gait stability. As the touch-down velocity decreases along the lower branch, the heading angle increases to overcome the potential energy of the spring and move the body forward past the foot placement point. For a given touch-down angle, the gaits of the lower branch ultimately destabilize via a saddle node bifurcation at a critical touch-down velocity, below which no periodic gaits exist. To achieve periodic gaits with average forward velocities below that of the bifurcation point requires larger touch-down velocities and heading angles. The upper branch of the gait family is comprised of these unstable gaits, which have larger lateral oscillations that cannot be stabilized by a fixed leg touch-down angle protocol. However, incorporating the leg touch-down protocol based on previous leg angles will enable modification of gait stability. Since periodic gait symmetry requires $\beta_n^{TD} = \beta_n^{LO} = \beta_{des}^{TD}$, changes in the parameters c_i will only change the stability of each gait, since each periodic gait remains periodic for any choices of c_i that satisfy the gait symmetry constraint (3.9).

We validate our numerical eigenvalue results by computing the eigenvalues analytically from the linearized Poincaré map. Since knowledge of the leg touch-down angle is required to fully define the state of the system, we augment our system state with the leg touch-down control law, such that the linearization of the Poincaré map about the fixed point for a single stance phase yields

$$Df = \begin{bmatrix} 1 & 0 & 0 \\ \cdots & 1 - \frac{\partial \Delta\psi}{\partial \delta_n^{TD}} & -\left(2 + \frac{\partial \Delta\psi}{\partial \beta_n^{TD}}\right) \\ \cdots & -c_2 \frac{\partial \Delta\psi}{\partial \delta_n^{TD}} & (c_1 - c_2) - c_2 \frac{\partial \Delta\psi}{\partial \beta_n^{TD}} \end{bmatrix}. \tag{3.10}$$

In the above, $\cdots$ represent values that do not enter into the eigenvalue computation and $\Delta\psi$ represents the leg angle swept during stance. The mapping above represents the mapping for a single stance phase; the full-stride map consists of a composition of the stance phase maps for a left and a right stance phase. Since only symmetric periodic gaits are investigated in this work, the stance phase maps for left and right stance phases are equivalent. As a result, while analytical expressions for the single stance phase map are computed below, eigenvalues for the full-stride mapping are simply the square of the eigenvalues for the single stance phase map. We determine the characteristic equation governing the eigenvalues, as detailed in Appendix A, as

$$\begin{aligned} z(\lambda) = (\lambda - 1) \Bigg[\lambda^2 + \left(-c_1 + c_2 + c_2 \frac{\partial \Delta\psi}{\partial \beta_n^{TD}} - 1 + \frac{\partial \Delta\psi}{\partial \delta_n^{TD}} \right) \lambda + \\ c_1 \left(1 - \frac{\partial \Delta\psi}{\partial \delta_n^{TD}} \right) - c_2 \left(1 + \frac{\partial \Delta\psi}{\partial \delta_n^{TD}} + \frac{\partial \Delta\psi}{\partial \beta_n^{TD}} \right) \Bigg] = 0 \end{aligned} \tag{3.11}$$

One eigenvalue of (3.11) is unity, corresponding to energy conservation, while the other

two emerge from the inner quadratic equation. The inner quadratic equation explicitly depends upon the leg angle swept during stance, $\Delta\psi$, an expression for which is constructed from the conservation of angular momentum and energy during the stance phase in [43], as summarized in Appendix A.

The characteristic equation (3.11) can be simplified further since, as detailed in Appendix A, $\frac{\partial\Delta\psi}{\partial\beta_n^{TD}} = -\frac{\partial\Delta\psi}{\partial\delta_n^{TD}}$, yielding the following expression for the two potentially non-unity eigenvalues

$$\lambda^2 + \left[-c_1 + c_2 + (1-c_2)\frac{\partial\Delta\psi}{\partial\delta_n^{TD}} - 1\right]\lambda + c_1\left(1 - \frac{\partial\Delta\psi}{\partial\delta_n^{TD}}\right) - c_2 = 0 \qquad (3.12)$$

This characteristic equation governs periodic gait stability for the LLS model with any leg representation; spring laws other than the linear one considered here simply result in a different definition of $\Delta\psi$. While straightforward, computing the derivative $\frac{\partial\Delta\psi}{\partial\delta_n^{TD}}$ required for the analytical eigenvalue computation is lengthy and left to Appendix A.

With the approximation for $\frac{\partial\Delta\psi}{\partial\delta_n^{TD}}$ developed in Appendix A, the analytical eigenvalue approximation is evaluated and compared to numerical results in Fig. 3.2. As illustrated, the analytically computed eigenvalues compare well with those computed numerically over almost the entire speed range, despite the approximation utilized in computing $\frac{\partial\Delta\psi}{\partial\delta_n^{TD}}$.

In contrast to the nominal leg touch-down protocol $\beta_{n+1}^{TD} = \beta_n^{TD}$, changes in the values for (c_1, c_2, c_3) result in a second eigenvalue, corresponding to the leg touch-down angle, moving within the unit circle. Periodic gaits under this leg touch-down protocol, for appropriate choices of (c_1, c_2, c_3), are therefore able to recover from perturbations to

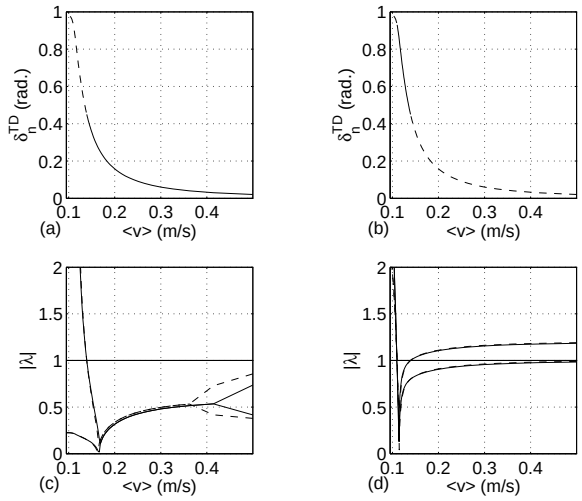

Figure 3.2: Comparison between numerical and analytical eigenvalue computations along a gait family for $d = 0$ and $\beta_{des}^{TD} = 1$. (a) Stable (solid) and unstable (dashed) periodic gaits for a gait family for $(c_1, c_2, c_3) = (-0.25, -0.1, 1.35)$ (b) Stable (solid) and unstable (dashed) periodic gaits for a gait family for $(c_1, c_2, c_3) = (0.2, 1.0, -0.2)$ (c) Eigenvalues of the periodic gaits of the gait family for $(c_1, c_2, c_3) = (-0.25, -0.1, 1.35)$ (d) Eigenvalues of the periodic gaits of the gait family for $(c_1, c_2, c_3) = (0.2, 1.0, -0.2)$. Numerical and analytical computations of the eigenvalues in panels (c) and (d) are represented by solid and dotted lines, respectively. All other model parameters are held constant at values characteristic of *Blaberus discoidalis*, as described in the text.

the leg touch-down angle. As well, the panels of Fig. 3.2 illustrate that gait stability can be dramatically affected through the choice of (c_1, c_2, c_3). Specifically, as illustrated in panels (b) and (d), appropriate choice of the c_i values can result in stabilization of gaits at the lower end of the speed range, which were previously unstable. However, choices of c_i that result in stabilization of the lower half of the speed range destabilize gaits at higher speeds. This result is expected, since while two fixed points exist for a given $(v_n^{TD}, \beta_{des}^{TD})$ combination, as illustrated in the first panel of Fig. 3.1, only one can be stable for a given choice of c_i.

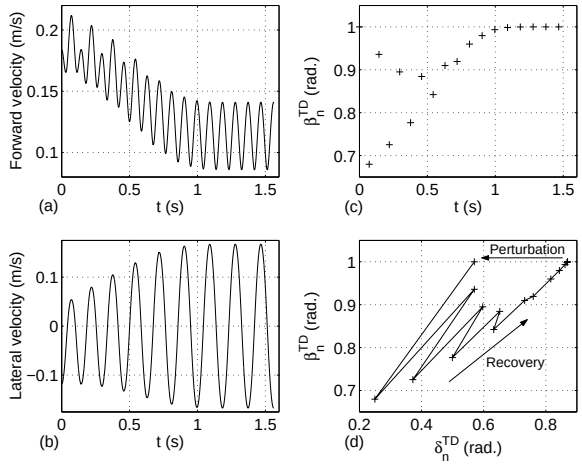

Figure 3.3: Recovery of a periodic gait, $(v_{des}^{TD}, \delta_{des}^{TD}, \beta_{des}^{TD}) = (0.2186, 0.87, 1)$ from an external perturbation in the heading angle, $\delta_{pert} = -0.3$ rad., for $(c_1, c_2, c_3) = (0.2, 1.0, -0.2)$, $d = 0$. (a) Forward velocity (b) Lateral velocity (c) Leg touch-down angle (β_n^{TD}) at the beginning of each stance phase (d) Leg touch-down and heading angle at the beginning of each stance phase. All other model parameters are held constant at values characteristic of *Blaberus discoidalis*, as described in the text.

An example of the performance of the control protocol in stabilizing a previously unstable periodic gait is illustrated in Fig. 3.3. The panels of Fig. 3.3 illustrate recovery of a periodic gait $(v_n^{TD}, \delta_n^{TD}, \beta_n^{TD}) = (0.2186, 0.87, 1.0)$ from a significant external perturbation in the heading angle, $\delta_{pert} = -0.3$ radians. While this periodic gait is strongly unstable for the previously studied leg touch-down protocol of $\beta_{n+1}^{TD} = \beta_n^{TD}$, with a heading angle eigenvalue of 26.4, utilizing the leg touch-down protocol (3.8) with $(c_1, c_2, c_3) = (0.2, 1.0, -0.2)$ produces gait stabilization with a maximum non-unity eigenvalue magnitude of 0.031. While the magnitude of the perturbation moves the orbit outside of the range of applicability of the linearized Poincaré map, for which the leg touch-down angle control was designed, the leg touch-down protocol is still able to recover the original periodic gait within approximately 14 stance phases. Stabilization

in this instance, and in other simulations, is achieved through relatively small (< 0.3 radians) deviations from the desired leg touch-down angle. Such magnitudes are consistent with the natural variation in foot placement exhibited by individual legs during both steady state locomotion [27] as well as during recovery from rapid impulse perturbations [23]. While the recovery rate exhibited in this instance is slower than that predicted by the linearized mapping eigenvalues, smaller perturbations, for which the linearized mapping has more relevance, demonstrate recovery rates closer to those predicted by the eigenvalues of the linearized Poincaré map. The stabilization illustrated in Fig. 3.3 is not unique to this instance, perturbations to other previously unstable periodic gaits also result in re-stabilization for appropriate choices of c_i, as will be examined further in section 3.1.4.

3.1.3 Gait stability for variations in c_i

While choices for c_i have a significant effect on periodic gait stability, insight into appropriate bounds for these parameters is difficult to obtain from the characteristic equation in the form given by (3.12). To determine bounds on c_i that ensure stability, we transform (3.12) via a bilinear transformation to obtain the characteristic equation

$$\begin{aligned} z(s) &= z(\lambda = \frac{1+s}{1-s})(1-s)^2 \\ &= (2-\frac{\partial \Delta\psi}{\partial \delta})(1+c_1-c_2)s^2 + 2(1-c_1(1-\frac{\partial \Delta\psi}{\partial \delta})+c_2)s + \\ &\quad \frac{\partial \Delta\psi}{\partial \delta}(1-c_1-c_2)\ . \end{aligned} \tag{3.13}$$

The characteristic equation in this form provides necessary and sufficient conditions for all eigenvalues of the mapping to remain within the unit circle. Specifically, for a second order characteristic equation, the Routh-Hurwitz criterion requires that all coefficients of the orders of s present in the characteristic equation be greater than zero for all eigenvalues to have magnitude less than unity. Since $\frac{\partial \Delta\psi}{\partial \delta} < 2$ [43], the following three conditions must be satisfied to obtain stable gaits

$$1 + c_1 - c_2 > 0 \tag{3.14}$$

$$1 - c_1 + \frac{\partial \Delta\psi}{\partial \delta} c_1 + c_2 > 0 \tag{3.15}$$

$$\frac{\partial \Delta\psi}{\partial \delta}(1 - c_1 - c_2) > 0 \tag{3.16}$$

Values for c_1, c_2 and $\frac{\partial \Delta\psi}{\partial \delta}$ that yield an equality in any of the above conditions result in a stability boundary, since at least one eigenvalue will have unity magnitude. While the first and third conditions produce stability boundaries in the (c_1, c_2) plane independent of $\frac{\partial \Delta\psi}{\partial \delta}$, the second condition produces a stability boundary whose slope is $1 - \frac{\partial \Delta\psi}{\partial \delta}$. Examining these conditions reveals that regions of stability or stability boundaries in the (c_1, c_2) plane are qualitatively different for $1 < \frac{\partial \Delta\psi}{\partial \delta} < 2$, $0 < \frac{\partial \Delta\psi}{\partial \delta} < 1$, and $\frac{\partial \Delta\psi}{\partial \delta} < 0$. Determining appropriate bounds on c_i to ensure for stability of a particular periodic gait requires identifying the association between $\frac{\partial \Delta\psi}{\partial \delta}$ and branches of periodic gaits of the gait family, to which we now turn.

Since each gait family, such as that illustrated in Fig. 3.1, is defined for a constant leg touch-down angle, the choice of c_i does not influence the value of $\frac{\partial \Delta\psi}{\partial \delta}$ for any of the periodic gaits comprising the gait family. However, the association between $\frac{\partial \Delta\psi}{\partial \delta}$ and

branches of the gait family is best illustrated for the nominal leg touch-down protocol of $(c_1, c_2, c_3) = (1, 0, 0)$, for which the characteristic equation (3.12) simplifies to

$$(\lambda - 1)\left(\lambda - \left(1 - \frac{\partial \Delta\psi}{\partial \delta}\right)\right) = 0\,. \tag{3.17}$$

It is clear from (3.17) and the gait family illustrations of Fig. 3.1 that $\frac{\partial \Delta\psi}{\partial \delta} = 0$ at the saddle node bifurcation point, which corresponds to the point separating the lower and upper branches of the gait family in the first panel of Fig. 3.1. For the lower branch of the gait family, $\frac{\partial \Delta\psi}{\partial \delta} > 0$, and for the upper branch $\frac{\partial \Delta\psi}{\partial \delta} < 0$. As a result, the sign of $\frac{\partial \Delta\psi}{\partial \delta}$ identifies which branch of the gait family the periodic gait belongs to, which is essential in identifying values of c_i that stabilize gaits of either the lower or upper branches via (3.14-3.16).

Contour plots of the maximum non-unity eigenvalue magnitude variation for representative periodic orbits as a function of (c_1, c_2) are presented in Fig. 3.4. Panels (a)-(c) illustrate eigenvalue magnitudes as computed from the analytical approximation for periodic orbits with $1 < \frac{\partial \Delta\psi}{\partial \delta} < 2$, $0 < \frac{\partial \Delta\psi}{\partial \delta} < 1$, and $\frac{\partial \Delta\psi}{\partial \delta} < 0$, respectively. Panels (d)-(f) present numerically computed eigenvalue magnitudes for comparison purposes. In all plots, the dotted lines indicate the stability boundaries of conditions (3.14-3.16). Since $\frac{\partial \Delta\psi}{\partial \delta}$ differs for each periodic orbit of a gait family, these plots are only representative of the stability regions for the range of $\frac{\partial \Delta\psi}{\partial \delta}$ considered; the slope of the bottom stability boundary as well as the specific eigenvalue variation within the stability boundaries is specific to a particular fixed point.

The panels of Fig. 3.4 when viewed from left to right correspond to moving along

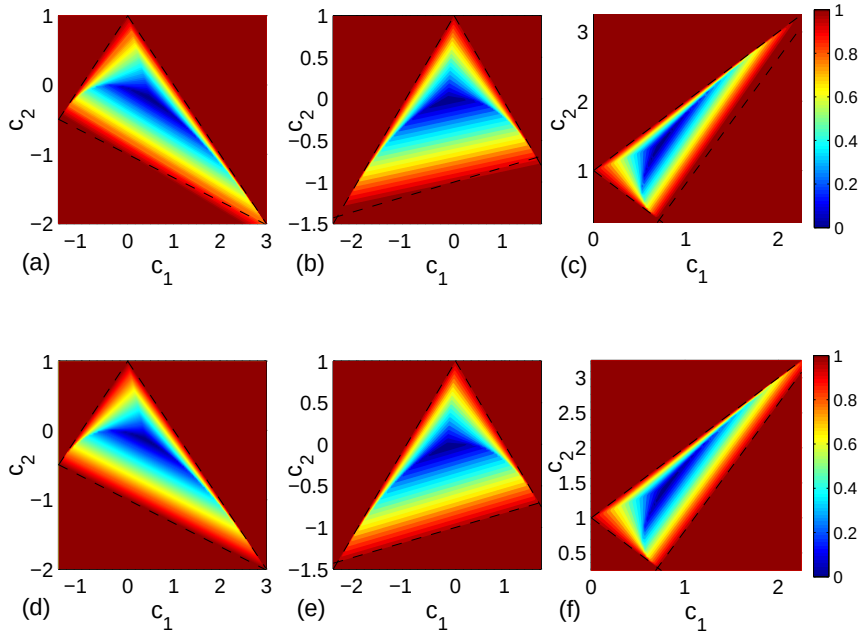

Figure 3.4: Contour plots of the maximum non-unity eigenvalue for representative periodic orbits, with $d = 0$, as a function of (c_1, c_2). Panels (a)-(c) illustrate the analytical approximation of the maximum non-unity eigenvalue, while panels (d)-(f) represent the numerical eigenvalue calculation for the periodic orbits of (a)-(c), respectively. (a) $(v_{des}^{TD}, \delta_{des}^{TD}, \beta_{des}^{TD}) = (0.256, 0.09, 1.0)$, $\frac{\partial \Delta\psi}{\partial \delta_n^{TD}} = 1.34$ (b) $(v_{des}^{TD}, \delta_{des}^{TD}, \beta_{des}^{TD}) = (0.192, 0.2, 1.0)$, $\frac{\partial \Delta\psi}{\partial \delta_n^{TD}} = 0.83$ (c) $(v_{des}^{TD}, \delta_{des}^{TD}, \beta_{des}^{TD}) = (0.175, 0.64, 1.0)$, $\frac{\partial \Delta\psi}{\partial \delta_n^{TD}} = -0.81$. Dashed lines in each plot represent the stability boundaries determined by equations (3.14-3.16). All other model parameters are held constant at values characteristic of *Blaberus discoidalis*, as described in the text.

the gait family of Fig. 3.1 from higher to lower average velocity. Examining panels (a) and (b) of Fig. 3.4 with this knowledge reveals that a large range of values of c_i stabilize the periodic gaits of the lower branch, although the lower bound of stabilizing c_2 values varies as determined by $c_2 = c_1(1 - \frac{\partial \Delta\psi}{\partial \delta}) - 1$. Considering the limiting cases of $\frac{\partial \Delta\psi}{\partial \delta} = 0$ and $\frac{\partial \Delta\psi}{\partial \delta} = 2$, we can conclude that values of (c_1, c_2) within the diamond defined by the lines $c_2 = c_1 + 1$, $c_2 = -c_1 + 1$, $c_2 = c_1 - 1$ and $c_2 = -c_1 - 1$ will ensure

stability for *all* gaits of the lower branch of the gait family. Examination of panel (c) reveals that the previously unstable periodic gaits of the upper branch can be stabilized through choice of c_i within the stability boundaries. Unfortunately, a region of c_i that guarantees stability for gaits of the upper branch cannot be constructed, since decreases in $\frac{\partial \Delta\psi}{\partial \delta}$ result in continual increases in the slope of the bottom stability boundary, thereby reducing the range of c_i values that yield stable gaits. While a wide range of c_i will therefore stabilize gaits of the upper branch near the saddle node bifurcation (where $\frac{\partial \Delta\psi}{\partial \delta}$ is small), the range of stabilizing c_i values decreases as one considers gaits further away from the saddle node bifurcation. In all instances, comparison of the analytical results of panels (a)-(c) with the numerical computations of (d)-(f) confirm that the analytical eigenvalue approximation remains relatively accurate over a wide range of c_i.

Additionally, these figures illustrate that gait stability can be improved from that of the nominal leg touch-down protocol of $\beta_{n+1}^{TD} = \beta_n^{TD}$ or $\beta_{n+1}^{TD} = \beta_{des}^{TD}$ through appropriate choice of c_i. For any periodic gait, values of c_i resulting in maximum stability (i.e. two zero eigenvalues) can be determined from (3.12) by setting the coefficients of the lower orders of λ to zero, yielding

$$c_1 = \frac{1 - \frac{\partial \Delta\psi}{\partial \delta}}{\frac{\partial \Delta\psi}{\partial \delta}\left(\frac{\partial \Delta\psi}{\partial \delta} - 2\right)} \tag{3.18}$$

$$c_2 = c_1 - \frac{1 - \frac{\partial \Delta\psi}{\partial \delta}}{\frac{\partial \Delta\psi}{\partial \delta} - 2} \tag{3.19}$$

$$c_3 = \frac{1}{\frac{\partial \Delta\psi}{\partial \delta}} \, . \tag{3.20}$$

While these relationships provide a means of calculating values of c_i that result in maxi-

mum stability for a particular periodic gait, they require knowledge of $\frac{\partial \Delta \psi}{\partial \delta}$ and therefore the full state of the system, thereby limiting their practical utility.

Determining additional information about the qualitative behavior of gaits as a function of c_i requires analysis of the possible bifurcations that may occur as c_i values cross stability boundaries. To determine the types of possible bifurcations that may occur, we substitute equalities for (3.14-3.16) into the original single stance phase characteristic equation and examine the square of the resulting eigenvalues. For the boundaries defined by $c_1 + c_2 = 1$ and $c_1 - c_2 = -1$, a single eigenvalue passes through 1, indicating a saddle node bifurcation. For the bottom boundary defined by $1 - c_1 + \frac{\partial \Delta \psi}{\partial \delta} c_1 + c_2 = 0$, a pair of complex conjugate eigenvalues pass through the unit circle, indicating a Hopf bifurcation. Simulations for c_i just outside of this stability boundary did not reveal any stable quasi-periodic gaits. Rather, while oscillations in stride variables appear quasi-periodic, they grow in magnitude with time.

3.1.4 Periodic gait recovery from perturbations

While eigenvalues of the linearized Poincaré map provide gait stability information, they do not indicate the range of perturbations for which the system will recover the original periodic gait. To determine the robustness of the control law to external perturbations, we subject each periodic gait of the gait family to a range of perturbations in the heading angle, δ_n^{TD}. For a gait family defined for a particular β_n^{TD}, limiting values of δ_n^{TD} occur at $\delta_n^{TD} = \beta_n^{TD}$ (mass directly compresses the spring) and $\delta_n^{TD} = \beta_n^{TD} - \pi/2$ (glancing contact). For each fixed point of the gait family, the starting value of δ_n^{TD} is varied

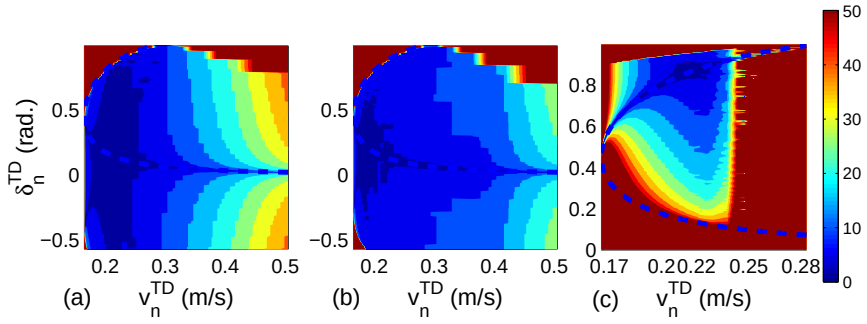

Figure 3.5: Contour plots of the number of stance phases required for recovery from external perturbations in δ_n^{TD} for $d = 0$ and $\beta_{des}^{TD} = 1$. Panels (a) and (b) illustrate the basin of stability for periodic gaits of the lower branch for (a) the nominal leg touch-down protocol $(c_1, c_2, c_3) = (1, 0, 0)$ and (b) the applied leg touch-down control law with $(c_1, c_2, c_3) = (-0.25, -0.1, 1.35)$. Panel (c) illustrates the basin of stability for periodic gaits of the upper branch for the leg touch-down control law with $(c_1, c_2, c_3) = (0.2, 1.0, -0.2)$. In each plot, the original periodic gait family is indicated with a dotted line. All other model parameters are held constant at values characteristic of *Blaberus discoidalis*, as described in the text.

between these limits and simulations are run for 100 stance phases. The number of stance phases required for the system to recover the original periodic gait (if applicable) is subsequently recorded. For the purposes of this work, recovery is defined as all stride variables returning and remaining within 1% of the original periodic gait. Simulations are conducted with a fixed set of c_i values representative of values that stabilize either the lower or upper branches of the gait family.

The panels of Fig. 3.5 illustrate the basin of stability for the nominal leg touch-down protocol $(c_1, c_2, c_3) = (1, 0, 0)$ as well as the control law with $(c_1, c_2, c_3) = (-0.25, -0.1, 1.35)$ and $(c_1, c_2, c_3) = (0.2, 1.0, -0.2)$. Perturbations in the heading angle considered in these simulations typically move the system out of the range for which the linearized Poincaré map has relevance, and for which the control law was designed. The basin of stability

for periodic gaits comprising the lower branch of the gait family is illustrated in the first two panels of Fig. 3.5 for both the nominal leg touch-down protocol and the leg touch-down control law, respectively. The results of these panels reveal that the control law is not only able to reproduce the large basin of stability evidenced by the fixed angle leg touch-down protocol, but is also able to improve the recovery rate for a large number of the gaits of the gait family. This improved recovery rate for higher speeds comes at a cost of a slightly reduced recovery rate for gaits at the lower end of the speed range. The third panel of Fig. 3.5 illustrates that not only is the control law capable of stabilizing the previously unstable periodic gaits of the upper branch of the gait family, but that the resulting stabilized gaits have a relatively large basin of stability.

3.2 Control effectiveness for $d \neq 0$

While attaching the effective leg laterally offset from the center of mass produces yawing motions that qualitatively resemble those of the insect [25, 41], it also couples the translational and rotational dynamics. This dynamic coupling creates difficulties in developing analytic solutions describing gait stability in a manner similar to the $d = 0$ case. As a result, numerical simulations are utilized to analyze the effectiveness of the leg touch-down control law for the $d \neq 0$ case.

As in the $d = 0$ case, a one parameter family of periodic gaits exists for each leg touch-down angle, parameterized by the touch-down velocity, v_n^{TD}. As illustrated in Fig. 3.6 for $\beta_n^{TD} = 1$, periodic gaits are significantly less stable as a result of the coupling of the translational and rotational dynamics, with the eigenvalue corresponding to

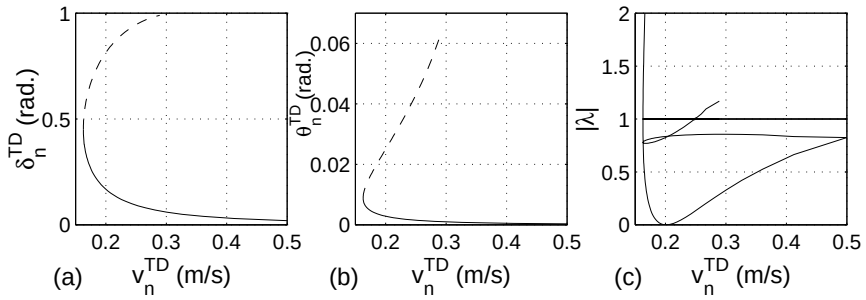

Figure 3.6: (a-b) Periodic gait family $(v, \delta, \theta, \dot{\theta})$ for $d = 0.002$ and $\beta_{des}^{TD} = 1$ as a function of the touch-down velocity, v_n^{TD}. Stable and unstable periodic gaits of the gait family are denoted by solid and dashed lines, respectively (c) Eigenvalue magnitudes of each periodic gait, with the gait identified by the touch-down velocity. All other model parameters were held constant at values characteristic of *Blaberus discoidalis*, as described in the text.

angular velocity remaining at a value near 0.8 for each gait of the lower branch. As a result, recovery rates evidenced for the $d \neq 0$ case are significantly slower than those of the $d = 0$ case. Additionally, since the system has a unity eigenvalue corresponding to body rotation, non-energetic gait perturbations result in stabilization back to the original gait in body coordinates, but not in inertial coordinates.

Dynamic coupling also significantly changes the Poincaré map of the system, upon which the original leg touch-down control law was based. While the original control law does not explicitly account for the presence of rotational dynamics in the heading angle map (and vice-versa), prescribing leg touch-down angle changes with respect to the body frame may still have utility for the $d \neq 0$ case. We therefore proceed with analyses similar to those utilized for the $d = 0$ case, first determining the effect of variations of (c_1, c_2) on gait stability. As illustrated in the panels of Fig. 3.7, gait stability can also be improved for $d \neq 0$ through the use of this control law. Each panel illustrates

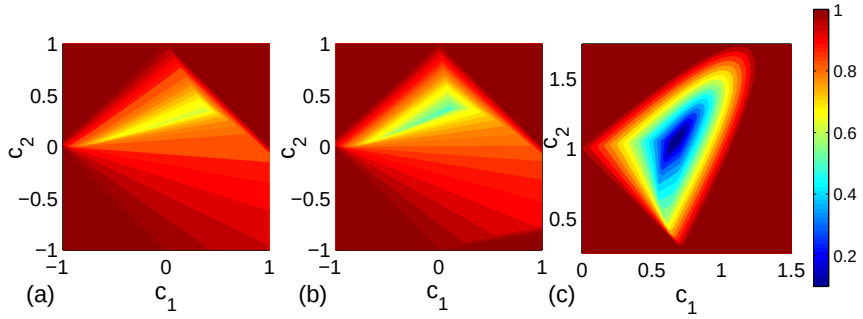

Figure 3.7: Contour plots of the maximum non-unity eigenvalue variation for representative periodic orbits with $d = 0.002$ as a function of (c_1, c_2). (a) $(v_{des}^{TD}, \delta_{des}^{TD}, \theta_{des}^{TD}, \dot{\theta}_{des}^{TD}, \beta_{des}^{TD}) = (0.253, 0.09, 0.0015, 0, 1.0)$, $\frac{\partial \Delta\psi}{\partial \delta_n^{TD}} = 1.57$ (b) $(v_{des}^{TD}, \delta_{des}^{TD}, \theta_{des}^{TD}, \dot{\theta}_{des}^{TD}, \beta_{des}^{TD}) = (0.189, 0.2, 0.0034, 0, 1.0)$, $\frac{\partial \Delta\psi}{\partial \delta_n^{TD}} = 0.96$ (c) $(v_{des}^{TD}, \delta_{des}^{TD}, \theta_{des}^{TD}, \dot{\theta}_{des}^{TD}, \beta_{des}^{TD}) = (0.172, 0.64, 0.015, 0, 1.0)$, $\frac{\partial \Delta\psi}{\partial \delta_n^{TD}} = -1.03$. All other model parameters are held constant at values characteristic of *Blaberus discoidalis*, as described in the text.

the performance of the control law for $d = 0.002$, for representative cases similar to those investigated for $d = 0$. While the maximum non-unity eigenvalue for the nominal leg touch-down protocol remains at about 0.8 for the entire lower branch, panels (a) and (b) illustrate that a maximum non-unity eigenvalue of magnitude $0.5 - 0.6$ can be attained by placing increased emphasis on the leg lift-off angle (i.e. increasing c_2) with c_1 slightly positive. Unlike the $d = 0$ case, maximal stability (two zero eigenvalues) cannot be attained through implementation of this control law. The third panel, however, illustrates that a maximum non-unity eigenvalue of approximately 0.1 can be attained to stabilize a gait of the upper branch of the gait family through appropriate selection of (c_1, c_2). It appears that the larger forces generated by gaits of the upper branch of the gait family provide more control authority than the forces generated for gaits of the lower branch, which aids in improving the stabilization of the rotational dynamics.

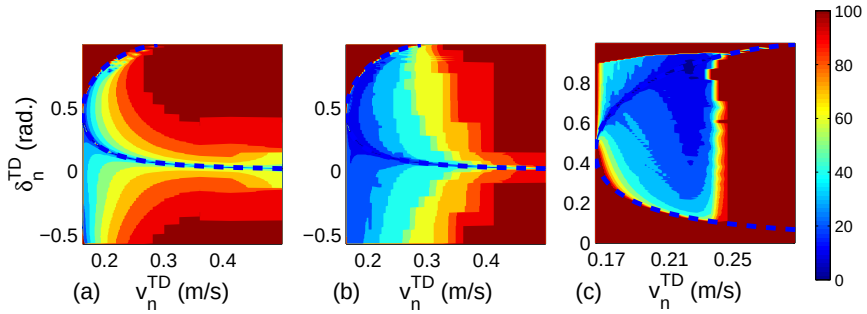

Figure 3.8: Contour plots of the number of stance phases required for recovery from external perturbations in δ_n^{TD} for $d = 0.002$ and $\beta_{des}^{TD} = 1$. Panels (a) and (b) illustrate the basin of stability for periodic gaits of the lower branch for (a) the nominal leg touch-down protocol $(c_1, c_2, c_3) = (1, 0, 0)$ and (b) the applied leg touch-down control law with $(c_1, c_2, c_3) = (-0.1, 0.3, 0.8)$. Panel (c) illustrates the basin of stability for periodic gaits of the upper branch for the leg touch-down control law with $(c_1, c_2, c_3) = (0.2, 1.0, -0.2)$. In each plot, the original gait family is indicated with a dotted line. All other model parameters are held constant at values characteristic of *Blaberus discoidalis*, as described in the text.

The recovery of periodic gaits from significant external perturbations in the heading angle δ_n^{TD} is illustrated in the panels of Fig. 3.8 for $d = 0.002$. Similar to the $d = 0$ case, implementing the leg angle control law enables recovery of the original periodic gaits for a wide range of perturbations, even though the control law was designed for the linearized, point mass system. Additionally, for periodic gaits of the lower branch of the gait family, implementing the control law significantly improves the recovery rate and enlarges the basin of stability. Periodic gaits for the upper branch of the gait family are not only stabilized through the control law, but actually exhibit a larger basin of stability than those of the $d = 0$ case. The recovery rate exhibited by these gaits is also better than that exhibited by gaits of the lower branch. This result lends further support to the argument that the larger forces exhibited for gaits of the upper branch provide more

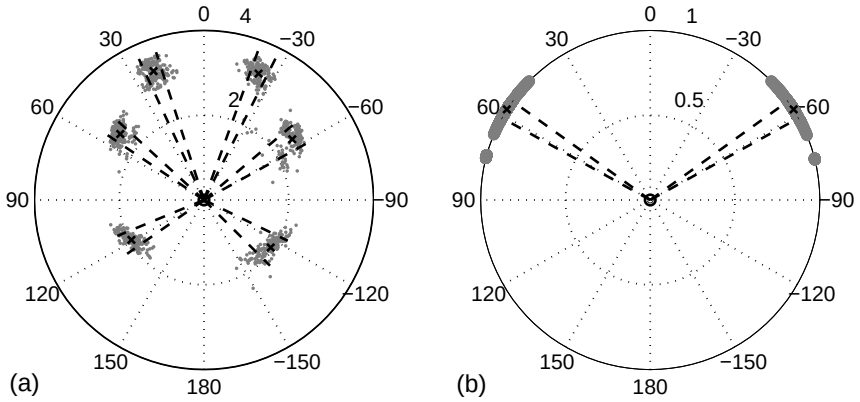

Figure 3.9: Body frame foot touch-down positions for (a) individual legs of the cockroach *Blaberus discoidalis*, obtained experimentally from six runs (S. Revzen, 2008, personal communication, Polypedal Lab, University of California at Berkeley) and (b) the controlled rigid body model recovering from perturbations in the heading angle. In each figure, dots indicate foot touch-down positions, an angle of zero degrees denotes the fore-aft body axis, circles indicate distance in cm, x values denote the mean foot touch-down position and dotted lines indicate the standard deviation in the leg touch-down angle. Model simulations utilized $d = 0.002$ and $(c_1, c_2, c_3) = (-0.1, 0.3, 0.8)$, with all other parameters characteristic of *Blaberus discoidalis*.

control authority over the rotational dynamics, leading to improved stabilization rates.

Variations in foot touch-down positions employed by cockroaches running over flat terrain are compared to those utilized in simulations in Fig. 3.9 and Table 3.1. Foot touch-down positions utilized by *Blaberus discoidalis* while running on a treadmill were extracted from experimental data collected and provided by S. Revzen (S. Revzen, 2008, personal communication, Polypedal Lab, University of California at Berkeley). In these experiments, video tracking was employed to capture both the center of mass motion and individual leg position relative to the center of mass throughout each run. The first panel of Fig. 3.9 illustrates the foot placement distributions of individual legs as determined from data sets of six different runs, with each run having an average fore-aft

velocity between $22-30$ cm/s. The second panel illustrates the foot placements utilized in simulations of the controlled rigid body model recovering from external perturbations in the heading angle. In these simulations, ten periodic gaits from the gait family for $d = 0.002$, with average fore-aft velocities between $20-30$ cm/s, were each subjected to external perturbations in the heading angle. The range of the perturbations imparted were identical to those investigated the perturbation recovery simulations of Fig. 3.8. Leg touch-down angles utilized during recovery from each of these perturbations were used to produce the second panel of Fig. 3.9.

Table 3.1: Leg touch-down angles from experimental runs and controlled simulations

	Left tripod			Right tripod			Model	
Foot	Front	Middle	Hind	Front	Middle	Hind	Left	Right
Min. angle (*deg.*)	12	-44	105	-14	42	-105	45.5	-45.5
Max. angle (*deg.*)	28	-76	137	-36	72	-155	76.2	-76.2
Mean angle (*deg.*)	21	-55	119	-23	52	-125	57.7	-57.7
Standard deviation (*deg.*)	3.4	5.6	6.2	3.5	4.3	9.5	3.3	3.4

As illustrated in the panels of Fig. 3.9 and summarized in Table 3.1, variations in leg touch-down angles employed by the controlled model in recovering from external perturbations are similar to those employed by individual legs of the insect running over flat terrain. While a wide range of touch-down angles is evidenced in both experiment and simulation, a majority of the leg touch-down angles utilized fall within a smaller range, as indicated by the standard deviation. The similarity in leg touch-down angle distribution between simulation and experiment does not indicate that such a control law is employed by running cockroaches, but rather that use of such a law remains plausible. Since small changes in leg touch-down angles are responsible for improvements in both

gait stability and robustness in reduced order model locomotion simulations, they may also prove beneficial for their insect counterparts.

3.3 Biological relevance

While the control strategy investigated in this work improves gait stability of a reduced order bipedal model of a hexapedal insect, insight into the possible biological relevance requires analyzing both the model assumptions and insect function. The reduced order model considered here is highly simplified; rather than modeling individual multi-jointed legs, the cumulative effect of three legs during a stance phase is represented by an elastic spring. Additionally, no leg recirculation strategy is employed to govern motion of the leg during the swing phase. Instead, the effective leg is positioned at the angle prescribed by the control law at the start of each stance phase. As a result, the leg touch-down protocol developed for the effective leg does not immediately translate to the touch-down angle of any single leg in the tripod, unless the legs are coordinated to reproduce the touch-down angle prescribed for the effective leg [33]. However, the improvements in gait stability and robustness evidenced by the simple leg angle adjustments investigated in this work invite the question of whether such a control law is employed in a decentralized fashion by individual legs during locomotion. Specifically, is the touch-down angle of a contralateral leg influenced by the initial leg touch-down angle and the leg angle swept by the corresponding leg of the opposite stance phase?

Prerequisites of any such law being employed by the insect include: the existence of mechanoreceptors that sense joint angles, a neural pathway through which the reflex

action acts, and sufficient time for signal transmission, processing and corresponding muscle action to occur. In the cockroach, the tonic signals emanating from hair plates, multipolar receptors and chordotonal organs effectively encode joint angles [57]. Since leg control in insects is handled locally, signals from these sense organs need only travel to the local thoracic ganglion to influence leg reflexes [7, 11]. Experiments in some insects suggest that information influencing leg coordination may be provided by interneurons that connect nearby ganglia [11, 6, 13]. Since these intersegmental reflexes appear weak, though, it seems more likely that the signals may instead affect contralateral leg coordination by modifying the amplitude and timing of leg movements as prescribed by the central pattern generator [29]. Such inter-leg reflexes have been exhibited in cockroaches, with stimulation of the tarso-pretarsal chordotonal organ producing a response in contralateral leg muscles [29]. It is unclear, however, if sufficient time exists for the communication and processing of these signals to affect the leg touch-down position of a contralateral leg in a means similar to that proposed in this work. Experiments suggest that the time required between sensing and muscle action ranges between $25 - 50$ ms, a significant portion of the duration of a stance phase of *Blaberus discoidalis* running at its preferred stride frequency of 10 Hz [24, 20]. Yet quicker neural pathways evidently do exist for some insect motions, as evidenced by the turning reflex exhibited in cockroaches in response to antennal sensing [8].

Ultimately, further experimental investigations are required to determine if inter-leg reflexes influence leg touch-down angles in high speed insect locomotion. These experiments will require accurate determination of individual leg joint angles, either through video tracking or appropriate leg angle sensors, such as those developed by [30]. While

correlations between the leg angles employed by the active and contralateral legs can be determined via external perturbation experiments, evidence of a reflex pathway responsible for the correlation will likely require neurobiological experiments. Specifically, an investigation in which the sense organs encoding joint angle are induced to produce erroneous signals may provide insight into this issue by revealing how the contralateral leg angles vary in response.

Chapter 4 – Leg recirculation in horizontal plane locomotion

4.1 Modeling leg recirculation

Models characterizing locomotion dynamics exist in forms of varying complexity. Full and Koditschek [16] have classified minimal models as templates and complex models that include more realistic representations of the physiology and morphology of the animal as anchors. Templates encapsulate the locomotion dynamics of the body using a minimum number of variables and serve as a target for control. Anchors, while more accurately reflecting animal structure and function, also embed the behavior of an associated template within it. In so doing, control effort applied to the anchor can result in the realization of the lower dimensional template dynamics.

In this study, leg recirculation protocols are developed and implemented in the LLS template to determine their impact on gait stability and robustness. Specifically, based upon results from previous experimental and analytical studies, this investigation examines the following three hypotheses:

H1 *Feedforward specification of the swing-leg angular velocity can produce stable periodic gaits*

H2 *Swing-leg angular velocity and acceleration at leg touch-down provide control authority to reorient system momentum in response to perturbations, thereby enabling selection of gait stability and robustness characteristics*

H3 *Gait stability and robustness is improved via leg retraction at leg touch-down*

By considering leg recirculation in the context of the LLS template, we intend to gain insight into the mechanics by which swing-leg recirculation impacts gait stability and robustness, which may be obfuscated in more anchored representations. More constitutive lateral plane models have been developed that include more anchored representations of leg function [27, 49], but neither of these multi-legged models incorporate swing-phase leg dynamics. We hope that the guiding principles identified in this study will help inform the design and implementation of swing-leg recirculation in such anchored representations.

Utilizing bio-inspiration from sprawled-posture insect locomotion, feedforward leg recirculation is developed for the LLS template to produce natural variations in the leg touch-down angle in response to perturbations away from a periodic orbit. The utilization of a primarily feedforward leg recirculation protocol, modulated by the leg angle and angular velocity values at the start of the swing phase and those desired at the end, is inspired primarily by the results of recent investigations into cockroach locomotion over rough terrain. For cockroaches running over rough terrain, a leg that misses the ground during a stance phase continues to retract, with muscle activation levels similar to those observed for legs in contact with the ground [52]. The subsequent delay in leg protraction after a missed step suggests that while leg recirculation is prescribed primarily in a feedforward manner, neural reflexes act on a stance-to-stance basis to modulate muscle activation levels [52].

The proposed feedforward control of the swing-leg angular velocity is also inspired by experimental studies showing that motor neuron activity is correlated with joint an-

gular velocities [56] and that leg velocity is controlled during swing [10], perhaps to follow a prescribed velocity and position [3]. Such control may result from the continual firing of motor neurons during the swing phase, as evidenced for stick insects and other smaller animals, which is evidently required to produce the required leg movement [21]. The results of cockroach locomotion over rough terrain [52] suggest that the resulting muscle activation may be prescribed in a feedforward manner, thereby yielding the swing leg motion observed without feedback control. Employing feedforward leg angular velocity control during swing also presumably requires relatively accurate sensing of leg joint angles and their rate of change at the beginning of the swing phase. Cockroaches possess a multitude of sense organs in their legs, of which several (hair plates, multipolar receptors and chordotonal organs) combine to effectively tonically encode joint angles and their rate of change [57, 29]. Signals from these sense organs may influence the amplitude and timing of leg movements as prescribed by the central pattern generator [29], and may thus play a role in modulating the swing phase dynamics at the initiation of the swing phase.

The broader concepts revealed by these experimental studies are employed in the model of leg recirculation developed in this study. In this formulation, accurate sensing of the leg angle and angular velocity at lift-off, in conjunction with a desired leg touchdown angle and angular velocity, is utilized at the instant of leg lift-off to prescribe the leg angular velocity for the entire swing phase. The functional form of this feedforward profile remains the same for all swing phases, but differences in the leg angle and angular velocity at lift-off produce in differences in swing frequency, magnitude and phase for individual swing phases. The model of leg recirculation developed in this study

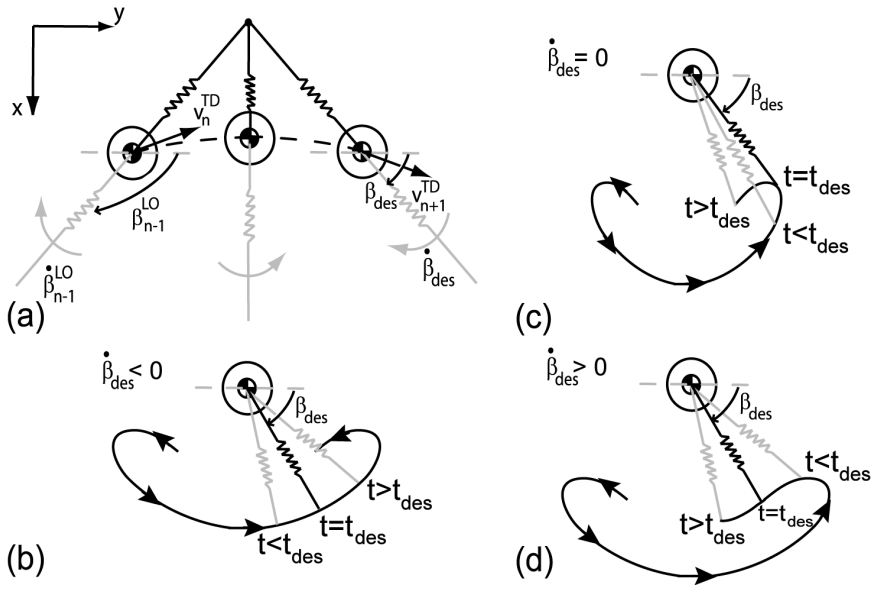

Figure 4.1: (a) Recirculation protocol illustrated for the right leg (grey) during the swing phase. Qualitative differences in the leg touch-down angle achieved for $t \neq t_{des}$ for (b) $\dot{\beta}_{des} < 0$, (c) $\dot{\beta}_{des} = 0$ and (d) $\dot{\beta}_{des} > 0$

therefore prescribes leg angular velocity in a feedforward manner, with feedback on a stance to stance basis producing small variations in the profile.

Development of an accurate leg recirculation model requires matching the leg angle and angular velocity at specific instants of the swing phase. As illustrated for the swing phase of the right leg in Fig. 4.1, the swing phase begins with the leg at an angle β_{n-1}^{LO} and an angular velocity of $\dot{\beta}_{n-1}^{LO}$. The leg must reverse its initial rearward angular velocity to swing forward, and our recirculation model requires that the leg attains a desired angle (β_{des}) with angular velocity ($\dot{\beta}_{des}$) at a specified time, t_{des}. With a duty factor of 0.5, the actual swing phase duration is determined by the stance phase duration of the opposite leg. As a result, the swing phase duration can differ from t_{des}, resulting in a leg touch-down angle and angular velocity different from those desired. For a symmetric

periodic orbit, both left and right stance phase durations will equal t_{des}, yielding a leg touch-down angle and angular velocity of β_{des} and $\dot{\beta}_{des}$, respectively.

In rapidly running cockroaches, the swing leg eventually reaches a minimum angle at which point it begins swinging rearward. A function that qualitatively matches the baseline characteristics of the leg swing profile with sufficient free parameters to match both the initial conditions and those at t_{des} is

$$\dot{\beta} = \omega \sin(at + \phi) \ , \tag{4.1}$$

where a, ϕ and ω represent the swing frequency, a phase shift, and the magnitude of the angular velocity, respectively. While leg recirculation in the insect occurs in three dimensions, this recirculation protocol can be viewed as a projection of the fully three-dimensional motion of the leg during swing onto the horizontal plane.

Utilizing this leg recirculation protocol in conjunction with the initial conditions and those at t_{des} produces three equations for the free parameters (ω, a, ϕ). Without loss of generality, each swing phase is assumed to commence with $t = 0$ in the equation governing leg recirculation. Matching the lift-off angular velocity of the leg yields an expression for the required phase shift

$$\phi = \sin^{-1}\left(\frac{\dot{\beta}_{n-1}^{LO}}{\omega}\right) \ . \tag{4.2}$$

Matching the angular velocity at $t = t_{des}$ yields

$$\dot{\beta}_{des} \quad = \quad \omega \sin(at_{des} + \phi) \tag{4.3}$$

$$= \omega\left(\cos(\phi)\sin(at_{des}) + \sin(\phi)\cos(at_{des})\right) \tag{4.4}$$

$$= \omega\left(\sqrt{1-\frac{(\beta_{n-1}^{LO})^2}{\omega^2}}\sin(at_{des}) + \frac{\dot{\beta}_{n-1}^{LO}}{\omega}\cos(at_{des})\right) . \tag{4.5}$$

Rearranging (4.5) to solve for ω results in

$$\omega = \sqrt{(\dot{\beta}_{n-1}^{LO})^2 + \left(\frac{\dot{\beta}_{des} - \dot{\beta}_{n-1}^{LO}\cos(at_{des})}{\sin(at_{des})}\right)^2} . \tag{4.6}$$

An equation governing the recirculation frequency a results from matching the desired leg touch-down angle β_{des} at t_{des}. Integrating the angular velocity profile (4.1) from $t = 0$ to $t = t_{des}$ yields

$$\beta_{des} = \beta_{n-1}^{LO} - \frac{\omega}{a}\left[\cos(at_{des}+\phi) - \cos(\phi)\right] \tag{4.7}$$

$$= \beta_{n-1}^{LO} - \frac{\omega}{a}\left[\sqrt{1-\frac{(\beta_{n-1}^{LO})^2}{\omega^2}}\left(\cos(at_{des})-1\right) - \frac{\beta_{n-1}^{LO}}{\omega}\sin(at_{des})\right] . \tag{4.8}$$

Utilizing (4.6) and simplifying yields

$$\beta_{des} = \beta_{n-1}^{LO} + \frac{\dot{\beta}_{des} + \dot{\beta}_{n-1}^{LO}}{a}\tan\left(\frac{at_{des}}{2}\right) . \tag{4.9}$$

At the beginning of the swing phase, a is determined from (4.9), and values for ω and ϕ are determined from (4.6) and (4.2), respectively. Once determined, these variables prescribe the angular velocity of the leg undergoing swing via (4.1), resulting in a leg

touch-down angle of

$$\beta_{n+1}^{TD} = \beta_{n-1}^{LO} - \frac{\omega}{a}\left[\cos(at+\phi) - \cos(\phi)\right] \ . \tag{4.10}$$

The equations governing leg recirculation are developed with respect to the body frame, and can therefore be applied to both the point mass and rigid body LLS models.

As in previous work on the LLS model, periodic gaits exist for a range of desired leg touch-down angles, β_{des}. While a periodic orbit associated with a particular β_{des} will not vary, as a function of $\dot{\beta}_{des}$, $\dot{\beta}_{des}$ will directly impact gait stability and robustness through its effect on the leg touch-down angle for swing phase durations different from t_{des}. Qualitatively, the differences in the expected leg touch-down angle, as a function $\dot{\beta}_{des}$, are illustrated in panels $(b)-(d)$ of Fig. 4.1. For a periodic orbit with $\dot{\beta}_{des} < 0$, the swing leg is moving forwards when it is placed down, such that swing phase durations less than t_{des} result in leg touch-down angles greater than β_{des}. If $t > t_{des}$, then the resulting leg touch-down angle is smaller than β_{des} for small deviations in t from t_{des}, but larger than β_{des} for sufficiently large deviations away from the desired swing phase duration. For $\dot{\beta}_{des} > 0$, $t > t_{des}$ results in leg touch-down angles larger than the desired value. Similar to the previous case, variations in the leg touch-down angle for $t < t_{des}$ depend upon the magnitude of the deviation away from t_{des}; small deviations lead to smaller leg touch-down angles than desired while much larger deviations lead to larger leg touch-down angles. A desired leg angular velocity at touch-down of $\dot{\beta}_{des} = 0$ presents a unique case. In this instance, any deviation in the stance phase duration of the opposite leg leads to a larger leg touch-down angle. The qualitatively different variations in the leg touch-down

angle that occur in each of these cases provide a means to investigate the impact of leg recirculation on gait stability and robustness.

4.2 Model simulations

Analytical and numerical investigations are conducted to determine the effect of leg recirculation on gait stability and robustness for the LLS model. Analytically, as presented in Appendix B, eigenvalues governing periodic gait stability are calculated for the point mass ($d = 0$) case and serve to validate our numerical results. Numerical simulations are subsequently employed to determine periodic gait characteristics, gait stability, and gait recovery from external perturbations.

All numerical simulations are performed utilizing the Runge-Kutta integrator *ode45* in Matlab. The instant of leg lift-off is determined, via the events functionality of *ode45*, to an accuracy of 10^{-8} by monitoring the force developed in the leg. Once the leg force returns to zero, the leg is lifted and the opposite stance phase begins. A Levenberg-Marquardt algorithm, as implemented in *fsolve*, is employed to identify initial states for the left stance phase $(v_n^{TD}, \delta_n^{TD}, \theta_n^{TD}, \dot{\theta}_n^{TD}, \beta_n^{TD})$ that result in an identical state for the subsequent left stance phase $(v_{n+2}^{TD}, \delta_{n+2}^{TD}, \theta_{n+2}^{TD}, \dot{\theta}_{n+2}^{TD}, \beta_{n+2}^{TD})$. The set of initial states identified by this algorithm are fixed points of the Poincaré map and periodic orbits of the continuous system. Gait stability is determined from the eigenvalues of Poincaré map linearized about the fixed point. Unstable gaits have at least one eigenvalue greater than unity in magnitude, while stable gaits have all eigenvalue magnitudes less than or equal to unity, with unity eigenvalues identifying directions of neutral stability.

Locomotion dynamics are governed by a composition of the left and right stance phase dynamics, resulting in a hybrid, piecewise-holonomic system [35]. While hybrid locomotion systems can display asymptotic stability [40], they are often best described in terms of partial asymptotic stability [18]. For these systems, fixed points and the corresponding periodic motions typically exhibit one or more neutral eigendirections (with Floquet multiplier = 1) which are often associated with conservation laws (e.g. energy conservation) or symmetries such as rotational invariance. For eigenvalues associated with such conservation laws, perturbations in neutral eigendirections do not result in recovery of the original gait, but rather the attainment of a new gait. For example, energetic perturbations to a periodic gait for the conservative LLS model result in the selection of a new touch-down velocity, since no means exists within the model to add or remove energy. However, perturbations in an eigendirection with an eigenvalue of magnitude less than one, such as the velocity heading angle, result in restabilization to the original periodic gait. Stability of periodic gaits considered in this work will be characterized in this manner.

In the results that follow, LLS model parameters are set to values representative of the cockroach *Blaberus discoidalis* [54, 25, 26, 41]: spring stiffness (k) of 2.25 N/m, mass (m) of 0.0025 kg, force-free leg length (l) of 0.01 m, moment of inertia (I) of 2.06×10^{-7} kg m^2. Because gait stability is improved by varying the stride frequency and length to match that observed experimentally in the cockroach [41, 49], a quartic polynomial curve fit is constructed from experimental stride length and frequency data [54] for the cockroach *Blaberus discoidalis* as a function of t_{des}. This fit is employed at each t_{des}, in conjunction with an approximation of the stride length of a periodic orbit

from stance phase geometry as $L_s = 4l\cos(\beta_{des})$ (see Fig. 2.1), to determine variations in β_{des} that approximately match stride length variations. The average forward velocity of the resulting gaits for this range of t_{des} is $< v >= 0.11 - 0.43$ m/s, which encompasses the preferred running speed of *Blaberus discoidalis*. Other model parameters, such as the spring stiffness and leg length, are chosen to adequately reproduce insect force and velocity profiles at the desired running speed of the insect, 0.25 m/s. Periodic gaits identified utilizing Matlab's *fsolve* algorithm are determined within an accuracy of 10^{-7}. Eigenvalues associated with these periodic gaits are computed from the linearized Poincaré map, the entries of which are computed numerically via central difference approximations.

Locomotion performance with leg recirculation is examined for both the point mass ($d = 0$) and rigid body ($d \neq 0$) models in the following section. Results for the point mass case are included in this study due to their possible relevance for other sprawled-posture animals and insects, as well as robotic implementations. While the center of pressure moves from fore to aft during a stance phase in the cockroach [54] and is not generally aligned with the center of mass, this is not necessarily true for other sprawled-posture creatures. Scaling relationships derived from dynamic similarity principles, as developed in [44], can therefore be utilized to extend these results for parameter ranges characteristic of other animals or insects.

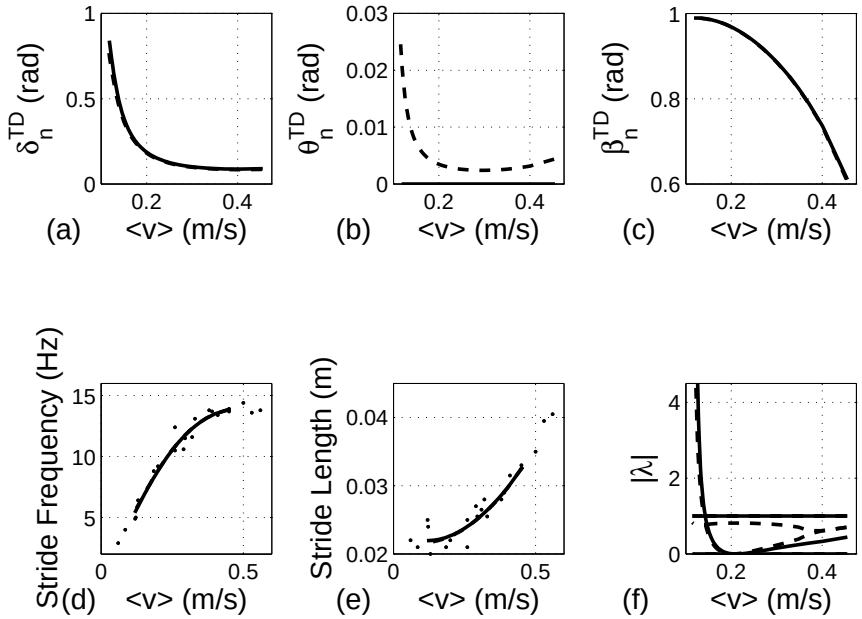

Figure 4.2: (a-c) Family of periodic gaits $(< v >, \delta_n^{TD}, \theta_n^{TD}, \dot{\theta}_n^{TD}, \beta_n^{TD})$ for $d = 0$ (solid) and $d = 0.002$ (dashed) as a function of the average forward velocity. All periodic gaits have $\dot{\theta_n^{TD}} = 0$. (d-e) Comparison of experimental stride frequency data on running cockroaches (dots) [54] to that of the illustrated gait families (lines). (f) Eigenvalue magnitudes $|\lambda|$ for each periodic gait of the gait families.

4.3 Results

4.3.1 Gait behavior for variations in t_{des}

A one-parameter family of periodic gaits exists for the LLS model with leg recirculation, parameterized by the desired stance phase duration (t_{des}). As illustrated in Fig. 4.2, families of periodic gaits $(v_n^{TD}, \delta_n^{TD}, \theta_n^{TD}, \dot{\theta}_n^{TD}, \beta_n^{TD})$ are identified numerically for both $d = 0$ and $d \neq 0$ for $t_{des} = 0.093 - 0.036$ seconds and $\dot{\beta}_{des} = 0$. Employing the leg recirculation protocol, for both the point mass and rigid body models, produces stable

periodic gaits, thus supporting our first hypothesis. Variation in gait stability over this speed range has similarities to that of the original LLS model for both $d = 0$ and $d \neq 0$. In both cases, as t_{des} increases the touch-down velocity decreases, and the associated periodic gaits destabilize as the velocity heading angle eigenvalue passes through the unit circle in a saddle-node bifurcation. For $d \neq 0$, the introduction of yawing dynamics decreases gait stability, with an eigenvalue corresponding to body angular velocity remaining near 0.8 for most of the gait family. As a result, recovery rates from small perturbations for the rigid body model occur over a much longer timescale than that required by gaits of the point mass case. While periodic gaits of both the original LLS model and the recirculation protocol share a unity eigenvalue corresponding to energy conservation, the eigenvalue corresponding to the leg touch-down angle is zero for leg recirculation as compared to the unity value of the original LLS model. This zero eigenvalue for the entire gait family is unique to the case of $\dot{\beta}_{des} = 0$; non-zero values of $\dot{\beta}_{des}$ result in an eigenvalue different than zero. Periodic gaits for values of t_{des} beyond that associated with the saddle-node bifurcation yield unstable gaits. However, unlike the original LLS model, gait stability and the location of the saddle-node bifurcation can be modified through appropriate choice of $\dot{\beta}_{des}$. Previously unstable periodic gaits for the original LLS model can therefore be stabilized, as examined in further detail in both Appendix B and the following section.

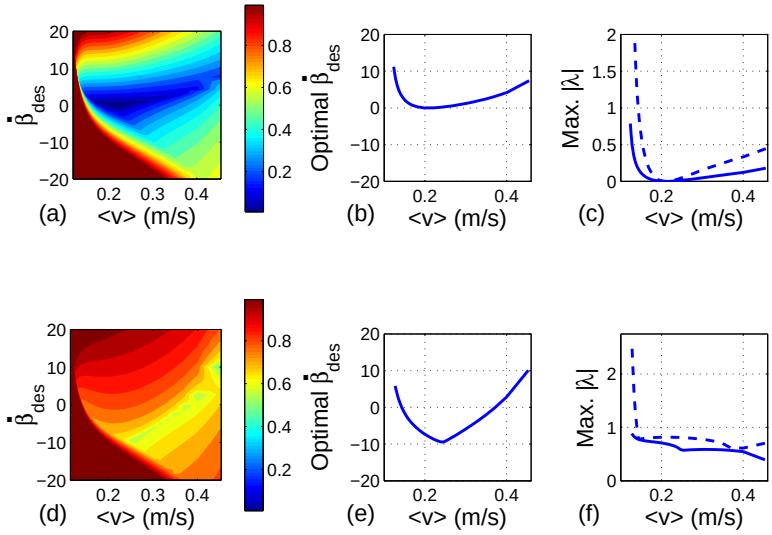

Figure 4.3: Variations in gait stability with $\dot{\beta}_{des}$ for $d = 0$ (top row) and $d = 0.002$ (bottom row). (a,d) Maximum non-unity eigenvalue contours for each periodic gait of the gait family as $\dot{\beta}_{des}$ is varied between -20 and 20 rad/sec for (b,e) Value of $\dot{\beta}_{des}$ that yields a minimum non-unity eigenvalue for each gait of the gait family. (c,f) Eigenvalue magnitude at the optimal value of $\dot{\beta}_{des}$ (solid) as compared to that for $\dot{\beta}_{des} = 0$ (dotted).

4.3.2 Gait behavior for variations in $\dot{\beta}_{des}$

With numerical eigenvalue calculations validated by analytical results, as detailed in Appendix B, we utilize numerical calculations to investigate gait stability as a function of $\dot{\beta}_{des}$. Eigenvalues of the full-stride Poincaré map, linearized about each fixed point, are numerically computed for $\dot{\beta}_{des}$ values between -20 and 20 rad/sec for the gait families of Fig. 4.2. For each fixed point and $\dot{\beta}_{des}$, the maximum non-unity eigenvalue is retained.

The eigenvalue contour plots of Fig. 4.3 illustrate the dependence of gait stability on the leg angular velocity at touch-down for both $d = 0$ and $d = 0.002$ and help validate our first two hypotheses. As illustrated, feedforward prescription of the leg angular

velocity during swing in the LLS model is capable of producing a range of stable periodic gaits. Additionally, gait stability depends upon the value of the leg angular velocity at leg touch-down. For the point mass model, increasing the rate of leg retraction at touch-down improves gait stability for each gait of the gait family, which is qualitatively similar to the results obtained for swing-leg retraction [51] in the LLS model for vertical plane locomotion. Gaits at the lower end of the speed range, which are nominally unstable for $\dot{\beta}_{des} = 0$, are stabilized for sufficiently large leg angular velocities at touch-down. While gait stability can be improved by retracting the leg at the touch-down instant, an optimal value of $\dot{\beta}_{des}$ exists, beyond which stability decreases until the gait destabilizes. The optimal choice of $\dot{\beta}_{des}$ for each gait in the gait family is illustrated in the second panel of Fig. 4.3. The larger values of $\dot{\beta}_{des}$ employed by the model at higher speeds may be a byproduct of explicitly matching the higher leg cycle frequencies utilized by insects at these higher speeds. At higher speeds, the stance phase durations decrease, and perturbations to these periodic gaits result in comparatively smaller deviations in the stance phase duration from the desired value. As a result, larger leg angular velocities are required at touch-down to achieve leg touch-down angle variations capable of quickly restabilizing the gait. At the lowest speeds, gait instability requires larger changes in the leg touch-down angle to appropriately reorient the momentum in response to external perturbations, which necessitates increases in the leg angular velocity at touch-down.

The contour plot of gait stability for $d = 0.002$ m exhibits improved stability for a different range of $\dot{\beta}_{des}$ than the point mass case, due to the coupling between translational and rotational dynamics introduced in the rigid body model. As in the point mass case, previously unstable gaits at the lower end of the speed range can be stabilized for

sufficiently large leg retraction velocities at touch-down. While these stability results and those at the higher end of the speed range qualitatively match those of the point mass model, gait stability in the middle of the speed range improves for leg protraction at touch-down, $\dot{\beta}_{des} < 0$. In this speed range, the least stable eigenvalue corresponds to the angular velocity of the body, $\dot{\theta}$. Improving body angular velocity stability evidently requires leg touch-down angle changes in response to perturbations similar to those evidenced in Fig. 4.1b rather than those employed in Fig. 4.1d that improve the stability of the velocity heading angle, which dominates stability at the lowest and highest speeds. We hypothesize that the gait stability improvement obtained by increased protraction rates for the rigid body model may be limited to this bipedal model; the forces produced by a combination of legs in a multi-legged model or insect might better compensate for disturbances in angular velocity without necessitating a forward leg angular velocity at touch-down. This hypothesis is bolstered by analysis of experimental data for the angular velocity of cockroach legs during the swing phase, all of which are typically retracting at touch-down, as examined in more detail in Section 4.3.3.

While gait stability can be improved via changes in the leg retraction or protraction velocity at touch-down, perturbation recovery simulations are required to determine if these local results extend to perturbations that move the system outside the range for which the linearization is valid. As a result, a series of perturbation simulations are conducted to quantify gait robustness for the recirculation protocol. Perturbations are applied to the velocity heading angle within the limits of glancing contact ($\delta_n^{TD} = -\frac{\pi}{2} + \beta_{des}$) and direct compression of the elastic leg ($\delta_n^{TD} = \beta_{des}$). For each periodic gait of the gait family, the initial velocity heading angle is set to values within these limits and

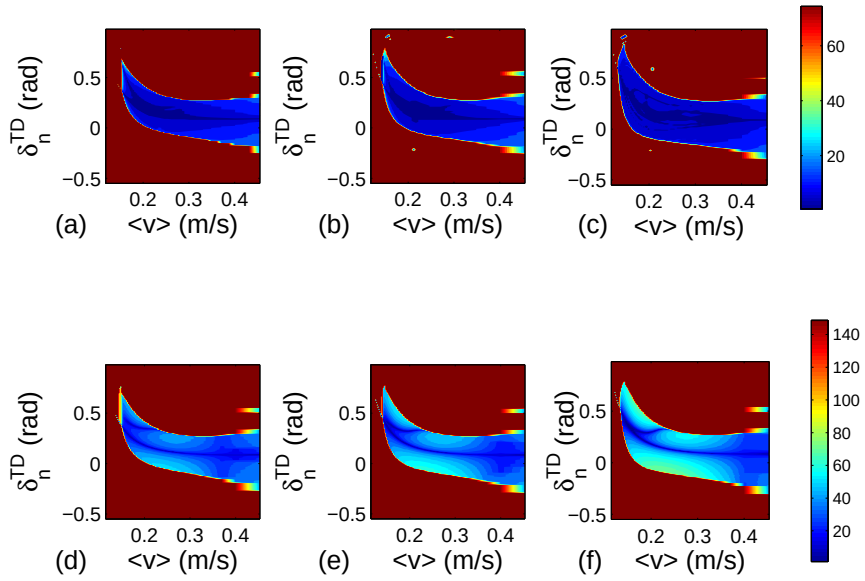

Figure 4.4: Contour plots of the number of stance phases required for recovery of periodic gaits from external perturbations in δ_n^{TD} for $d = 0$ (top row) and $d = 0.002$ (bottom row) with (a,d) $\dot{\beta}_{des} = -2.5$ rad/sec (b,e) $\dot{\beta}_{des} = 0$ rad/sec (c) $\dot{\beta}_{des} = 5$ rad/sec and (f) $\dot{\beta}_{des} = 2.5$ rad/sec.

simulations are conducted for 75 ($d = 0$) or 150 ($d = 0.002$) stance phases. In total, 17,806 perturbation simulations are conducted for each gait family. In each simulation, the number of stance phases required for all the system states to return and stay within 1% of the original periodic gait is recorded, if applicable.

The panels of Fig. 4.4 illustrate the numerically computed basin of stability for the LLS model with leg recirculation implemented for several values of $\dot{\beta}_{des}$. Quantitative comparisons are presented in Table 4.1. For the point mass model, employing leg retraction with a leg touch-down angular velocity $\dot{\beta}_{des} = 5$ rad./s increases the number of gaits that recover from the applied perturbations by 68.6% as compared to the number that recover for leg protraction with $\dot{\beta}_{des} = -2.5$ rad./s. Part of the expansion of the basin of

Table 4.1: Basin of stability and recovery basin as a function of $\dot{\beta}_{des}$

	Recovery percentage	Avg. number of steps required ($\pm$ standard deviation)
Recirculation model		
$d = 0$		
$\dot{\beta}_{des} = -2.5$	16.9%	9.8 ± 8.4
$\dot{\beta}_{des} = 0$	21.3%	9.1 ± 6.7
$\dot{\beta}_{des} = 5$	28.5%	7.3 ± 4.1
$d = 0.002$		
$\dot{\beta}_{des} = -2.5$	17.6%	33.9 ± 10.4
$\dot{\beta}_{des} = 0$	22.0%	39.2 ± 18.0
$\dot{\beta}_{des} = 2.5$	25.7%	44.3 ± 17.3
Original LLS Model		
$d = 0$	80.0%	9.4 ± 9.3
$d = 0.002$	73.4%	51.7 ± 22.7

stability is due to stabilization of additional gaits at the lower end of the speed range that were previously unstable. Additionally, the average number of steps required to recover the original periodic gait drops by 25.5% for the same variation in $\dot{\beta}_{des}$. These results conclusively validate the third hypothesis for the point mass case. For the rigid body model with $d = 0.002$, while gait stability improves with $\dot{\beta}_{des} < 0$ for gaits in the middle of the speed range, the number of gaits that recover from the applied perturbations increases by 46% for $\dot{\beta}_{des} = 2.5$ rad./s as compared to that exhibited for $\dot{\beta}_{des} = -2.5$ rad./s. This improvement comes at a cost of a decrease in the recovery rate of almost 31%. However, the benefit of the expanded operating range may offset the decrease in stability that occurs. Employing leg retraction at touch-down for the rigid body model will therefore remain less stable than other alternatives, but will yield recovery from a larger range of external perturbations.

As evident from the results of Table 4.1, the basin of stability is at best 35% of that obtained for the original LLS model with a fixed leg touch-down angle for both the point mass and rigid body case. While the basin of stability is therefore much smaller, the recovery rate is improved by 22.3% and 14.3% for $(d, \dot{\beta}_{des}) = (0, 5)$ and $(d, \dot{\beta}_{des}) = (0.002, 2.5)$, respectively. The reduction in the stability basin is not unexpected, because as the external perturbations in the heading angle increase in magnitude the deviation in the stance duration from the desired stance duration also increases. While the difference in the leg touch-down angle from the desired angle therefore increases in magnitude as a result of the recirculation protocol, this difference is larger than that needed to effect recovery. While enough control authority therefore exists, the leg touch-down angle employed produces leg forces that are not appropriately directed to reorient the system momentum, leading to destabilization of the velocity heading angle and continued movement away from the original periodic orbit. As a result, both leg angular velocity and angular acceleration may play a role in gait robustness. Smaller angular accelerations than those present in the current formulation in the latter portion of the swing phase may effectively limit the range of leg touch-down angles that occur for perturbations away from a periodic orbit. Modifications to the leg recirculation protocol that incorporate this concept are considered in further detail as the recirculation profile is compared to that observed experimentally in Section 4.3.3.

4.3.3 Comparison to experimental results

The leg recirculation protocol is developed with the intention of qualitatively matching the swing profile employed by individual legs of sprawled-posture insects during locomotion. The leg angular velocity profiles utilized in the model are now compared to those employed by running cockroaches to determine both the relative accuracy of the profile and whether profile refinements that result in better matches to experimental data positively affect the basin of stability.

Experimental data of individual leg position and velocity, relative to the body frame, for cockroaches running over flat terrain was collected utilizing video tracking by S. Revzen (S. Revzen, 2008, personal communication, Polypedal Lab, University of California at Berkeley). The nominal leg recirculation protocol utilized in this work is compared to the leg angular velocity computed from the experimental data for the middle leg of the cockroach *Blaberus discoidalis* over a series of four different runs, with each run having an average fore-aft velocity between $22 - 30$ cm/s. The middle leg of the insect was selected for comparison purposes because, unlike the front and rear legs, the fore-aft force profile exhibited by this leg resembles that produced by the effective leg of the LLS recirculation model. While the swing leg angular velocity profiles exhibited by all legs qualitatively match those of the model, examination of the model and experimental profiles in Fig. 4.5 reveals that the experimental profile has a more complicated structure in the second half of the swing phase.

Specifically, it appears that a decrease occurs in the leg angular acceleration during the second half of the swing phase that results in a slower variation in the leg angular

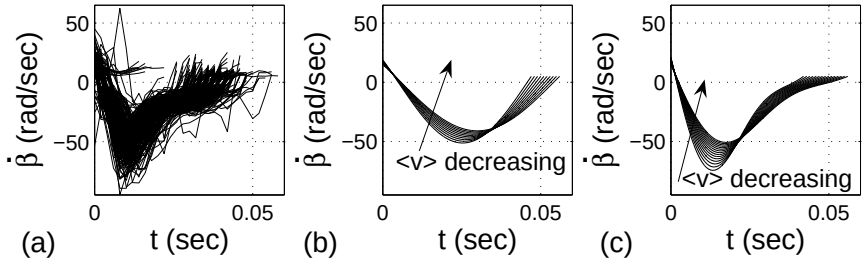

Figure 4.5: (a) Leg angular velocity during the swing phase for the middle legs of running cockroaches, as calculated from experimental data collected and provided by S. Revzen (S. Revzen, 2008, personal communication, Polypedal Lab, University of California at Berkeley). (b) Calculated leg angular velocity during the swing phase for fixed points of the $d = 0.002$ gait family, with average forward velocities $< v >= 0.20 - 0.25$ m/s (c) Calculated leg angular velocity during the swing phase for fixed points of the $d = 0.002$ gait family, for the modified leg recirculation protocol with $c_1 = 0.5$, $c_2 = 0.2$ and $< v >= 0.20 - 0.30$ m/s

velocity before leg touch-down.

The importance of this difference in the swing profile is investigated by including higher order frequencies in the recirculation protocol to better match that exhibited experimentally. Specifically, the following leg recirculation formulation is considered

$$\dot{\beta} = \omega \left[\sin(at) + c_1 \sin(2at) + c_2 \sin(3at) + c_3 \right] , \tag{4.11}$$

where c_1 and c_2 are chosen to better match the experimental profile. An expression for c_3 results from matching the initial leg angular velocity $c_3 = \frac{\dot{\beta}_{n-1}^{LO}}{\omega}$. The conditions on the leg angle and angular velocity at $t = t_{des}$ produce coupled equations in ω and a that are solved numerically at the beginning of each swing phase. As illustrated in Fig. 4.5c, the refined recirculation protocol with $c_1 = 0.5$ and $c_2 = 0.2$ results in better agreement with the experimental profile and has a smaller angular acceleration near $t = t_{des}$.

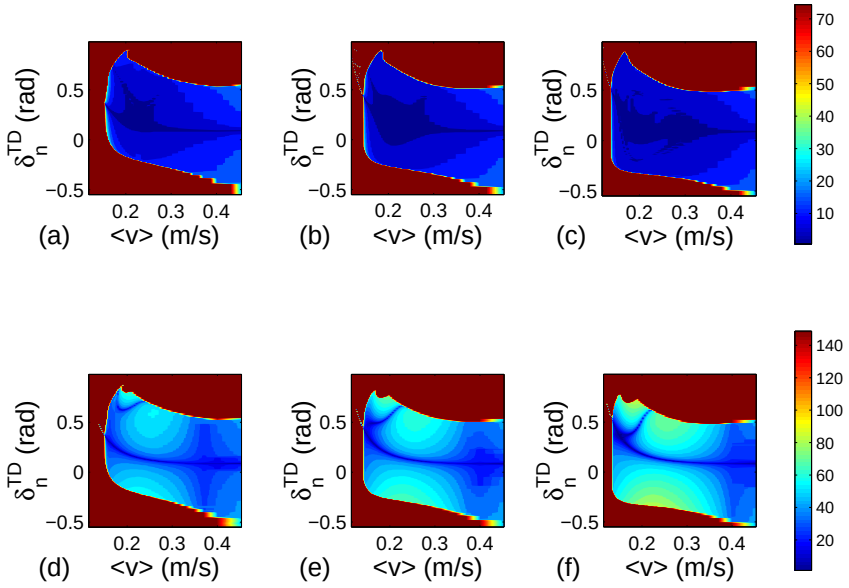

Figure 4.6: Contour plots of the number of stance phases required for recovery of periodic gaits from external perturbations in δ_n^{TD} for the modified recirculation protocol with $c_1 = 0.5$ and $c_2 = 0.2$. Recovery simulations are performed for $d = 0$ (a-c) and $d = 0.002$ (d-f) with (a,d) $\dot{\beta}_{des} = -2.5$ rad/sec (b,e) $\dot{\beta}_{des} = 0$ rad/sec and (c,f) $\dot{\beta}_{des} = 2.5$ rad/sec.

The performance of the refined protocol for $(c_1, c_2) = (0.5, 0.2)$ is examined by conducting perturbation recovery simulations similar to those performed previously for both the point mass and rigid body models. As illustrated in Fig. 4.6 and detailed in Table 4.2, the refined recirculation protocol produces a stability basin for both the point mass and rigid body models that is essentially twice the size of that produced by the original model. The improved recovery basin indicates that the model can recover from a larger range of perturbations, similar to its insect counterpart, which is able to recover from external lateral perturbations of up to 85% of its momentum in only a few stance phases [24]. While the model in its current form cannot recover from energetic pertur-

Table 4.2: Basin of stability and recovery basin for refined recirculation protocol as a function of $\dot{\beta}_{des}$

	Recovery percentage	Avg. number of steps required ($\pm$ standard deviation)
$d = 0$		
$\dot{\beta}_{des} = -2.5$	37.1%	10.1 ± 9.1
$\dot{\beta}_{des} = 0$	44.7%	7.9 ± 6.5
$\dot{\beta}_{des} = 2.5$	50.9%	7.3 ± 5.9
$d = 0.002$		
$\dot{\beta}_{des} = -2.5$	37.8%	40.9 ± 11.3
$\dot{\beta}_{des} = 0$	45.0%	44.4 ± 13.8
$\dot{\beta}_{des} = 2.5$	50.5%	50.4 ± 17.3

bations, its ability to recover from half of the perturbations investigated suggests that the feedforward leg recirculation evidenced in the insect [52] may be a viable control strategy. The basins of stability for the refined leg recirculation formulation are also improved from the original formulation, yet variations in recovery rate and the basin of stability as a function of $\dot{\beta}_{des}$ remain similar to those obtained for the original protocol. For $d = 0$, values of $\dot{\beta}_{des} > 0$ enlarge the basin of stability, improving the recovery rate at lower and higher speeds, while slightly reducing the recovery rate in the middle of the speed range. For $d = 0.002$, increasing $\dot{\beta}_{des} > 0$ enlarges the stability basin, but reduces the recovery rate at lower speeds while improving it at higher speeds. However, the average recovery rate evidenced by the periodic gaits for $\dot{\beta}_{des} = 2.5$ rad./s is 23.2% less than that observed for $\dot{\beta}_{des} = -2.5$ rad./s. The basin of stability results for both the point mass and rigid body models suggest that while leg angular velocity is important for gait stability, angular acceleration near leg touch-down also influences the basin of stability. Reducing the angular acceleration during the second half of the swing phase

may be beneficial for the insect, since it results in smaller changes in leg touch-down angles in recovery from external perturbations.

Similarity between leg touch-down angles employed by the refined leg recirculation protocol and the leg touch-down angle control law developed in Chapter 3 is examined via perturbation simulations. Perturbation recovery simulations are conducted for the rigid body model for both strategies, with parameters in the control law set to those utilized in Chapter 3 for $d = 0.002$. For simulations in which both strategies recover the original periodic gait, the first five leg angles utilized in recovery are retained for comparison purposes. The coefficient of determination (r^2 and associated p value), as derived from the Pearson product-moment coefficient for these values, is employed as a measure of similarity of the actuation strategies for each protocol. Comparisons are made for the entire gait family across the entire range of perturbations previously considered.

As illustrated in Fig. 4.7, the leg angles utilized in restabilization from an external perturbation for each protocol appear to have a relatively strong correlation for many of the perturbations simulated. For each $\dot{\beta}_{des}$, as the perturbed heading angle δ_n^{TD} increases from negative to positive the associated correlation coefficient rapidly changes from a positive value close to 1 to a negative value close to -1, yielding a small band of perturbations for which the strategies are relatively uncorrelated. Further increases in δ_n^{TD} yield decreases in the correlation coefficient, until the recirculation strategy is no longer able to recover the original periodic gait. Additionally, as $\dot{\beta}_{des}$ decreases, positive correlations between the leg touch-down angles employed exist for a wider range of perturbations.

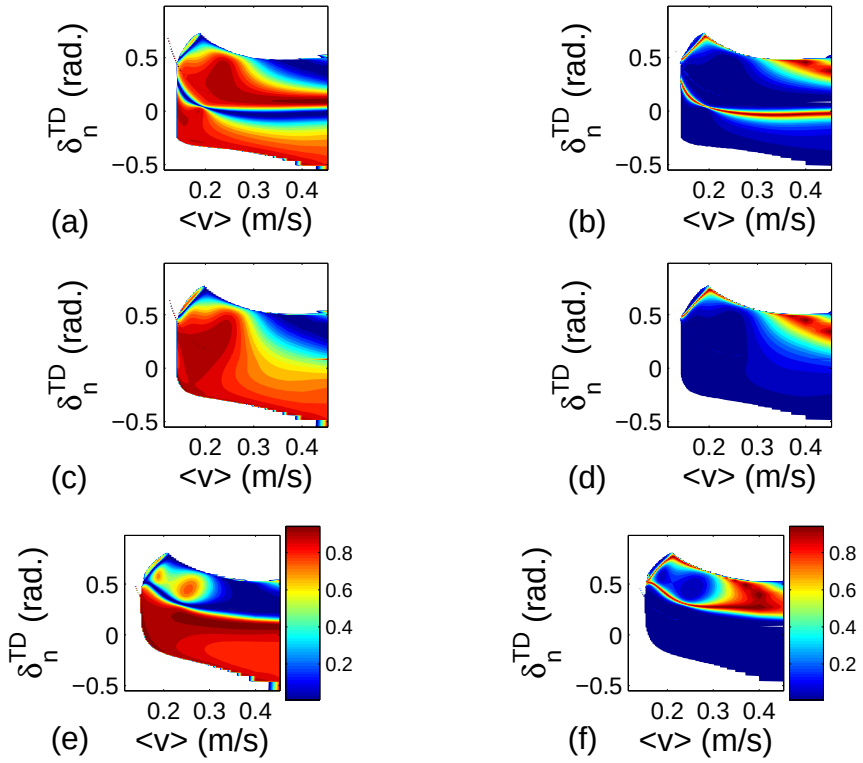

Figure 4.7: Contour plots of r^2 (first column) and associated p value (second column) determined for the first five leg touch-down angles utilized in recovery from external perturbations by the leg angle control law and the refined leg recirculation protocol. Perturbation recovery simulations are conducted for the rigid body model with $d = 0.002$, with leg touch-down angle control law parameters set to $(c_1, c_2, c_3) = (-0.1, 0.3, 0.8)$ and leg recirculation parameters set to $(c_1, c_2) = (0.5, 0.2)$. Results are determined for (a-b) $\dot{\beta}_{des} = 2.5$ rad/sec, (c-d) $\dot{\beta}_{des} = 0$ rad/sec and (e-f) $\dot{\beta}_{des} = -2.5$ rad/sec

These results suggest that the refined leg recirculation protocol produces variations in leg touch-down angles, in response to perturbations, that are qualitatively similar to those employed by the leg touch-down angle control law for a relatively wide range of perturbations. Failure of the recirculation protocol to recover from as wide as a range of perturbations as the leg touch-down angle control law is certainly due in part to the

fact that large external perturbations in δ_n^{TD} result in large changes in the duration of the swing phase, resulting in destabilizing variations in the leg touch-down angle. Such issues do not exist for the leg touch-down angle control law, since swing phase dynamics are not included. However, these results also suggest that deviations in the leg touch-down angles employed by the leg recirculation protocol for larger positive perturbations in δ_n^{TD}, as compared to those utilized by the leg touch-down control law, may also be responsible for decreased basin of stability evidenced.

Chapter 5 – Leg control with actuation

5.1 Incorporating leg actuation

While conservative leg function in the traditional LLS formulation appears to accurately represent steady state locomotion dynamics, leg structures present in animals and insects serve to store and return, dissipate, and produce energy during a single stride. Thus, it appears that the energy variation observed during a stance phase is the result of the coordination of muscles, joints and tendons producing negative and positive work, the net result of which are the apparent spring-like dynamics represented by the model. Recent studies in insects [12] have demonstrated that leg function differs significantly from its spring-like counterpart in the LLS model, and suggest that the ability of legs to manage energy absorption and production is important in locomotion.

While the nominal LLS template maintains a constant force-free leg length $l = l_0$ during each stance phase to produce an energetically conservative system, we seek to actuate the force-free leg length during stance to better model the balance of energy storage, dissipation and production that must occur.

A simple model for energy absorption and production during each stance phase is therefore proposed via actuation of the force-free leg length ($l(t)$). While the actuation protocol is kept simple in an effort to better understand the basic effects energy absorption and production have on gait dynamics and stability, it is also intended that

it effectively model the net energetic effect that may result from muscle groups acting together in a predetermined pattern[53]. To model such patterns, we consider that the musculature may act in a cyclical fashion; it may absorb energy during the first half of the stance phase to serve as a braking mechanism, yet actively produce energy to propel the body forward during the second half of the stance phase. To obtain periodic orbits, the energy absorption and production must be equal over the course of the stance phase, such that the energy at the beginning and end of the stance phase are equal. As well, to retain force and velocity profiles that resemble those produced by the LLS template, energy absorption and production should be symmetric about mid-stance for periodic orbits and only slightly out of phase for non-periodic gaits. These requirements are satisfied by prescribing a model for force-free leg length actuation during each stance phase of the form

$$l(t) = l_0 - l_{dev} \sin(\frac{\pi t}{t_{des}}) \tag{5.1}$$

similar to that utilized in the lateral plane climbing template[19]. Here, l_{dev} represents the maximal deviation from a nominal leg length l_0, and t represents stance duration. Selection of t_{des} implicitly defines the average forward speed of a periodic gait, such that periodic gaits for a range of forward speeds can be determined by varying t_{des}. The fractional length change l_{dev} impacts both the energy change for perturbations away from a periodic orbit as well as gait stability. While the force-free leg length varies, the force developed in the leg is still governed by the linear spring law ($F_{leg} = k(l(t) - \zeta)$). Without loss of generality, each stance phase is assumed to begin with $t = 0$, which yields a constant leg touch-down length of $l = l_0$. Because leg lift-off occurs at the

instant the force developed in the spring returns to zero, incorporating this actuation protocol results in leg lift-off lengths (l) that deviate from l_0, as evidenced by examining the actuation protocol (Equation 5.1). It is important to note that while the force-free leg actuation protocol considered in this paper introduces a non-conservative force, re-deriving the equations of motion using Lagrange's equations with generalized forces results in the same equations of motion as of the original LLS model (Equations 2.1, 2.2, and 2.3). The equations of motion only differ in that l becomes a prescribed function of time, as prescribed by (Equation 5.1), and forces developed in the leg therefore arise from a combination of the clock-driven changes in l and the axial dynamics.

The energy of the non-actuated LLS system is comprised of the kinetic energy of the mass and the potential energy of the spring. In the non-actuated system, the work done by the spring on the mass during compression or extension equals the change in the amount of potential energy stored in the spring, resulting in energy conservation. In our actuated model, the formulation for the work done by the leg during each stance phase remains the same as that of the nominal LLS model; the work is the time integral of the leg force multiplied by the rate of change of the leg length,

$$W = \int_0^t k(l-\zeta)\dot{\zeta}\, dt \ . \tag{5.2}$$

Actuation of the force-free leg length during the stance phase, as prescribed by (Equation 5.1), modulates the spring force such that the change in energy stored in the spring does not equal the work done by the spring in compression or extension. As a result, energy is no longer conserved and fluctuations in energy occur during the stance phase.

In the actuated model, energy is removed from the system by leg actuation during leg compression and is added to the system during leg extension. For a periodic gait with stance phase duration t_{des} and $l_{dev} > 0$, gait symmetry in ζ and $\dot{\zeta}$ about mid-stance ensures that the energy absorbed during the first half of the stance phase equals that added during the latter half, such that the energy at lift-off equals that at touch-down. For non-periodic gaits, symmetry about mid-stance is no longer guaranteed because the leg is lifted once it returns to the force-free length, which is not necessarily the touch-down length of $l = l_0$. As is evident from (Equation 5.1), gaits with stance phase durations longer than t_{des} have a leg length at lift-off greater than l_0. The increased duration of leg extension results in a net energy increase, thereby increasing the velocity of the mass at the end of the stance phase and potentially reducing the duration of future stance phases. In a similar manner, gaits with stance phase durations less than t_{des} result in net reductions in system energy, and serve to reduce the system velocity. As a result, it is expected that incorporating this actuation protocol into the LLS model will stabilize the center of mass velocity. By the same reasoning $l_{dev} < 0$ is expected to destabilize center of mass velocity.

This simple and analytically amenable actuation scheme also has the advantage of being easily adapted to the energy-dissipation realities of robot instantiation. Simply by shifting the phasing of the feed-forward actuation the asymmetry of the energy removal and addition can be adapted to compensate for the inevitable mechanical losses in a robotic system.

Incorporating the leg angle control protocols considered in the previous chapters yields improved gait stability, as compared to the original LLS model. Specifically,

changes in the leg touch-down angle, whether resulting from a leg angle control law or natural leg recirculation, provide control authority over the velocity heading angle, enabling modification of the associated eigenvalue. As detailed previously, stability can therefore be improved through appropriate choice of either the leg angle control parameters c_i or the desired leg angular velocity at touch-down $\dot{\beta}_{des}$. With these leg angle control strategies, the resulting gaits are not only stable with respect to the velocity heading angle, but are also stable with respect to the leg touch-down angle. As such, appropriately small perturbations in either the velocity heading angle or the leg touch-down angle result in re-stabilization to the original periodic gait. While these periodic gaits can reject disturbances in these states, they remain only partially asymptotically stable due to energy conservation. Because the model formulation contains no means to input or extract energy, an eigenvalue corresponding to energy conservation remains unity in both situations, yielding only Lyapunov stability. As such, applied energetic perturbations result in recovery to a nearby periodic gait rather than the original gait.

In this chapter, we therefore investigate performance of a prescribed, feedforward leg actuation strategy (Equation 5.1) developed to approximate the feedforward muscle activation utilized by insects when running over rough terrain. Ultimately, the goal of this line of research is to combine prescribed, feedforward leg actuation characteristic of sprawled-posture insects with the leg angle control and recirculation strategies previously investigated to produce completely asymptotically stable periodic gaits for the point mass LLS model. Producing asymptotically stable periodic gaits in this fashion would lend support to the hypothesis that insects employ a hierarchical control system, with recovery from transient disturbances resulting from a combination of preflexes,

prescribed feedforward actuation and low level neural control, such as that required to place the leg at its next touch-down position. In this hypothesized control formulation, significant neural feedback only occurs in response to the presence of persistent disturbances, such as changes in slope or substrate.

5.2 Leg actuation with a fixed leg touch-down angle

Incorporating leg actuation into the LLS model destroys energy conservation, which has been critical in developing the analytical approximations of gait stability examined in both the previous chapters as well as other investigations [18, 39, 48]. While the qualitative arguments regarding gait stability under the influence of leg actuation presented in the previous section still hold, we must resort to numerical simulations to determine the dynamical behavior, stability and robustness of the model when employing leg actuation strategies.

As such, we investigate model performance over a wide range of velocity heading angles between the limits of pure fore-aft motion as the leg touches down ($\delta_n^{TD} = 0$) to direct compression of the spring ($\delta_n^{TD} = \beta_{des}^{TD}$). Initially, we consider a fixed leg touch-down angle, as utilized previously, of $\beta_{des}^{TD} = 1.0$ radians. The numerical simulations of the model with leg actuation and a fixed leg touch-down angle are developed and performed using the Runge-Kutta integrator, *ode45*, available in Matlab. The event functionality of *ode45* is employed to detect instants of leg lift-off and touch-down with a tolerance of 1×10^{-8}. Periodic orbits are identified by driving the difference between the initial states ($v_n^{TD},\ \delta_n^{TD},\ \beta_n^{TD}$) and those at the next leg touch-down ($v_{n+1}^{TD},\ \delta_{n+1}^{TD},\ \beta_{n+1}^{TD}$)

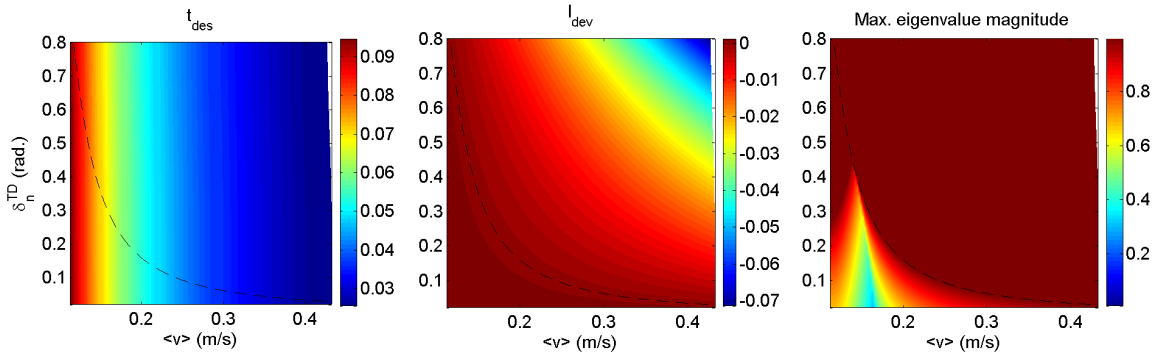

Figure 5.1: Surface of periodic gaits with leg actuation and a fixed leg touch-down angle of $\beta_{des} = 1.0$ radians. Contour plots, from left to right, identify: values of the desired stance phase duration (t_{des}) as a function of the average forward velocity ($< v >$) and the touch-down velocity heading angle (δ_n^{TD}), values of the leg actuation amplitude l_{dev}, and the maximum eigenvalue magnitude. The dashed line in each panel identifies the gait family for $l_{dev} = 0$. All other parameters are held at values characteristic of the cockroach *Blaberus discoidalis*, as identified previously.

to zero via a Levenberg-Marquardt algorithm, as implemented in *fsolve* in Matlab.

Numerically determined periodic orbits for the LLS model with leg actuation and a fixed leg touch-down angle are presented along with the maximum eigenvalue magnitude governing gait stability in Figure 5.1. As in previous chapters, we define a family of periodic gaits as the values of the velocity v_n^{TD} and t_{des} that yield periodic gaits for a constant leg actuation amplitude l_{dev} and leg touch-down angle β_{des}^{TD} as the velocity heading angle δ_n^{TD} is varied between its limits. A single gait family, characteristic of $l_{dev} = 0$, is illustrated in Figure 5.1a-b as a dashed line, where each point $(v_n^{TD}, \delta_n^{TD}, l_{dev}, t_{des}, \beta_{des}^{TD})$ on the line represents the initial conditions for a periodic orbit of the continuous system. Repeating this process for other values of the leg actuation amplitude results in additional gait families, thereby creating the surface of periodic gaits illustrated in Figure 5.1a-b.

In the original LLS formulation ($l_{dev} = 0$) an eigenvalue corresponding to energy conservation is necessarily unity, indicating that the model cannot recover the original periodic gait when subjected to an energetic perturbation. Incorporating the feedforward leg actuation protocol developed earlier (Equation 5.1) into the model destroys energy conservation, such that all eigenvalues differ from unity for $l_{dev} \neq 0$. As hypothesized previously, the sign of the actuation amplitude is important for stability, as illustrated in Figure 5.1c. Because $l_{dev} = 0$ represents the energetically conservative case, continuity of solutions suggests that deviations in l_{dev} away from zero will yield periodic gaits with an eigenvalue corresponding to the system energy that deviates from unity. As illustrated in Figure 5.1c, periodic gaits with $l_{dev} < 0$ are unstable, while those with $l_{dev} > 0$ are partially asymptotically stable. Unlike previous stability analyses, the maximum eigenvalue variation illustrated in Figure 5.1c corresponds to the system energy rather than the velocity heading angle. As a result, energetic perturbations result in quicker recovery in the velocity heading angle and slower recovery in the system velocity. While $l_{dev} > 0$ can yield gaits that stabilize the system energy, leg actuation alone cannot produce re-stabilization to the original periodic orbit in response to perturbations in the leg touch-down angle. As a result, periodic gaits with leg actuation alone are only partially asymptotically stable and perturbations in the leg touch-down angle result in the attainment of a nearby periodic orbit. Attaining complete asymptotic stability will therefore require combining this leg actuation strategy with leg angle control strategies, as investigated later in this chapter.

The periodic gaits identified for a constant leg touch-down angle with leg actuation possess gait characteristics that resemble those of both the nominal LLS model as well

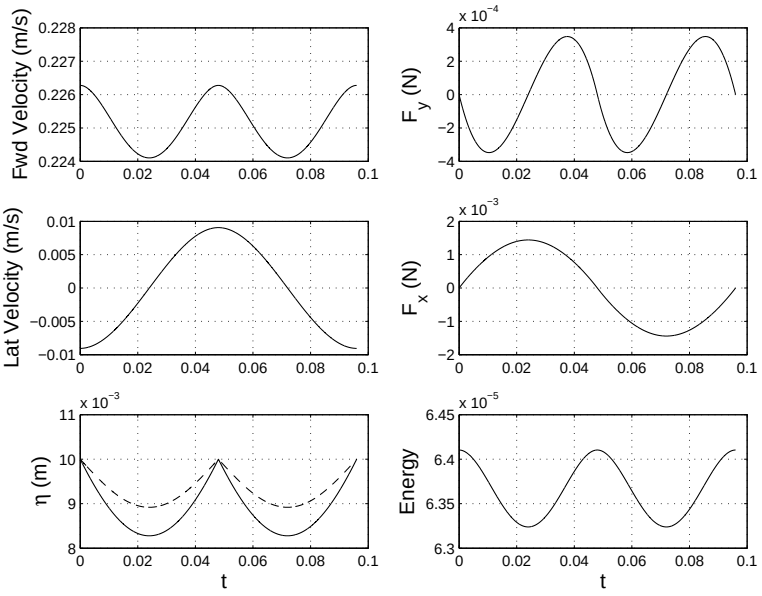

Figure 5.2: Illustration of the gait characteristics for a periodic gait $(v_n^{TD}, \delta_n^{TD}, \beta_n^{TD}) = (0.2265, 0.04, 1)$ with leg actuation of $l_{dev} = 0.0011$m and $v_{des} = 0.2251$ m/s, $t_{des} = 0.0480$ s. All other model parameters are set to values characteristic of *Blaberus discoidalis* as described in the text. The dotted line in the bottom left panel represents the variation in the force-free leg length during the stride.

as well as experimentally determined cockroach locomotion profiles, as illustrated in Figure 5.2. As hypothesized in [1, 12], absorption and production of energy in phase with the compression and extension of the leg result in force and velocity profiles that resemble those of a LLS model without energy variations. Yet, as illustrated in the bottom right panel, energy variations occur during the stride due to the variation in the force-free leg length. Variations in the force-free leg length also serve to reduce the amount of force developed in the leg during the stride, thereby reducing the variations in fore-aft and lateral velocity during each stance phase.

5.3 Improving gait stability via combined strategies

As evidenced for our results with a fixed leg touch-down angle, producing gaits that are completely asymptotically stable requires both leg actuation and a strategy for changing the leg touch-down angle in response to external perturbations. In this section, we therefore consider the performance of the point mass LLS model with both leg actuation and the leg angle control strategy developed previously.

5.3.1 Combined leg actuation and leg angle control

As in our previous analysis of the leg angle control strategy, we only consider choices for our control parameters c_i that satisfy the gait symmetry constraint $\sum_{i=1}^{3} c_i = 1$. Choices of c_i that satisfy this constraint preserve gait symmetry and ensure that the periodic gait surface identified for the LLS model with leg actuation remain periodic when the leg angle control protocol is included. As a result, our choices of c_i only impact gait stability, to which we now turn.

In the conservative LLS model with leg angle control, it was found that the c_i values could be chosen to improve stability of either previously stable or unstable periodic gaits. In a similar manner, c_i values can be chosen in our combined actuation and leg angle control formulation to modify stability of our previously stable gaits or to stabilize those that were previously unstable (i.e. those for which $l_{dev} < 0$). While we did not pursue a formal optimization of our c_i values for each fixed point of the gait surface, we were able to identify combinations of c_i values that yielded acceptable results for the cases $l_{dev} > 0$ and $l_{dev} < 0$.

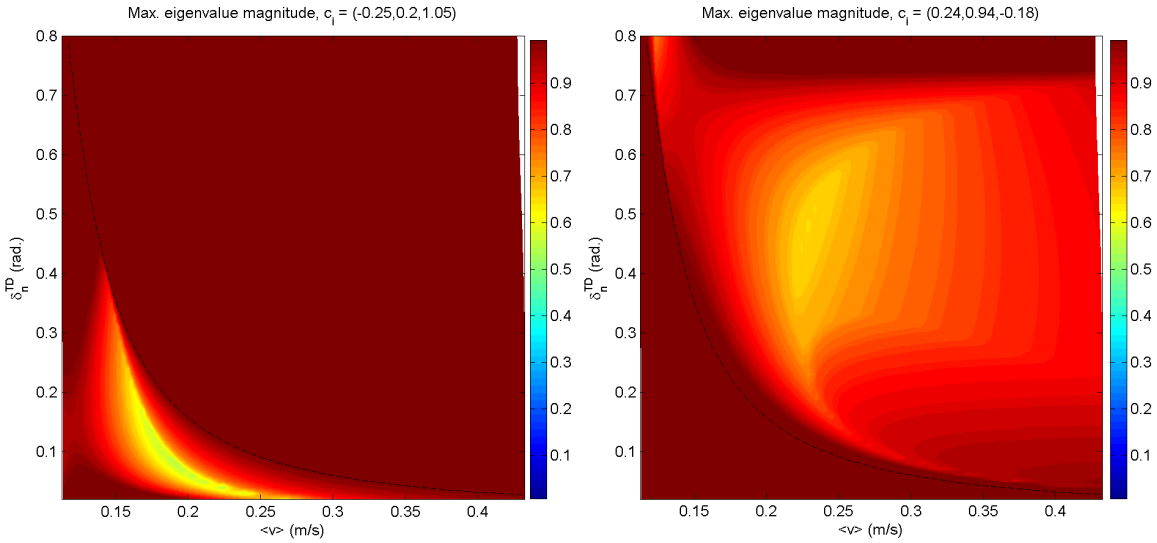

Figure 5.3: Contour plots of the maximum eigenvalue magnitude with leg actuation and leg angle control, for the surface of periodic gaits previously identified in Figure 5.1. The left and right panels illustrate results with $c_i = (-0.25, 0.2, 1.05)$ and $c_i = (0.24, 0.94, -0.18)$ respectively. The dashed line in each panel identifies the gait family for $l_{dev} = 0$. All other parameters are held at values characteristic of the cockroach *Blaberus discoidalis*, as identified previously.

We illustrate the changes in gait stability obtained through our combined strategy in the panels of Figure 5.3. For $l_{dev} > 0$, our choice of $c_i = (-0.25, 0.2, 1.05)$ produces a range of stable gaits similar to that obtained by leg actuation with a fixed leg touch-down angle. As is evident from Figure 5.3a and summarized in Table 5.1, both the number of gaits stabilized and the relative stability for our combined leg actuation and leg angle control strategy is less than that obtained for leg actuation with a fixed leg touch-down angle. Calculating the maximum eigenvalue magnitude for each gait of the gait surface with $c_i = (0.24, 0.94, -0.18)$ reveals that this set of c_i values is able to stabilize a large fraction of those gaits that were previously unstable with $l_{dev} < 0$. While it would appear

Table 5.1: Gait stability for leg actuation and combined strategies

	All l_{dev}	$l_{dev} > 0$		$l_{dev} < 0$	
	% Gaits Stabilized	% Gaits Stabilized	Mean Max. $\|\lambda\|$ (Stable Gaits)	% Gaits Stabilized	Mean Max. $\|\lambda\|$ (Stable Gaits)
Leg Actuation:					
$c_i = (0,0,1)$	24.8	70.5	0.75 ± 0.16	0	*NA*
Leg Actuation + Angle Control:					
$c_i = (-0.25, 0.2, 1.05)$	21.5	60.1	0.86 ± 0.11	0	*NA*
$c_i = (0.24, 0.94, -0.18)$	57.7	0	*NA*	89.0	0.85 ± 0.08

that the gaits stabilized for $l_{dev} > 0$ are generally more stable than those stabilized for $l_{dev} < 0$, both sets of gaits share eigenvalues of a similar magnitude (on the order of 0.85). As such, all gaits stabilized via leg actuation and leg angle control will recover relatively slowly from small external perturbations.

Comparison of our stability results for the combined strategy with those obtained from leg actuation alone are a bit misleading, considering that the gaits for the leg actuation strategy and a fixed leg touch-down angle are only *partially* asymptotically stable, due to neutral stability in the leg touch-down angle. In contrast, the gaits identified for the combined strategy are *completely* asymptotically stable and are therefore able to recover from any appropriately small perturbation. The evidenced decrease in gait stability is due largely to coupling that occurs between the strategies. For example, a change in the leg touch-down angle affects the initial leg compression velocity $\dot{\zeta} = v_n^{TD} \cos(\beta_n^{TD} - \delta_n^{TD})$, which will therefore result in a change in the work done during the stance phase $W = \int_0^t k(l(t) - \zeta)\dot{\zeta} dt$. While the coupling between the strategies does not preclude attaining completely asymptotically stable gaits, it does appear to slightly reduce the combined effectiveness, as compared to individual control strategies.

5.3.2 Gait robustness to energetic perturbations

Our gait stability results provide insight into how quickly a periodic orbit will recover from small perturbations. However, these local stability results do not necessarily predict how well gaits will recover from larger perturbations that may move the system outside of the range for which the local Poincaré map has relevance. As a result, we also conduct simulations of periodic gaits subjected to lateral impulses. These simulations are utilized to determine the range of perturbations from which the system can recover for both the leg actuation protocol with a fixed leg touch-down angle and the leg actuation protocol with leg angle control.

Perturbations are applied in numerical simulations in a manner representative of the perturbation experiments of Jindrich and Full [24]. In these experiments, lateral impulsive perturbations were applied to running cockroaches via a roach-mounted device that utilized chemical propellants to accelerate a small ball bearing. The experimental apparatus and the resulting applied force profile from the experimental work are illustrated in Fig. 5.4. Perturbations applied in numerical simulations employ a piecewise linear approximation of the force profile to produce an impulse in the lateral direction. The perturbation force profile of Fig. 5.4 is applied beginning at an instant $t_{des}/8$ into a left stance phase and lasts for 0.004s. Perturbation force magnitudes are varied to impart impulses up to 85% of the linear momentum of system, similar to those applied in experiment, with the peak force occurring 0.0029s after the perturbation begins. A representative example of gait recovery in one of these perturbation simulations, characteristic of leg actuation and leg angle control, is illustrated in the bottom row of Fig.

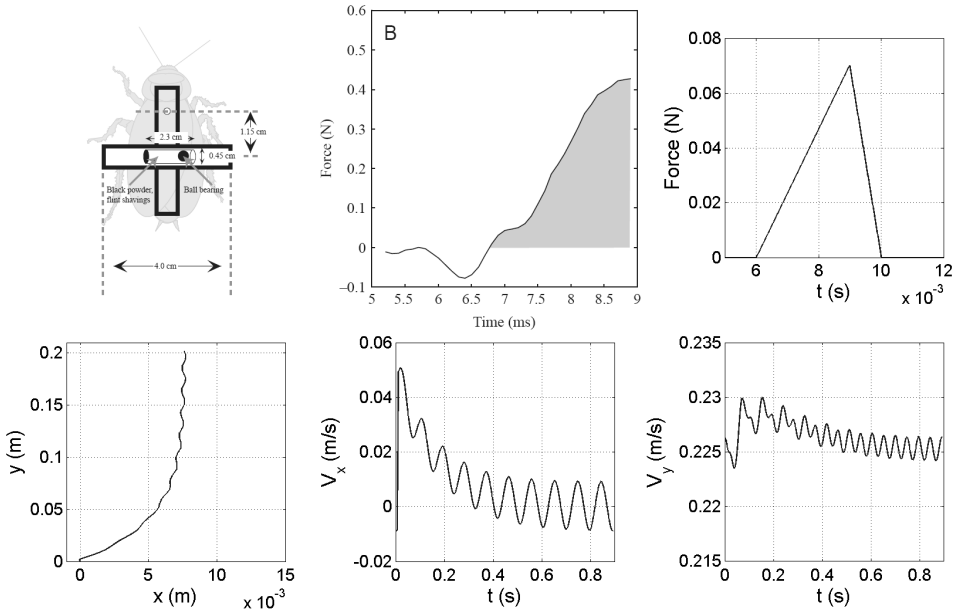

Figure 5.4: Impulse perturbation formulation and recovery from an external perturbation. (a-b) Experimental perturbation impulse apparatus and associated lateral force produced [24]. (c) Piecewise-linear approximation of the applied perturbation force for an impulsive perturbation of 25% of the linear momentum for an average speed of 0.225 m/s. (d-f) Recovery of a periodic gait $(v_n^{TD}, \delta_n^{TD}, \beta_n^{TD}) = (0.2265, 0.04, 1)$ in response to the impulsive perturbation, with $v_{des} = 0.2251$ m/s, $t_{des} = 0.0480$ s. All other model parameters are set to values characteristic of *Blaberus discoidalis* as described in the text.

5.4. In this instance, the unperturbed gait corresponds to locomotion at the preferred speed of the insect (0.225 m/s). A perturbation impulse of 25% of the linear momentum of the model is applied during the first stance. While the perturbation causes the system to deviate from the periodic orbit, it appears to recover the periodic gait within eleven stance phases after the perturbation.

Perturbation simulations are subsequently conducted for a gait family for each of the control strategies: leg actuation with a fixed leg touch-down angle and leg actuation

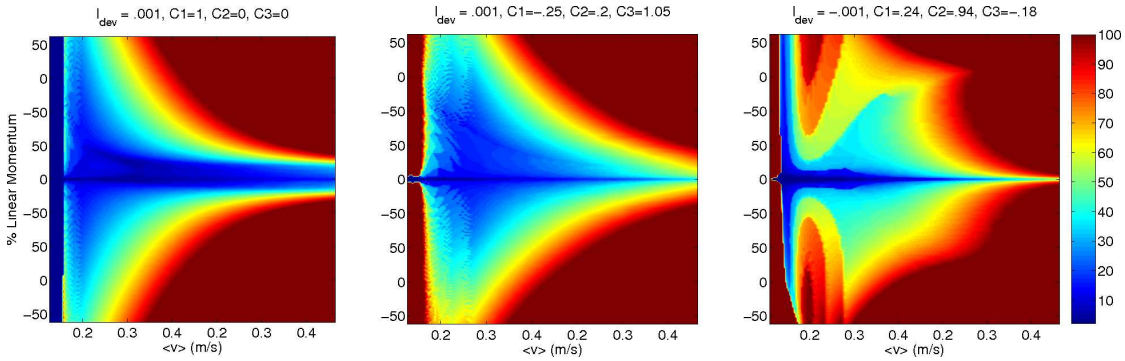

Figure 5.5: Contour plots of the number of stance phases required for periodic gaits to recover from impulse perturbations of up to 85% of the linear momentum of the point mass. (a) Recovery with actuation and fixed leg touch-down protocol. (b) Recovery with actuation and leg angle control ($l_{dev} > 0$). (c) Recovery with actuation and leg angle control ($l_{dev} < 0$).

with leg angle control. The maximum impulsive perturbation applied at each forward speed is 85% of the linear momentum of the system. The lateral perturbation force is applied in either the positive or negative direction; signs of the perturbation percentages in Fig. 5.5 reflect the direction of the perturbation. In each perturbation simulation the perturbation is applied during the left stance phase at $t_{des}/8$. At the end of each stance phase, the percent deviation from the original periodic gait is computed for all state variables. The number of steps required (up to 100) for all state variables to return and stay within 1% of the original periodic gait is subsequently recorded.

Comparison of our perturbation recovery results for the combined control strategy for ($l_{dev} < 0$) with those of ($l_{dev} > 0$) shows that it requires a larger number of steps for the model to recover when ($l_{dev} < 0$) even though the eigenvalues are similar. The eigenvalues no longer accurately predict recovery since the perturbations are outside the linear range of the Poincaré map. Longer recovery time for ($l_{dev} < 0$) can be attributed

Table 5.2: Gait surface recovery from external perturbations for leg actuation and combined strategies

	Percent recovered (stable gaits)	Recovery rate (number of steps)
Leg Actuation:		
$(l_{dev}, c_i) = (0.001, 1, 0, 0)$	76.3	38.4 ± 23.7
Leg Actuation + Leg Angle Control:		
$(l_{dev}, c_i) = (0.001, -0.25, 0.2, 1.05)$	80.5	44.2 ± 22.5
$(l_{dev}, c_i) = (-0.001, 0.24, 0.94, -0.18)$	83.5	56.4 ± 25.1

to the destabilizing effect it has on velocity as explained earlier. The leg touch down angle control law however has sufficient control authority to overcome this instability. Combined leg actuation and leg angle control with ($l_{dev} > 0$) may be considered the better strategy since we obtain complete asymptotic stability with a lower number of steps for recovery compared to the ($l_{dev} < 0$) case.

Chapter 6 – Conclusions

The lateral leg spring (LLS) model has been shown to accurately represent horizontal plane locomotion characteristics of sprawled posture insects such as the cockroach Blaberus discoidalis. While passively stable periodic gaits result from employing a constant leg touch-down angle for this model, utilizing a similar protocol for point mass model of locomotion in three dimensions produces only unstable periodic gaits. The previous LLS models are only partially asymptotically stable since they cannot recover from perturbations in mass center velocity and leg touch down angle. Further, previous LLS models have not addressed leg motion during the swing phase. In the leg angle control work, we develop a simple control law that prescribes variations in the leg touch-down angle in response to external perturbations. The leg swing protocols we develop prescribe the angular velocity of the swing leg relative to the body in a feedforward manner, yielding natural variations in the leg touch down angle in response to perturbations away from a periodic orbit. These leg control mechanisms provide control authority in re-orienting system momentum thus improving stability and robustness of previous LLS models. We also introduce energy variations to the LLS model enabling recovery in mass center velocity. Finally we combine leg angle control with energy variations for the point mass LLS model, obtain complete asymptotic stability in body coordinates and examine the basin of stability of our model in response to energetic perturbations of the type experimentally imparted on running cockroaches. The leg angle control,

leg swing and energy variation protocols developed are intended to be consistent with neural activity and muscle activation of running cockroaches.

We have developed a leg touch-down control law for horizontal plane locomotion, based upon linear state feedback principles applied to the Poincaré map of the system. Dependence of the control law on the heading angle is removed by considering consecutive iterates of the Poincaré map and using the heading angle mapping. The resulting leg touch-down protocol depends solely upon leg angles of the previous stance phase and a desired leg touch-down angle. Incorporating the control law results in a model that combines the stabilizing effect of preflexes with low level neural control that may be responsible for leg touch-down angle changes evidenced experimentally in response to external perturbations. Periodic gait stability is analytically computed by examining the eigenvalues of the single stance phase Poincaré map. We examine stability variations as a function of the parameters of the control law and perform numerical simulations to determine the effectiveness of the control law in the presence of significant external perturbations to the touch-down heading angle.

For the point mass case, we find bounds on control law parameters that ensure stability, and show that periodic gait stability can be improved from the nominal, fixed leg touch-down angle protocol. Additionally, the control law can be used to stabilize previously unstable periodic gaits through appropriate choice of the control law parameters. When subjected to an external perturbation in the heading angle, we find that gaits stabilize back to the original gait utilizing relatively small changes in leg touch-down angles. Systematic investigation of the recovery of each periodic gait of the gait family in response to a range of perturbations in the heading angle reveals that the controlled system

maintains a basin of stability similar in size to that of the fixed leg touch-down protocol. Recovery rates, when viewed over the entire speed range, are generally better for the controlled system. As well, previously unstable gaits can not only be stabilized through application of the control, but also exhibit relatively large basins of stability. The control law is also shown, via numerical simulation, to improve gait stability, basin of stability, and recovery rates for the rigid body case ($d \neq 0$).

In our legswing work, the LLS model for lateral plane locomotion is extended through the development of a leg recirculation policy. This protocol prescribes the angular velocity of the leg during the swing phase in a feedforward manner, similar to the functionality evidenced experimentally for cockroaches running over rough terrain [52]. The resulting model combines the stabilizing effect of preflexes, as represented by the effective elastic leg, with low level neural control governing leg motion during the swing phase. Incorporating the protocol produces natural variations in the leg touch-down angle in response to external perturbations. A family of periodic gaits is computed for the model by varying the desired swing phase duration and gait stability is computed analytically from the single-stance Poincaré map. Variations in gait stability are analyzed as a function of a desired angular velocity of the swing leg at touch-down, $\dot{\beta}_{des}$, and numerical simulations are employed to determine the performance of the protocol in the presence of external perturbations in the velocity heading angle.

Specifically, based upon results from previous experimental and analytical studies, this investigation examines the following three hypotheses:

H1 *Feedforward specification of the swing-leg angular velocity can produce stable periodic gaits*

H2 *Swing-leg angular velocity and acceleration at leg touch-down provide control authority to reorient system momentum in response to perturbations, thereby enabling selection of gait stability and robustness characteristics*

H3 *Gait stability and robustness is improved via leg retraction at leg touch-down*

Results for both the point mass and rigid body models clearly support our first two hypotheses and demonstrate the importance of leg recirculation in the LLS template. Inclusion of feedforward leg recirculation in the template yields a family of periodic gaits, whose stability and robustness characteristics depend upon the shape of the leg recirculation profile employed. However, gait stability and robustness results for the point mass and rigid body models provided mixed support for the final hypothesis that leg retraction at touch-down improves *both* gait stability and robustness to external perturbation. For the point mass case, both gait stability and robustness are improved by retracting the leg at touch-down ($\dot{\beta}_{des} > 0$). Increased retraction rates can move the saddle node bifurcation to lower average forward velocities, thereby stabilizing previously unstable gaits. While the basin of stability remains much smaller than that obtained for the original LLS model with a fixed leg touch-down angle, recovery rates evidenced with leg recirculation are generally better. Simulation results for the rigid body model with leg recirculation suggest that gait stability is improved for leg retraction ($\dot{\beta}_{des} > 0$) at low and high speeds while leg protraction ($\dot{\beta}_{des} < 0$) improves stability for gaits in the middle of the speed range. Investigation into recovery from external perturbations reveals that while the recovery rate is generally better for leg protraction at touch-down, the basin of stability is larger for cases where the leg is retracting at touch-down. As a result,

while leg retraction appears to provide a slightly larger basin of stability, leg protraction provides improved stability for gaits near the middle of the speed range considered. Ultimately, the choice of a touch-down leg angular velocity must balance consideration of both gait stability and robustness to external perturbation.

Because stability basins for both the point mass and rigid body models with the original leg recirculation protocol are small in comparison to the range of perturbations from which the cockroach is able to recover [24], the angular velocity profiles during swing are compared to those observed experimentally for running cockroaches. Based on this comparison, higher order frequencies are added into the recirculation protocol to yield lower leg angular accelerations near $t = t_{des}$. Gait recovery simulations conducted for this modified recirculation protocol demonstrate a basin of stability double that obtained previously, with recovery rates similar to those demonstrated for the original protocol. The larger basin of stability evidenced for the refined protocol suggests that feedforward control of the leg angular velocity may represent a viable control strategy for the insect.

While leg protraction ($\dot{\beta}_{des} < 0$) improves gait stability for a large range of gaits for the rigid body model with $d = 0.002$, examination of locomotion data for the cockroach reveals that, on average, each leg is retracting at touch-down. As a result, one avenue for future work includes examination of gait stability and robustness for a multi-legged rigid body model, with leg recirculation protocols developed and implemented for each individual leg. A limitation of the bipedal LLS template has been its inability to produce forces capable of effectively reproducing the magnitude of yawing motions exhibited by the insect. This results in reduced control authority for the body angular velocity, which represents the largest eigenvalue for the rigid body model. We hypothesize that larger,

net effective forces produced by a multi-legged model might better stabilize the body angular velocity such that leg retraction at touch-down will help improve gait stability.

The LLS model augmented with leg angle control or legswing protocols is still energetically conservative thus yielding only partial asymptotic stability relative to mass center velocity. In our leg actuation work, we investigate the performance of a prescribed feedforward leg actuation strategy developed to approximate the feedforward muscle activation utilized by insects when running over rough terrain thus destroying energy conservation. We vary the force free length ($l(t)$) of the spring in a prescribed feedforward manner, ($l(t) = l_0 - l_{dev}\sin(\frac{\pi t}{t_{des}})$). Our leg actuation work is limited to the point mass model. A surface of periodic gaits with leg actuation and a fixed leg touchdown angle were obtained numerically. The numerical eigenvalues were computed for this gait surface with a fixed leg touch down protocol. Stable gaits were obtained for $l_{dev} > 0$ and unstable gaits were obtained for $l_{dev} < 0$ as expected. We obtain completely asymptotically stable gaits by combining our leg actuation and leg angle control protocols. We modify the stability of previously stable gaits and stabilize previously unstable gaits ($l_{dev} < 0$ gaits) by choosing c_i values appropriately. Slower eigen values were obtained for the completely asymptotically stable combined leg actuation and leg angle control strategy compared to the partially asymptotically stable leg actuation and fixed leg touch down strategy. This can be attributed to the coupling that occurs for the combined control strategy which results in slower eigen values. This coupling that occurs for the combined control strategy however does not preclude us from attaining completely asymptotically stable gaits in body coordinates.

Robustness of this energetically non conservative point mass model to external en-

ergetic impulse perturbations as done in experiments on running cockroaches were examined for the partially asymptotically stable model with a fixed leg touch down protocol and leg actuation. Similarly, robustness of the completely asymptotically stable point mass model with combined leg angle control and leg actuation was also examined. These Robustness studies were carried out for the gait family defined by $l_{dev} = 0.001$m. The basin of stability for the completely asymptotically stable model incorporating combined leg actuation and leg angle control remained similar to that of the partially asymptotically stable model with leg actuation and a fixed leg touch down protocol. The perturbations imparted were outside the linear range of the Poincaré map. Finally we carry out similar robustness studies for the gait family defined by $l_{dev} = -0.001$m, which was unstable with the fixed leg touch down control strategy. Incorporating leg angle control with appropriate c_i values yielded a large basin of stability for this previously unstable gait family. The longer recovery time observed for $l_{dev} < 0$ can be attributed to the destabilizing effect it has on velocity as explained in the text.

The energetic control approach proposed and analyzed here also adapts easily to mechanical robot designs due to the essentially feedforward nature of the actuation protocol and the simplicity of the sensing requirements. Furthermore, the controller can be implemented in a simple mechanism and can easily be extended to deal with the mechanical losses in the system. This approach to regulating system energy also provides an alternative to existing actuation schemes, and its analytical tractability may lead to improved stability properties and move us closer to designing robots that can safely run over unstructured terrain. In the future we plan to combine leg recirculation with leg actuation and obtain completely asymptotically stable gaits in body coordinates while

specifying a feedforward swing protocol. We also plan to include frictional and energy losses in the model, investigate these control protocols on inclines and embed them in more anchored models.

Bibliography

[1] R. McN. Alexander. *Elastic Mechanisms in Animal Movement*. Cambridge University Press, Cambridge, 1988.

[2] R. Altendorfer, D. Koditschek, and P. Holmes. Stability analysis of legged locomotion models by symmetry-factored return maps. *Intl. Journal of Robotics Research*, 23(11):979–1000, 2004.

[3] U. Bassler and A. Buschges. Pattern generation for stick insect walking movements - multisensory control of a locomotor program. *Brain Research Rev.*, 27:65–88, 1998.

[4] R. Blickhan. The spring-mass model for running and hopping. *J. Biomechanics*, 11/12:1217–1227, 1989.

[5] R. Blickhan and R.J. Full. Similarity in multi-legged locomotion: bouncing like a monopode. *J. Comp. Physiol. A*, 173:509–517, 1993.

[6] M. Burrows. *The Neurobiology of an Insect Brain*. Oxford University Press, Oxford New York Tokyo, 1996.

[7] M. Burrows and M.V.S. Siegler. Spiking local interneurons mediate local reflexes. *Science*, 217:650–652, 1982.

[8] J. Camhi and E. Johnson. High frequency steering maneuvers mediated by tactile cues: antennal wall-following in the cockroach. *J. Exp. Biology*, 202:631–643, 1999.

[9] J. Cham and M. Cutkosky. Dynamic stability of open-loop hopping. *ASME J. of Dynamics Systems, Meas. and Control*, to appear, 2007.

[10] J. Dean and H. Cruse. Evidence for the control of velocity as well as position in leg protraction and retraction by the stick insect. *Exp. Brain Res.*, 15:263–274, 1986.

[11] F. Delcomyn. Walking robots and the central and peripheral control of locomotion in insects. *Autonomous Robots*, 7:259–270, 1999.

[12] D. Dudek and R. Full. Passive mechanical properties of legs from running insects. *J. Exp. Biol.*, 209:1502–1515, 2006.

[13] C. Fourtner and C. Kaars. Anatomy of the central nervous system and its usefulness as a model for neurobiology. In Masler E. Huber, I. and B.R. Rao, editors, *Cockroaches as models for neurobiology: applications in biomedical research, Volume I*, pages 65–87. CRC Press, Boca Raton, 1990.

[14] R. Full, K. Autmn, J. Chung, and A. Ahn. Rapid negotiation of rough terrain by the death-head cockroach. *American Zoologist*, 38:81A, 1998.

[15] R.J. Full, R. Blickhan, and L.H. Ting. Leg design in hexpedal runners. *J. Exp. Biol.*, 158:369–390, 1991.

[16] R.J. Full and D.E. Koditschek. Templates and anchors: neuromechanical hypotheses of legged locomotion on land. *J. Exp. Biol.*, 202:3325–3332, 1999.

[17] R.J. Full and M.S. Tu. Mechanics of six-legged runners. *J. Exp. Biol.*, 148:129–146, 1990.

[18] R. Ghigliazza, R.M. Altendorfer, P. Holmes, and D. Koditschek. A simply stabilized running model. *SIAM Journal on Applied Dynamical Systems*, 2(2):187–218, 2003.

[19] D. I. Goldman, T. S. Chen, D. M. Dudek, and R. J. Full. Dynamics of rapid vertical climbing in a cockroach reveals a template. *Journal of Experimental Biology*, 209:2990–3000, 2006.

[20] P. Holmes, R.J. Full, D. Koditschek, and J. Guckenheimer. Dynamics of legged locomotion: models, analysis, and challenges. *SIAM Review*, 48(2):207–304, 2006.

[21] S. Hooper, C. Guschlbauer, M. Blumel, P. Rosenbaum, M. Gruhn, T. Akay, and A. Buschges. Neural control of unloaded leg posture and of leg swing in stick insect, cockroach, and mouse differs from that in larger animals. *J. of Neuroscience*, 29(13):4109–4119, 2009.

[22] A. Hurwitz. On the conditions under which an equation has only roots with negative real parts. In R. Ballman and R. Kalaba, editors, *Selected papers on mathematical trends in control theory*. Dover, New York, 1964.

[23] D. Jindrich. *Stability, maneuverability, and control of rapid hexapedal locomotion*. Univ. California, Berkeley, 2001.

[24] D. Jindrich and R.J. Full. Dynamic stabilization of rapid hexapedal locomotion. *J. Exp. Biol.*, 205:2803–2823, 2002.

[25] R. Kram, B. Wong, and R.J. Full. Three-dimensional kinematics and limb kinetic energy of running cockroaches. *J. Exp. Biol.*, 200:1919–1929, 1997.

[26] T.M. Kubow and R.J. Full. The role of the mechanical system in control: a hypothesis of self-stabilization in hexapedal runners. *Phil. Trans. Roy Soc. Lond. B*, 354:849–861, 1999.

[27] R. Kukillaya and P. Holmes. A hexapedal jointed-leg model for insect locomotion in the horizontal plane. *Biol. Cybernetics*, 97(5-6):379–395, 2007.

[28] A. Kuo. Stabilization of lateral motion in passive dynamic walking. *Intl. Journal of Robotics Research*, 18(9):917–930, 1999.

[29] G.S. Larsen, S.F. Frazier, and S.N. Zill. The tarso-pretarsal chordotonal organ as an element in cockroach walking. *J. Comp. Physiol. A*, 180:683–700, 1997.

[30] H. Lee, R. Cooper, B. Mika, D. Clayton, R. Garg, J. Gonzalez, S.B. Vinson, S. Khatri, and H. Liang. Polymeric sensors to monitor cockroach locomotion. *IEEE Sensors Journal*, 7(12):1698–1702, 2007.

[31] J. Lee, A. Lamperski, J. Schmitt, and N. Cowan. Task-level control of the lateral leg spring model of cockroach locomotion. *Lecture notes in control and information sciences*, 340:167–188, 2006.

[32] T. McGeer. Passive bipedal running. *Proc. Roy. Soc. Lond.*, B 240:107–134, 1990.

[33] M. Raibert. *Legged Robots that Balance*. MIT Press, Cambridge, MA, 1986.

[34] S. Revzen, D. Koditschek, and R. Full. Testing feedforward control models in rapid running insects using large perturbations. *Integr. Comp. Biol.*, 45:1061, 2005.

[35] A. Ruina. Non-holonomic stability aspects of piecewise holonomic systems. *Reports on Mathematical Physics*, 42(1/2):91–100, 1998.

[36] U. Saranli, M. Buehler, and D. Koditschek. Rhex: A simple and highly mobile hexapod robot. *Intl. Journal of Robotics Research*, 20(7):616–631, 2001.

[37] J. Schmitt. Simple feedback control of running. *Lecture notes in control and information sciences*, 340:361–381, 2006.

[38] J. Schmitt. A simple stabilizing control for sagittal plane locomotion. *J. Comp. Nonlinear Dyn.*, 1(4):348–357, 2006.

[39] J. Schmitt. A simple stabilizing control for sagittal plane locomotion. *J. Computational and Nonlinear Dynamics*, 1:348–357, 2006.

[40] J. Schmitt. Incorporating energy variations into controlled sagittal plane locomotion dynamics. In *Proc. of the Intl. Design Engineering and Technical Conf. IDETC07*, 2007.

[41] J. Schmitt, M. Garcia, R. Razo, P. Holmes, and R.J. Full. Dynamics and stability of legged locomotion in the horizontal plane: A test case using insects. *Biological Cybernetics*, 86(5):343–353, 2002.

[42] J. Schmitt and P. Holmes. Mechanical models for insect locomotion: Dynamics and stability in the horizontal plane – Application. *Biological Cybernetics*, 83(6):517–527, 2000.

[43] J. Schmitt and P. Holmes. Mechanical models for insect locomotion: Dynamics and stability in the horizontal plane – Theory. *Biological Cybernetics*, 83(6):501–515, 2000.

[44] J. Schmitt and P. Holmes. Mechanical models for insect locomotion: Stability and parameter studies. *Physica D*, 156(1-2):139–168, 2001.

[45] W.J. Schwind and D.E. Koditschek. Characterization of monopod equilibrium gaits. Preprint, Dept. of EECS, University of Michigan, 1998.

[46] W.J. Schwind and D.E. Koditschek. Approximating the stance map of a 2 dof monoped runner. *J. Nonlinear Science*, 10(5):533–568, 2000.

[47] J. Seipel and P. Holmes. Running in three dimensions: analysis of a point-mass sprung-leg model. *Intl. J. Robotics Research*, 24(8), 2005.

[48] J. Seipel and P. Holmes. A simple model for clock-actuated legged locomotion. *Regular and Chaotic Dynamics*, 12(5):502–520, 2007.

[49] J. Seipel, P. Holmes, and R. Full. Dynamics and stability of insect locomotion: a hexapedal model for horizontal plane motions. *Biol. Cybern.*, 91:76–90, 2004.

[50] A. Seyfarth, H. Geyer, M. Gunther, and R. Blickhan. A movement criterion for running. *J. of Biomechanics*, 35:649–655, 2002.

[51] A. Seyfarth, H. Geyer, and H. Herr. Swing-leg retraction: a simple control model for stable running. *J. Exp. Biology*, 206:2547–2555, 2003.

[52] S. Sponberg and R. Full. Neuromechanical response of musculo-skeletal structures in cockroachs during rapid running on rough terrain. *J. Exp. Biol.*, 211:433–446, 2008.

[53] L. Ting and J. Macpherson. A limited set of muscle synergies for force control during a postural task. *J. Neurophys.*, 93:609–613, 2005.

[54] L.H. Ting, R. Blickhan, and R.J. Full. Dynamic and static stability in hexapedal runners. *J. Exp. Biol.*, 197:251–269, 1994.

[55] A. Tryba and R. Ritzmann. Multi-joint coordination during walking and foothold searching in the blaberus cockroach ii: extensor motor pattern. *J. Neurophysiol.*, 83:3337–3350, 2000.

[56] J.T. Watson and R.E. Ritzmann. Leg kinematics and muscle activity during treadmill running in the cockroach, blaberus discoidalis: I. slow running. *J. Comp. Physiol. A.*, 182:11–22, 1998.

[57] S.N. Zill. Mechanoreceptors: exteroceptors and proprioceptors. In I. Huber, E. Masler, and B.R. Rao, editors, *Cockroaches as models for neurobiology: applications in biomedical research, Volume II*, pages 247–267. CRC Press, Boca Raton, 1990.

APPENDICES

Appendix A – Chapter 3 Appendix

The eigenvalues of the single stance phase Poincaré map with leg touch-down angle control are determined from $\det(\lambda I - Df) = 0$, where I is the identity matrix and Df is the Jacobian matrix of equation (3.10). Evaluating the determinant yields

$$\left[\left(\lambda - 1 + \frac{\partial \Delta\psi}{\partial \delta_n^{TD}}\right)\left(\lambda + c_2\frac{\partial \Delta\psi}{\partial \beta_n^{TD}} - (c_1 - c_2)\right) - c_2\frac{\partial \Delta\psi}{\partial \delta_n^{TD}}\left(2 + \frac{\partial \Delta\psi}{\partial \beta_n^{TD}}\right)\right] * (\lambda - 1) = 0\,. \tag{A.1}$$

Expanding the interior of this expression and collecting like terms yields the characteristic equation presented in (3.11).

The characteristic equation can be further simplified by examining the relationship between $\frac{\partial \Delta\psi}{\partial \delta_n^{TD}}$ and $\frac{\partial \Delta\psi}{\partial \beta_n^{TD}}$. The expression for the leg angle swept during a given stance phase is developed in [43], as

$$\Delta\psi = \int_{\zeta_b}^{l} \frac{2 v_n^{TD} l \sin(\beta_n^{TD} - \delta_n^{TD}) d\zeta}{\zeta\sqrt{((v_n^{TD})^2 - k/m(\zeta - l)^2)\zeta^2 - l^2 (v_n^{TD})^2 \sin^2(\beta_n^{TD} - \delta_n^{TD})}} \tag{A.2}$$

where ζ_b is the largest positive root of the equation

$$m l^2 (v_n^{TD})^2 \sin^2(\beta_n^{TD} - \delta_n^{TD}) + k(\zeta_b - l)^2 \zeta_b^2 - m\zeta_b^2 (v_n^{TD})^2 \;=\; 0\,. \tag{A.3}$$

Defining the integrand of (A.2) as

$$f(\zeta,\delta_n^{TD},\beta_n^{TD}) = \frac{2v_n^{TD}l\sin(\beta_n^{TD}-\delta_n^{TD})}{\zeta\sqrt{((v_n^{TD})^2-k/m(\zeta-l)^2)\zeta^2-l^2(v_n^{TD})^2\sin^2(\beta_n^{TD}-\delta_n^{TD})}} = \frac{g}{h} \quad (A.4)$$

Leibniz's rule can be used to evaluate the expressions

$$\frac{\partial\Delta\psi}{\partial\delta_n^{TD}} = \int_{\zeta_b}^{l}\frac{\partial f(\zeta,\delta_n^{TD},\beta_n^{TD})}{\partial\delta_n^{TD}}d\zeta - f(\zeta_b,\delta_n^{TD},\beta_n^{TD})\frac{\partial\zeta_b}{\partial\delta_n^{TD}} \quad (A.5)$$

$$\frac{\partial\Delta\psi}{\partial\beta_n^{TD}} = \int_{\zeta_b}^{l}\frac{\partial f(\zeta,\delta_n^{TD},\beta_n^{TD})}{\partial\beta_n^{TD}}d\zeta - f(\zeta_b,\delta_n^{TD},\beta_n^{TD})\frac{\partial\zeta_b}{\partial\beta_n^{TD}}\,. \quad (A.6)$$

The development of any relationship between $\frac{\partial\Delta\psi}{\partial\delta_n^{TD}}$ and $\frac{\partial\Delta\psi}{\partial\beta_n^{TD}}$ therefore requires computing $\frac{\partial f(\zeta,\delta,\beta)}{\partial\delta_n^{TD}}$, $\frac{\partial f(\zeta,\delta,\beta)}{\partial\beta_n^{TD}}$, $\frac{\partial\zeta_b}{\partial\delta_n^{TD}}$ and $\frac{\partial\zeta_b}{\partial\beta_n^{TD}}$. We proceed by first constructing expressions for $\frac{\partial f(\zeta,\delta,\beta)}{\partial\delta_n^{TD}}$ and $\frac{\partial f(\zeta,\delta,\beta)}{\partial\beta_n^{TD}}$, which requires evaluating the following partial derivatives

$$\frac{\partial g}{\partial\delta_n^{TD}} = -2v_n^{TD}l\cos(\beta_n^{TD}-\delta_n^{TD}) \quad (A.7)$$

$$\frac{\partial g}{\partial\beta_n^{TD}} = 2v_n^{TD}l\cos(\beta_n^{TD}-\delta_n^{TD}) = -\frac{\partial g}{\partial\delta_n^{TD}} \quad (A.8)$$

$$\frac{\partial h}{\partial\delta_n^{TD}} = \frac{\zeta l^2(v_n^{TD})^2\sin(2(\beta_n^{TD}-\delta_n^{TD}))}{2\sqrt{((v_n^{TD})^2-k/m(\zeta-l)^2)\zeta^2-l^2(v_n^{TD})^2\sin^2(\beta_n^{TD}-\delta_n^{TD})}} \quad (A.9)$$

$$\frac{\partial h}{\partial\beta_n^{TD}} = \frac{-\zeta l^2(v_n^{TD})^2\sin(2(\beta_n^{TD}-\delta_n^{TD}))}{2\sqrt{((v_n^{TD})^2-k/m(\zeta-l)^2)\zeta^2-l^2(v_n^{TD})^2\sin^2(\beta_n^{TD}-\delta_n^{TD})}} \quad (A.10)$$

$$= -\frac{\partial h}{\partial\delta_n^{TD}}\,. \quad (A.11)$$

Using the above relations in the quotient rule yields the desired expressions for the

partial derivatives

$$\frac{\partial f(\zeta,\delta_n^{TD},\beta_n^{TD})}{\partial \beta_n^{TD}} = \frac{\frac{\partial g}{\partial \beta_n^{TD}}h - \frac{\partial h}{\partial \beta_n^{TD}}g}{h^2} \quad (A.12)$$

$$= \frac{-\frac{\partial g}{\partial \delta_n^{TD}}h + \frac{\partial h}{\partial \delta_n^{TD}}g}{h^2} \quad (A.13)$$

$$= -\frac{\partial f(\zeta,\delta_n^{TD},\beta_n^{TD})}{\partial \delta_n^{TD}}\,. \quad (A.14)$$

Evaluating $\frac{\partial \zeta_b}{\partial \delta_n^{TD}}$ and $\frac{\partial \zeta_b}{\partial \beta_n^{TD}}$ requires implicit differentiation of (A.3), yielding

$$\frac{\partial \zeta_b}{\partial \beta_n^{TD}} = -\frac{ml^2(v_n^{TD})^2\sin(\beta_n^{TD}-\delta_n^{TD})\cos(\beta_n^{TD}-\delta_n^{TD})}{k\zeta_b(\zeta_b-l)(2\zeta_b-l)-m\zeta_b(v_n^{TD})^2} \quad (A.15)$$

$$\frac{\partial \zeta_b}{\partial \delta_n^{TD}} = \frac{ml^2(v_n^{TD})^2\sin(\beta_n^{TD}-\delta_n^{TD})\cos(\beta_n^{TD}-\delta_n^{TD})}{k\zeta_b(\zeta_b-l)(2\zeta_b-l)-m\zeta_b(v_n^{TD})^2} = -\frac{\partial \zeta_b}{\partial \beta_n^{TD}} \quad (A.16)$$

The relationship between $\frac{\partial \Delta\psi}{\partial \delta_n^{TD}}$ and $\frac{\partial \Delta\psi}{\partial \beta_n^{TD}}$ is established by substituting (A.14) and (A.16) into (A.5), which yields

$$\frac{\partial \Delta\psi}{\partial \delta_n^{TD}} = -\frac{\partial \Delta\psi}{\partial \beta_n^{TD}}\,. \quad (A.17)$$

Utilizing this result in the characteristic equation given by (3.11) yields the simplified single stance phase characteristic equation presented in (3.12).

Having computed the simplified characteristic equation, it is clear that computing the eigenvalues governing gait stability requires computing $\frac{\partial \Delta\psi}{\partial \delta_n^{TD}}$. While [43] presents an analytical expression for $\Delta\psi$, the complexity of the expression precludes analytical computation of the derivatives. As in [44], the required derivatives are instead computed by approximating $\Delta\psi$ via the Schwind-Koditschek approximation [46]. This quadrature estimation method employs a linear approximation in the mean value function to ap-

proximate the integral. Using this approximation, $\Delta\psi$ is approximated as

$$\Delta\psi = \frac{2lv_n^{TD}\sin(\beta_n^{TD}-\delta_n^{TD})(l-\zeta_b)}{\hat{\zeta}\sqrt{((v_n^{TD})^2-k/m(\hat{\zeta}-l)^2)\hat{\zeta}^2-l^2(v_n^{TD})^2\sin^2(\beta_n^{TD}-\delta_n^{TD})}} \quad (A.18)$$

$$\hat{\zeta} = \frac{3\zeta_b+l}{4}. \quad (A.19)$$

We compute an approximation of $\frac{\partial\Delta\psi}{\partial\delta_n^{TD}}$ using our approximation of $\Delta\psi$ presented (A.18-A.19), simplified further as

$$\Delta\psi = \frac{p}{q} \quad (A.20)$$

$$p = 128lv_n^{TD}\sin(\beta_n^{TD}-\delta_n^{TD})(l-\zeta_b) \quad (A.21)$$

$$q = (3\zeta_b+l)\sqrt{s} \quad (A.22)$$

$$s = (16(v_n^{TD})^2-\frac{9k}{m}(\zeta_b-l)^2)(3\zeta_b+l)^2 - 256l^2(v_n^{TD})^2\sin^2(\beta_n^{TD}-\delta_n^{TD}). \quad (A.23)$$

With the expression for $\frac{\partial\zeta_b}{\partial\delta_n^{TD}}$ provided in (A.16), calculation of $\frac{\partial\Delta\psi}{\partial\delta_n^{TD}}$ proceeds directly from the quotient rule

$$\frac{\partial\Delta\psi}{\partial\delta_n^{TD}} = \frac{q\frac{\partial p}{\partial\delta_n^{TD}}-p\frac{\partial q}{\partial\delta_n^{TD}}}{q^2} \quad (A.24)$$

with

$$\frac{\partial p}{\partial\delta_n^{TD}} = -128lv_n^{TD}(\cos(\beta_n^{TD}-\delta_n^{TD})(l-\zeta_b)+\frac{\partial\zeta_b}{\partial\delta_n^{TD}}\sin(\beta_n^{TD}-\delta_n^{TD})) \quad (A.25)$$

and

$$\frac{\partial q}{\partial \delta_n^{TD}} = 3\frac{\partial \zeta_b}{\partial \delta_n^{TD}}\sqrt{s} + \frac{(3\zeta_b + l)(t\frac{\partial \zeta_b}{\partial \delta_n^{TD}} - x\frac{\partial \zeta_b}{\partial \delta_n^{TD}} + uv_n^{TD}\cos(\beta_n^{TD} - \delta_n^{TD}))}{2\sqrt{s}} \quad \text{(A.26)}$$

where

$$t = 6(3\zeta_b + l)(16(v_n^{TD})^2 - \frac{9k}{m}(\zeta_b - l)^2) \quad \text{(A.27)}$$

$$u = 512l^2 v_n^{TD}\sin(\beta_n^{TD} - \delta_n^{TD}) \quad \text{(A.28)}$$

$$x = \frac{18k}{m}(\zeta_b - l)(3\zeta_b + l)^2 \,. \quad \text{(A.29)}$$

Appendix B – Chapter 4 Appendix

B.1 Analytical eigenvalue approximation for $d = 0$

Analytical investigations into gait stability provide insight into the importance of the choice of $\dot{\beta}_{des}$ in the leg recirculation protocol and serve to validate our numerical results. Analytical computation of the eigenvalues governing local gait stability first requires determination of the Poincaré map. Using conservation of energy and conservation of angular momentum about the foot placement point, in conjunction with the stance phase geometry and the leg recirculation protocol, results in the following single-stance phase Poincaré map

$$v_{n+1}^{TD} = v_n^{TD} \tag{B.1}$$

$$\delta_{n+1}^{TD} = \delta_n^{TD} + \pi - \Delta\psi - 2\beta_n^{TD} + (-1)^n \dot{\theta}_n \tau \tag{B.2}$$

$$\theta_{n+1}^{TD} = \theta_n^{TD} + \dot{\theta}_n \tau \tag{B.3}$$

$$\beta_{n+1}^{TD} = \beta_{n-1}^{LO} - \frac{\omega}{a}\left(\cos(a\tau + \phi) - \cos(\phi)\right) , \tag{B.4}$$

where $\Delta\psi$ represents the change in ψ during the stance phase. A fixed point of the mapping requires $\dot{\theta}_n = 0$ and a stance phase duration of $\tau = t_{des}$, such that $\beta_{n+1}^{TD} = \beta_{des} = \beta_n^{TD}$. A full stride map consists of the composition of the mappings for a left and right stance phase. Due to the structure of the Jacobian for $d = 0$, the full stride

eigenvalues of the symmetric periodic gaits studied are simply the square of the single stance phase eigenvalues. As a result, the analytical eigenvalues computed for the single stance phase map are squared for comparison with those determined numerically.

The Jacobian for a periodic orbit results from evaluating the partial derivatives of the single stance phase Poincaré map. While the first two rows of the resulting Jacobian follow easily from the associated derivatives of the velocity and heading angle mappings (B.1-B.2), the components of the third row are not as easily determined. Expanding the $\cos(a\tau+\phi)$ term in the leg touch-down mapping (B.4) yields

$$\beta_{n+1}^{TD} = \beta_{n-1}^{LO} - \frac{1}{a}\left[\sqrt{\omega^2 - \left(\dot{\beta}_{n-1}^{LO}\right)^2}\left(\cos(a\tau)-1\right) - \dot{\beta}_{n-1}^{LO}\sin(a\tau)\right] . \tag{B.5}$$

Evaluating the derivative of (B.5) with respect to δ_n^{TD} yields

$$\frac{\partial \beta_{n+1}^{TD}}{\partial \delta_n^{TD}} = \left[\sqrt{\omega^2 - \left(\dot{\beta}_{n-1}^{LO}\right)^2}\sin(a\tau) + \dot{\beta}_{n-1}^{LO}\cos(a\tau)\right]\frac{\partial \tau}{\partial \delta_n^{TD}} . \tag{B.6}$$

Substituting the relationship

$$\sqrt{\omega^2 - \left(\dot{\beta}_{n-1}^{LO}\right)^2} = \frac{\dot{\beta}_{des} - \dot{\beta}_{n-1}^{LO}\cos(at_{des})}{\sin(at_{des})} \tag{B.7}$$

into (B.6) and evaluating (B.6) at a fixed point (where $\tau = t_{des}$) results in the expression

$$\begin{aligned}\frac{\partial \beta_{n+1}^{TD}}{\partial \delta_n^{TD}} &= \left[\frac{\left(\dot{\beta}_{des} - \dot{\beta}_{n-1}^{LO}\cos(at_{des})\right)}{\sin(at_{des})}\sin(at_{des}) + \dot{\beta}_{n-1}^{LO}\cos(at_{des})\right]\frac{\partial \tau}{\partial \delta_n^{TD}} && \text{(B.8)}\\ &= \dot{\beta}_{des}\frac{\partial \tau}{\partial \delta_n^{TD}} . && \text{(B.9)}\end{aligned}$$

The relationship

$$\frac{\partial \beta_{n+1}^{TD}}{\partial \beta_n^{TD}} = \dot{\beta}_{des} \frac{\partial \tau}{\partial \beta_n^{TD}} \tag{B.10}$$

follows from (B.5) in a similar manner.

The resulting Jacobian is therefore

$$Df = \begin{bmatrix} 1 & 0 & 0 \\ \cdots & 1 - \frac{\partial \Delta\psi}{\partial \delta_n^{TD}} & \left(-2 - \frac{\partial \Delta\psi}{\partial \beta_n^{TD}}\right) \\ \cdots & \dot{\beta}_{des} \frac{\partial \tau}{\partial \delta_n^{TD}} & \dot{\beta}_{des} \frac{\partial \tau}{\partial \beta_n^{TD}} \end{bmatrix}, \tag{B.11}$$

where $(\cdots)$ represent terms that do not enter into the eigenvalue calculation. The map is further simplified by the relationships $\frac{\partial \Delta\psi}{\partial \beta_n^{TD}} = -\frac{\partial \Delta\psi}{\partial \delta_n^{TD}}$ and $\frac{\partial \tau}{\partial \beta_n^{TD}} = -\frac{\partial \tau}{\partial \delta_n^{TD}}$, as determined in the Section B.2, yielding the characteristic equation

$$(\lambda - 1)\left[\lambda^2 + \left(\dot{\beta}_{des} \frac{\partial \tau}{\partial \delta_n^{TD}} + \frac{\partial \Delta\psi}{\partial \delta_n^{TD}} - 1\right)\lambda + \dot{\beta}_{des} \frac{\partial \tau}{\partial \delta_n^{TD}}\right] = 0\,. \tag{B.12}$$

Conservation principles can be used to develop quadratures for τ and $\Delta\psi$ as in [43]. Because these quadratures, as presented in Section B.2, are complex incomplete elliptic integrals, the partial derivatives required to compute the gait eigenvalues are instead computed from the Schwind-Koditschek [45] approximation of the quadratures. While straightforward, the details of the approximation and the development of the required partial derivatives is left to Section B.2.

As expected, one eigenvalue, corresponding to energy conservation, remains unity for this model while the other two result from evaluation of the inner quadratic equation. Because the characteristic equation explicitly depends upon $\dot{\beta}_{des}$, the choice of the leg

angular velocity at touch-down will affect both of the remaining eigenvalues, which correspond to the leg touch-down angle and velocity heading angle. For the original LLS model, the eigenvalue corresponding to leg touch-down was neutrally stable (i.e. 1) and the velocity heading eigenvalue was $1-\frac{\partial \Delta\psi}{\partial \delta_n^{TD}}$. Because $\frac{\partial \Delta\psi}{\partial \delta_n^{TD}} < 2$ for all gaits [43], gait stability in the original model was determined by the sign of $\frac{\partial \Delta\psi}{\partial \delta_n^{TD}}$, with $\frac{\partial \Delta\psi}{\partial \delta_n^{TD}} < 0$ yielding unstable gaits and $\frac{\partial \Delta\psi}{\partial \delta_n^{TD}} = 0$ identifying the saddle node bifurcation point. Transforming the characteristic equation (B.12) for the recirculation model by a bilinear transformation provides additional insight into how the inclusion of leg recirculation changes gait stability. After the transformation, the characteristic equation becomes

$$\begin{aligned} z(s) &= z(\lambda = \frac{1+s}{1-s})(1-s)^2 \\ &= (2-\dot{\beta}_{des}\frac{\partial \tau}{\partial \delta_n^{TD}} - \frac{\partial \Delta\psi}{\partial \delta_n^{TD}})s^2 + (2-\dot{\beta}_{des}\frac{\partial \tau}{\partial \delta_n^{TD}})s + 2\dot{\beta}_{des}\frac{\partial \tau}{\partial \delta_n^{TD}} + \frac{\partial \Delta\psi}{\partial \delta_n^{TD}} \\ . \end{aligned} \tag{B.13}$$

Applying the Routh-Hurwitz criterion [22] to the characteristic equation in this form yields the following conditions on $\dot{\beta}_{des}$ for the remaining eigenvalues to remain within the unit circle

$$-\frac{1}{2}\frac{\partial \Delta\psi}{\partial \delta_n^{TD}} < \dot{\beta}_{des}\frac{\partial \tau}{\partial \delta_n^{TD}} < min\left(2\ ,\ 2-\frac{\partial \Delta\psi}{\partial \delta_n^{TD}}\right)\ . \tag{B.14}$$

While (B.14) provides upper and lower bounds on the values of $\dot{\beta}_{des}$ for gait stability, it also reveals that periodic gaits can remain stable for $\frac{\partial \Delta\psi}{\partial \delta_n^{TD}} < 0$, for sufficiently large $\dot{\beta}_{des}$. As a practical result, this suggests that increasing the leg angular velocity at touch-down at lower speeds (where $\frac{\partial \Delta\psi}{\partial \delta_n^{TD}} < 0$) can move the saddle-node bifurcation to a lower

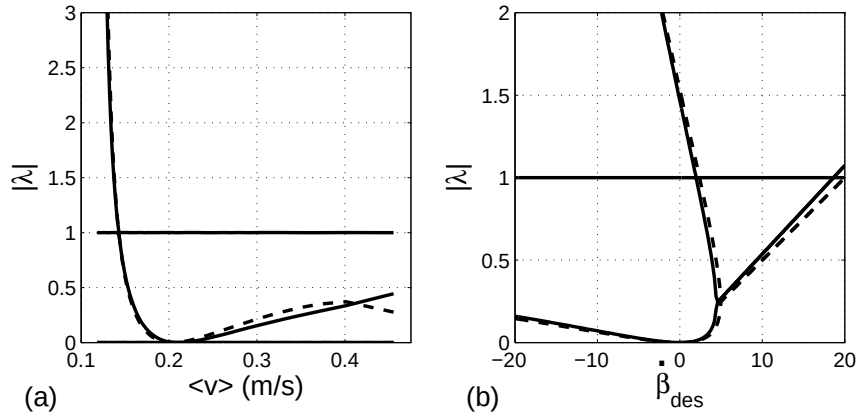

Figure B.1: Comparison between numerical (solid) and analytical (dashed) eigenvalue computations (a) along the gait family identified for $d = 0$; with $\dot{\beta}_{des} = 0$ and (b) as a function of the leg angular velocity at touch-down, $\dot{\beta}_{des}$, for the fixed point $(< v >, \delta_n^{TD}, \beta_n^{TD}) = (0.138, 0.509, 0.988)$ with $t_{des} = 0.08$ and $d = 0$.

speed, thereby stabilizing previously unstable periodic gaits of the original LLS model. Conversely, negative values of $\dot{\beta}_{des}$ will move the saddle-node bifurcation to higher average forward velocities, thereby destabilizing previously stable gaits.

The analytical eigenvalue expression (B.12) is evaluated for each fixed point of the gait family utilizing the approximations developed for the required partial derivatives, as developed in Section B.2. As illustrated in the first panel of Fig. B.1, the analytically approximated eigenvalues adequately match those computed numerically over the entire gait family, despite the approximations utilized in computing the partial derivatives. These results also extend to other choices of $\dot{\beta}_{des}$ which are different from zero although they are not illustrated here. Note the unity eigen value due to energy conservation and the zero eigen value due to $\dot{\beta}_{des} = 0$. The importance of the choice of $\dot{\beta}_{des}$, as previously discussed, is illustrated in the second panel of Fig. B.1 for a nominally unstable periodic

gait ($|\lambda| = 1.47$) for the recirculation model with $\dot{\beta}_{des} = 0$. While this gait cannot be stabilized in the original LLS formulation, varying the leg angular velocity at touchdown in the recirculation model modifies the eigenvalues, stabilizing the gait for $\dot{\beta}_{des} > 2$ rad/sec.

B.2 Supporting calculations

The characteristic equation governing the eigenvalues (B.12) was determined from the Jacobian (B.11) and simplified via the relations $\frac{\partial \Delta\psi}{\partial \beta_n^{TD}} = -\frac{\partial \Delta\psi}{\partial \delta_n^{TD}}$ and $\frac{\partial \tau}{\partial \beta_n^{TD}} = -\frac{\partial \tau}{\partial \delta_n^{TD}}$. Demonstrating that these equalities hold requires an expression for the leg angle swept during a given stance phase, which is developed in [43] as

$$\Delta\psi = \int_{\zeta_b}^{l} \frac{2 v_n^{TD} l \sin(\beta_n^{TD} - \delta_n^{TD}) d\zeta}{\zeta \sqrt{((v_n^{TD})^2 - k/m(\zeta - l)^2)\zeta^2 - l^2 (v_n^{TD})^2 \sin^2(\beta_n^{TD} - \delta_n^{TD})}} \tag{B.15}$$

where ζ_b is the largest positive root of the equation

$$m l^2 (v_n^{TD})^2 \sin^2(\beta_n^{TD} - \delta_n^{TD}) + k(\zeta_b - l)^2 \zeta_b^2 - m\zeta_b^2 (v_n^{TD})^2 \;=\; 0\,. \tag{B.16}$$

Defining the integrand of (B.15) as

$$\begin{aligned} f(\zeta, \delta_n^{TD}, \beta_n^{TD}) &= \frac{2 v_n^{TD} l \sin(\beta_n^{TD} - \delta_n^{TD})}{\zeta \sqrt{((v_n^{TD})^2 - k/m(\zeta - l)^2)\zeta^2 - l^2 (v_n^{TD})^2 \sin^2(\beta_n^{TD} - \delta_n^{TD})}} \\ &= \frac{g}{h} \end{aligned} \tag{B.17}$$

Leibniz's rule can be used to evaluate the expressions

$$\frac{\partial \Delta\psi}{\partial \delta_n^{TD}} = \int_{\zeta_b}^{l} \frac{\partial f(\zeta, \delta_n^{TD}, \beta_n^{TD})}{\partial \delta_n^{TD}} d\zeta - f(\zeta_b, \delta_n^{TD}, \beta_n^{TD}) \frac{\partial \zeta_b}{\partial \delta_n^{TD}} \tag{B.18}$$

$$\frac{\partial \Delta\psi}{\partial \beta_n^{TD}} = \int_{\zeta_b}^{l} \frac{\partial f(\zeta, \delta_n^{TD}, \beta_n^{TD})}{\partial \beta_n^{TD}} d\zeta - f(\zeta_b, \delta_n^{TD}, \beta_n^{TD}) \frac{\partial \zeta_b}{\partial \beta_n^{TD}} \, . \tag{B.19}$$

The development of any relationship between $\frac{\partial \Delta\psi}{\partial \delta_n^{TD}}$ and $\frac{\partial \Delta\psi}{\partial \beta_n^{TD}}$ therefore requires computing $\frac{\partial f(\zeta,\delta,\beta)}{\partial \delta_n^{TD}}$, $\frac{\partial f(\zeta,\delta,\beta)}{\partial \beta_n^{TD}}$, $\frac{\partial \zeta_b}{\partial \delta_n^{TD}}$ and $\frac{\partial \zeta_b}{\partial \beta_n^{TD}}$. We proceed by first constructing expressions for $\frac{\partial f(\zeta,\delta,\beta)}{\partial \delta_n^{TD}}$ and $\frac{\partial f(\zeta,\delta,\beta)}{\partial \beta_n^{TD}}$, which requires evaluating the following partial derivatives

$$\frac{\partial g}{\partial \delta_n^{TD}} = -2 v_n^{TD} l \cos(\beta_n^{TD} - \delta_n^{TD}) \tag{B.20}$$

$$\frac{\partial g}{\partial \beta_n^{TD}} = 2 v_n^{TD} l \cos(\beta_n^{TD} - \delta_n^{TD}) = -\frac{\partial g}{\partial \delta_n^{TD}} \tag{B.21}$$

$$\frac{\partial h}{\partial \delta_n^{TD}} = \frac{\zeta l^2 (v_n^{TD})^2 \sin(2(\beta_n^{TD} - \delta_n^{TD}))}{2\sqrt{((v_n^{TD})^2 - k/m(\zeta - l)^2)\zeta^2 - l^2 (v_n^{TD})^2 \sin^2(\beta_n^{TD} - \delta_n^{TD})}} \tag{B.22}$$

$$\frac{\partial h}{\partial \beta_n^{TD}} = \frac{-\zeta l^2 (v_n^{TD})^2 \sin(2(\beta_n^{TD} - \delta_n^{TD}))}{2\sqrt{((v_n^{TD})^2 - k/m(\zeta - l)^2)\zeta^2 - l^2 (v_n^{TD})^2 \sin^2(\beta_n^{TD} - \delta_n^{TD})}} \tag{B.23}$$

$$= -\frac{\partial h}{\partial \delta_n^{TD}} \, . \tag{B.24}$$

Using the above relations in the quotient rule yields the desired expressions for the partial derivatives

$$\frac{\partial f(\zeta, \delta_n^{TD}, \beta_n^{TD})}{\partial \beta_n^{TD}} = \frac{\frac{\partial g}{\partial \beta_n^{TD}} h - \frac{\partial h}{\partial \beta_n^{TD}} g}{h^2} \tag{B.25}$$

$$= \frac{-\frac{\partial g}{\partial \delta_n^{TD}} h + \frac{\partial h}{\partial \delta_n^{TD}} g}{h^2} \tag{B.26}$$

$$= -\frac{\partial f(\zeta, \delta_n^{TD}, \beta_n^{TD})}{\partial \delta_n^{TD}} . \tag{B.27}$$

Evaluating $\frac{\partial \zeta_b}{\partial \delta_n^{TD}}$ and $\frac{\partial \zeta_b}{\partial \beta_n^{TD}}$ requires implicit differentiation of (B.16), yielding

$$\frac{\partial \zeta_b}{\partial \beta_n^{TD}} = -\frac{ml^2(v_n^{TD})^2 \sin(\beta_n^{TD} - \delta_n^{TD}) \cos(\beta_n^{TD} - \delta_n^{TD})}{k\zeta_b(\zeta_b - l)(2\zeta_b - l) - m\zeta_b(v_n^{TD})^2} \tag{B.28}$$

$$\frac{\partial \zeta_b}{\partial \delta_n^{TD}} = \frac{ml^2(v_n^{TD})^2 \sin(\beta_n^{TD} - \delta_n^{TD}) \cos(\beta_n^{TD} - \delta_n^{TD})}{k\zeta_b(\zeta_b - l)(2\zeta_b - l) - m\zeta_b(v_n^{TD})^2} = -\frac{\partial \zeta_b}{\partial \beta_n^{TD}} \tag{B.29}$$

The relationship between $\frac{\partial \Delta\psi}{\partial \delta_n^{TD}}$ and $\frac{\partial \Delta\psi}{\partial \beta_n^{TD}}$ is established by substituting (B.27) and (B.29) into (B.18), which yields

$$\frac{\partial \Delta\psi}{\partial \delta_n^{TD}} = -\frac{\partial \Delta\psi}{\partial \beta_n^{TD}} . \tag{B.30}$$

Proceeding in a similar fashion for $\frac{\partial \tau}{\partial \beta_n^{TD}}$ requires the expression for the stance phase duration developed in [43]

$$\tau = 2\int_{\zeta_b}^{l} \frac{\zeta d\zeta}{\sqrt{((v_n^{TD})^2 - k/m(\zeta - l)^2)\zeta^2 - l^2(v_n^{TD})^2 \sin^2(\beta_n^{TD} - \delta_n^{TD})}} \tag{B.31}$$

where ζ_b once again is determined from (B.16). Defining the integrand of (B.31) as

$$f(\zeta, \delta_n^{TD}, \beta_n^{TD}) = \frac{2\zeta}{\sqrt{((v_n^{TD})^2 - k/m(\zeta - l)^2)\zeta^2 - l^2(v_n^{TD})^2 \sin^2(\beta_n^{TD} - \delta_n^{TD})}} = \frac{g}{h} \tag{B.32}$$

Leibniz's rule can be used to evaluate the expressions

$$\frac{\partial \tau}{\partial \delta_n^{TD}} = \int_{\zeta_b}^{l} \frac{\partial f(\zeta, \delta_n^{TD}, \beta_n^{TD})}{\partial \delta_n^{TD}} d\zeta - f(\zeta_b, \delta_n^{TD}, \beta_n^{TD}) \frac{\partial \zeta_b}{\partial \delta_n^{TD}} \tag{B.33}$$

$$\frac{\partial \tau}{\partial \beta_n^{TD}} = \int_{\zeta_b}^{l} \frac{\partial f(\zeta, \delta_n^{TD}, \beta_n^{TD})}{\partial \beta_n^{TD}} d\zeta - f(\zeta_b, \delta_n^{TD}, \beta_n^{TD}) \frac{\partial \zeta_b}{\partial \beta_n^{TD}} \, . \tag{B.34}$$

The development of the relationship between $\frac{\partial \tau}{\partial \delta_n^{TD}}$ and $\frac{\partial \tau}{\partial \beta_n^{TD}}$ therefore requires computing $\frac{\partial f(\zeta,\delta,\beta)}{\partial \delta_n^{TD}}$, $\frac{\partial f(\zeta,\delta,\beta)}{\partial \beta_n^{TD}}$, $\frac{\partial \zeta_b}{\partial \delta_n^{TD}}$ and $\frac{\partial \zeta_b}{\partial \beta_n^{TD}}$. We proceed by constructing expressions for $\frac{\partial f(\zeta,\delta,\beta)}{\partial \delta_n^{TD}}$ and $\frac{\partial f(\zeta,\delta,\beta)}{\partial \beta_n^{TD}}$, which requires evaluating the following partial derivatives

$$\frac{\partial g}{\partial \delta_n^{TD}} = 0 \tag{B.35}$$

$$\frac{\partial g}{\partial \beta_n^{TD}} = 0 \tag{B.36}$$

$$\frac{\partial h}{\partial \delta_n^{TD}} = \frac{l^2 (v_n^{TD})^2 \sin(2(\beta_n^{TD} - \delta_n^{TD}))}{2\sqrt{((v_n^{TD})^2 - k/m(\zeta - l)^2)\zeta^2 - l^2 (v_n^{TD})^2 \sin^2(\beta_n^{TD} - \delta_n^{TD})}} \tag{B.37}$$

$$\frac{\partial h}{\partial \beta_n^{TD}} = \frac{-l^2 (v_n^{TD})^2 \sin(2(\beta_n^{TD} - \delta_n^{TD}))}{2\sqrt{((v_n^{TD})^2 - k/m(\zeta - l)^2)\zeta^2 - l^2 (v_n^{TD})^2 \sin^2(\beta_n^{TD} - \delta_n^{TD})}} \tag{B.38}$$

$$= -\frac{\partial h}{\partial \delta_n^{TD}} \, . \tag{B.39}$$

Using the above relations in the quotient rule yields the desired expressions for the partial derivatives

$$\frac{\partial f(\zeta, \delta_n^{TD}, \beta_n^{TD})}{\partial \beta_n^{TD}} = \frac{\frac{\partial g}{\partial \beta_n^{TD}} h - \frac{\partial h}{\partial \beta_n^{TD}} g}{h^2} \tag{B.40}$$

$$= \frac{\frac{\partial h}{\partial \delta_n^{TD}} g}{h^2} \tag{B.41}$$

and

$$\frac{\partial f(\zeta,\delta_n^{TD},\beta_n^{TD})}{\partial \delta_n^{TD}} = \frac{\frac{\partial g}{\partial \delta_n^{TD}}h - \frac{\partial h}{\partial \delta_n^{TD}}g}{h^2} \tag{B.42}$$

$$= -\frac{\frac{\partial h}{\partial \delta_n^{TD}}g}{h^2} \tag{B.43}$$

$$= -\frac{\partial f(\zeta,\delta_n^{TD},\beta_n^{TD})}{\partial \beta_n^{TD}}\,. \tag{B.44}$$

The relationship between $\frac{\partial \tau}{\partial \delta_n^{TD}}$ and $\frac{\partial \tau}{\partial \beta_n^{TD}}$ is established by substituting (B.44) and (B.29) into (B.33), which yields

$$\frac{\partial \tau}{\partial \delta_n^{TD}} = -\frac{\partial \tau}{\partial \beta_n^{TD}}\,. \tag{B.45}$$

Computing the eigenvalues governing gait stability from the characteristic equation (B.12) requires determining $\frac{\partial \Delta\psi}{\partial \delta_n^{TD}}$ and $\frac{\partial \tau}{\partial \delta_n^{TD}}$. While [43] presents an analytical solution for $\Delta\psi$ and τ, the complexity of the expression precludes analytical computation of the derivatives. As in [44], the required derivatives are instead computed by approximating $\Delta\psi$ and τ via the Schwind-Koditschek approximation [46]. This quadrature estimation method employs a linear approximation in the mean value function to approximate the integral. Using this approximation, $\Delta\psi$ is approximated as

$$\Delta\psi = \frac{2lv_n^{TD}\sin(\beta_n^{TD}-\delta_n^{TD})(l-\zeta_b)}{\hat{\zeta}\sqrt{((v_n^{TD})^2 - k/m(\hat{\zeta}-l)^2)\hat{\zeta}^2 - l^2(v_n^{TD})^2\sin^2(\beta_n^{TD}-\delta_n^{TD})}} \tag{B.46}$$

$$\hat{\zeta} = \frac{3\zeta_b + l}{4}\,. \tag{B.47}$$

Employing the approximation for τ yields

$$\tau = \frac{2\hat{\xi}\,(l-\zeta_b)}{\sqrt{((v_n^{TD})^2 - k/m(\hat{\xi}-l)^2)\hat{\xi}^2 - l^2(v_n^{TD})^2\sin^2(\beta_n^{TD}-\delta_n^{TD})}}\,. \tag{B.48}$$

We compute an approximation of $\frac{\partial\Delta\psi}{\partial\delta_n^{TD}}$ using our approximation of $\Delta\psi$ presented (B.46-B.47), simplified further as

$$\begin{aligned}
\Delta\psi &= \frac{p}{q} && \text{(B.49)}\\
p &= 128 l v_n^{TD}\sin(\beta_n^{TD}-\delta_n^{TD})(l-\zeta_b) && \text{(B.50)}\\
q &= (3\zeta_b + l)\sqrt{s} && \text{(B.51)}\\
s &= (16(v_n^{TD})^2 - \frac{9k}{m}(\zeta_b - l)^2)(3\zeta_b+l)^2 - 256 l^2 (v_n^{TD})^2\sin^2(\beta_n^{TD}-\delta_n^{TD})\\
. && && \text{(B.52)}
\end{aligned}$$

With the expression for $\frac{\partial\zeta_b}{\partial\delta_n^{TD}}$ provided in (B.29), calculation of $\frac{\partial\Delta\psi}{\partial\delta_n^{TD}}$ proceeds directly from the quotient rule

$$\frac{\partial\Delta\psi}{\partial\delta_n^{TD}} = \frac{q\frac{\partial p}{\partial\delta_n^{TD}} - p\frac{\partial q}{\partial\delta_n^{TD}}}{q^2} \tag{B.53}$$

with

$$\frac{\partial p}{\partial\delta_n^{TD}} = -128 l v_n^{TD}(\cos(\beta_n^{TD}-\delta_n^{TD})(l-\zeta_b) + \frac{\partial\zeta_b}{\partial\delta_n^{TD}}\sin(\beta_n^{TD}-\delta_n^{TD})) \tag{B.54}$$

and

$$\frac{\partial q}{\partial \delta_n^{TD}} = 3\frac{\partial \zeta_b}{\partial \delta_n^{TD}}\sqrt{s} + \frac{(3\zeta_b + l)(t\frac{\partial \zeta_b}{\partial \delta_n^{TD}} - x\frac{\partial \zeta_b}{\partial \delta_n^{TD}} + uv_n^{TD}\cos(\beta_n^{TD} - \delta_n^{TD}))}{2\sqrt{s}} \tag{B.55}$$

where

$$t = 6(3\zeta_b + l)(16(v_n^{TD})^2 - \frac{9k}{m}(\zeta_b - l)^2) \tag{B.56}$$

$$u = 512l^2 v_n^{TD}\sin(\beta_n^{TD} - \delta_n^{TD}) \tag{B.57}$$

$$x = \frac{18k}{m}(\zeta_b - l)(3\zeta_b + l)^2 \, . \tag{B.58}$$

In a similar fashion, we compute $\frac{\partial \tau}{\partial \delta_n^{TD}}$ using our approximation of τ presented in (B.48), simplified further as

$$\tau = \frac{m}{n} \tag{B.59}$$

$$m = 8\left(l^2 + 2l\zeta_b - 3\zeta_b^2\right) \tag{B.60}$$

$$n = \sqrt{(16(v_n^{TD})^2 - \frac{9k}{m}(\zeta_b - l)^2)(3\zeta_b + l)^2 - 256l^2(v_n^{TD})^2\sin^2(\beta_n^{TD} - \delta_n^{TD})} = \sqrt{s} \tag{B.61}$$

.

The calculation of $\frac{\partial \tau}{\partial \delta_n^{TD}}$ then proceeds directly from the quotient rule as

$$\frac{\partial \tau}{\partial \delta_n^{TD}} = \frac{n\frac{\partial m}{\partial \delta_n^{TD}} - m\frac{\partial n}{\partial \delta_n^{TD}}}{n^2} \tag{B.62}$$

with

$$\frac{\partial m}{\partial \delta_n^{TD}} = (16l - 48\zeta_b)\frac{\partial \zeta_b}{\partial \delta_n^{TD}} \tag{B.63}$$

$$\frac{\partial n}{\partial \delta_n^{TD}} = \frac{(t-x)\frac{\partial \zeta_b}{\partial \delta_n^{TD}} + uv_n^{TD}\cos(\beta_n^{TD} - \delta_n^{TD})}{2\sqrt{s}}\,. \tag{B.64}$$

The analytical eigenvalue calculation employs these approximations, resulting in the eigenvalue variation illustrated in Fig. B.1.